

1 **Chemical characterization of oxygenated organic compounds**
2 **in gas-phase and particle-phase using iodide-CIMS with**
3 **FIGAERO in urban air**

4 Chenshuo Ye¹, Bin Yuan^{2,3,*}, Yi Lin^{2,3}, Zelong Wang^{2,3}, Weiwei Hu⁴, Tiange Li^{2,3}, Wei
5 Chen⁴, Caihong Wu^{2,3}, Chaomin Wang^{2,3}, Shan Huang^{2,3}, Jipeng Qi^{2,3}, Baolin Wang⁵,
6 Chen Wang⁵, Wei Song⁴, Xinming Wang⁴, E Zheng^{2,3}, Jordan E. Krechmer⁶, Penglin
7 Ye⁷, Zhanyi Zhang^{2,3}, Xuemei Wang^{2,3}, Douglas R. Worsnop⁶, Min Shao^{2,3,1,*}

8 ¹ College of Environmental Sciences and Engineering, Peking University, Beijing
9 100871, China

10 ² Institute for Environmental and Climate Research, Jinan University, Guangzhou
11 511443, China

12 ³ Guangdong-Hongkong-Macau Joint Laboratory of Collaborative Innovation for
13 Environmental Quality, Guangzhou 511443, China

14 ⁴ Guangzhou Institute of Geochemistry, Chinese Academy of Sciences, Guangzhou
15 511443, China

16 ⁵ School of Environmental Science and Engineering, Qilu University of Technology,
17 Jinan 250353, China

18 ⁶ Aerodyne Research, Inc. 45 Manning Rd., Billerica, MA, USA

19 ⁷ Shanghai Key Laboratory of Atmospheric Particle Pollution and Prevention (LAP³),
20 Department of Environmental Science and Engineering, Fudan University, Shanghai
21 200438, China

22 *Correspondence to: byuan@jnu.edu.cn; mshao@pku.edu.cn

23

24 Abstract

25 The characterization of oxygenated organic compounds in urban areas remains a
26 pivotal gap in our understanding of the evolution of organic carbon under polluted
27 environments, as the atmospheric processes involving interactions between organics
28 and inorganic compoundss, anthropogenic pollutants and natural emissions lead to the
29 formation of various and complex secondary products. Here, we describe
30 measurements of an iodide chemical ionization time-of-flight mass spectrometer
31 installed with a Filter Inlet for Gases and AEROsols (FIGAERO-I-CIMS) in both gas-
32 phase and particle-phase at an urban site in Guangzhou, a typical mega-city in southern
33 China, during the autumn of 2018. Abundant oxygenated organic compounds
34 containing 2--5 oxygen atoms were observed, including organic acids, multi-functional
35 organic compoundss typically emitted ~~form~~ from biomass burning, oxidation products
36 of biogenic hydrocarbons and aromatics. Photochemistry played dominant roles in the
37 formation of gaseous organic acids and isoprene-derived organic nitrates, while
38 nighttime chemistry contributed significantly to the formation of monoterpene-derived
39 organic nitrates and inorganics. Nitrogen-containing organic compounds occupied a
40 significant fraction of the total signal in both the gas and particle phases, with elevated
41 fractions at higher molecular weights. Measurements of organic compounds in particle
42 phase by FIGAERO-I-CIMS explained $24 \pm 0.8\%$ of the total organic aerosol mass
43 measured by aerosol mass spectrometer (AMS), and the fraction increased for more
44 aged organic aerosol. The systematical~~ly~~ interpretation of mass spectra of the
45 FIGAERO-I-CIMS in the urban area of Guangzhou provides a holistic view of
46 numerous oxygenated organic compounds in the urban atmosphere, which can serve as
47 a reference for the future field measurements by FIGAERO-I-CIMS in polluted urban
48 regions.

49

50 **1 Introduction**

51 In urban air, atmospheric chemical processes are varied and complex, as the result
52 of large emissions of both anthropogenic pollutants and biogenic volatile organic
53 compounds, associated with strong interactions with each other (He et al., 2014; Karl
54 et al., 2018; Shrivastava et al., 2019). Consequently, strong formation of secondary
55 pollutants, e.g. ozone and secondary organic aerosol (SOA), are observed in urban and
56 downwind regions (Huang et al., 2015; Zhang et al., 2014). ~~Previous literature suggests~~
57 ~~that oxygenated organic compounds are not fully accounted in some earlier studies,~~
58 ~~which may explain some of the discrepancies between observations and models for~~
59 ~~many provide a vital link between advanced chemical mechanisms and the model-~~
60 ~~observation discrepancy for many~~ unaddressed issues in atmospheric chemistry.
61 Oxygenated organic compounds They are supposed to be the top candidates for missing
62 OH reactivity observed in various environments including pristine rainforests and
63 urbanized areas (Noelscher et al., 2016; Yang et al., 2016, 2017). The photolysis of
64 carbonyls serves as a critical radical source driving ozone formation in highly polluted
65 industrialized areas (Edwards et al., 2014; Liu et al., 2012; Xue et al., 2016). Although
66 it has been discovered a long time ago that oxygenated organic compounds make up a
67 substantial fraction of submicron aerosol mass (Kroll and Seinfeld, 2008), enormous
68 difficulty still exists in accurately predicting formation and evolution of SOA (de Gouw
69 et al., 2005; Hodzic et al., 2010; Volkamer et al., 2006).

70 One of the biggest ~~obstacles to problems hindering our understanding~~
71 ~~in~~understand the role of oxygenated organic compounds is the characterization of these
72 extremely complicated and diverse chemicals which encompass tens of thousands of
73 individual species spanning a wide range of volatility. Chemical ionization mass
74 spectrometry (CIMS) is a powerful technique for the molecular-level characterization
75 of oxygenated organic compounds because of the following advantages (Zhao, 2018):
76 direct measurements and fast time response to capture the rapid temporal change of
77 short-lifetime intermediates; soft ionization providing chemical information on
78 molecular level; selective ionization ensuring measurements for specific classes of

79 species. Iodide anion ionizes species mainly through adduction (Iyer et al., 2016) and
80 is used for the detection of oxygenated organic compounds particularly organic
81 compounds with 2--5 oxygen atoms (Lee et al., 2014; Lopez-Hilfiker et al., 2016; Riva
82 et al., 2019). It has been shown that I-CIMS is an excellent technique to investigate
83 oxidation processes of volatile organic compounds (VOCs) and formation of SOA
84 (Isaacman-VanWertz et al., 2018). Installed with a thermal desorption inlet that collects
85 and heats aerosol to evaporate organic compounds-coatings, e.g. Filter Inlet for Gases
86 and AEROSols (FIGAERO, Lopez-Hilfiker et al., 2014) and Micro Orifice
87 Volatilization Impactor (MOVI-HRToF-CIMS, (Yatavelli et al., 2012), the CIMS
88 instruments are capable of analyzing particle-phase species and gas-particle partitioning
89 in a semi-continuous way (Stark et al., 2017; Stolzenburg et al., 2018).

90 Although FIGAERO-CIMS has gained recent popularity in atmospheric
91 chemistry research, much of the published work was done in chambers or in the
92 laboratory (D'Ambro et al., 2017, 2018; Hammes et al., 2019; Lopez-Hilfiker et al.,
93 2015), there is a growing trend for As for the applications of FIGAERO-I-CIMS in field
94 campaigns, most work has been mostly performed in forest or rural areas (Huang et al.,
95 2019; Hunter et al., 2017; Lee et al., 2016, 2018b), and systematic analysis of
96 measurements in urban atmosphere by FIGAERO-I-CIMS is still limited (Le Breton
97 et al., 2018b). In this study, we present the measurement results using this
98 instrumentation FIGAERO-I-CIMS during a coordinated campaign in Guangzhou, a
99 megacity in the Pearl River Region of China. We provide an overview of gas-phase and
100 particle-phase oxygenated species detected in the mass spectra of FIGAERO-I-CIMS
101 during the campaign. The bulk chemical properties of organic compounds in both gas
102 phase and particle phase will also be discussed.

103 **2 Methods**

104 **2.1 Measurement site and supporting data**

105 Measurements were conducted during the coordinated campaign “Particles,
106 Radicals and Intermediates from oxidation of primary Emissions over the Great Bay
107 Area” (PRIDE-GBA) in October and November 2018. The Great Bay Area (GBA)

108 refers to a highly industrialized and urbanized area in southern China, including two
109 Special Administrative Regions of Hong Kong and Macao, and nine cities surrounding
110 the Pearl River estuary. Affected by the subtropical monsoon climate, the weather in
111 the region was characterized by high temperatures and relative humidity (RH) as well
112 as sufficient sunshine— (global solar radiation of the Pearl River Delta region in Fall,
113 2016 was ~1200 MJ/m², (Liu et al., 2018)(Changhuan et al., 2018)(Wang and LinHo,
114 2002; Yihui and Chan, 2005). The city of Guangzhou lies ~~on~~in the north of the GBA
115 and south ~~to~~of the mountains. Therefore, the city is extensively influenced by both
116 anthropogenic and biogenic emissions. The urban site ~~in Guangzhou~~ was located at
117 Guangzhou Institute of Geochemistry, Chinese Academy of Sciences (23.14°N,
118 113.36°E). Online instruments sampled from inlets set up in laboratories on the eighth-
119 floor or ninth-floor (about 25 meters above the ground).

120 In addition to FIGAERO-I-CIMS discussed later, measurements data from a suite
121 of other instruments were also used in this work. A high-resolution time-of-flight
122 aerosol mass spectrometer (HR-ToF-AMS, Aerodyne Research, Inc.) was deployed to
123 provide chemical composition and many other parameters of ambient aerosol including
124 f60, liquid water content (LWC), particulate organic nitrates and elemental ratios (Hu
125 et al., 2016, 2018). The parameter f60 is the ratio of the integrated signal at m/z 60 to
126 the total signal of organic components and is used as a tracer for biomass burning
127 emissions (Cubison et al., 2011). LWC of aerosol was taken as the sum of water
128 contributed by inorganic components which ~~was~~was predicted by ISORROPIA II
129 model and organic components which was calculated based on the organic
130 hygroscopicity parameter (Fountoukis and Nenes, 2007; Guo et al., 2015). Based on
131 AMS data, oOrganic nitrate concentrations were ~~calculated~~determined by 2-3 times
132 lower based on AMS data as their NO₂⁺/NO⁺ ratios for organic nitrate than inorganic
133 nitrates are typically 2-3 times lower than separated from NH₄NO₃ and the measured
134 ratio can be used to separately quantify inorganic and organic nitrates based on their
135 difference in NO₂⁺/NO⁺ ratio (Fry et al., 2013). The calculation method of elemental
136 ratios based on AMS data has been described elsewhere (Aiken et al., 2007;
137 Canagaratna et al., 2015). Detailed information about AMS measurements from the

138 PRIDE-GBA campaign ~~are is~~ forthcoming in a separate manuscript. An online GC-
139 MS/FID (Wuhan Tianhong Instrument Co., Ltd) and a proton transfer reaction time-of-
140 flight mass spectrometer (PTR-ToF-MS, Ionicon Analytic GmbH) (Yuan et al., 2017)
141 served as the analytical techniques for measuring isoprene and other VOCs (e.g.
142 monoterpenes, aromatics and a few oxygenated VOCs) (Wu et al., 2020), respectively.
143 Trace gases (CO, O₃, NO and NO₂) were measured by commercial gas monitors
144 (Thermo Fisher Scientific Inc.) (Wang et al., 2020d). Photolysis rates were measured
145 by PFS-100 photolysis spectrometer (Focused Photonics Inc.). ~~Fig. S1 shows the diet~~
146 ~~Description of the conditions prevailing during the campaign is shown in Fig. S1,~~
147 ~~including changes of meteorological data, trace gases, the photolysis rate of NO₂~~
148 ~~(j_{NO_2} , $j_{(NO_2)}$) and important VOCs (isoprene, monoterpenes, toluene and benzene).~~
149 Temperature and RH were measured by a Vantage Pro2 weather station (Davis
150 Instruments Corp.). ~~Time series and diurnal profiles of meteorological parameters, trace~~
151 ~~gases, the photolysis rate of NO₂ (j_{NO_2}) along with several important VOCs (isoprene,~~
152 ~~monoterpenes, toluene and benzene) are shown in Figure S1. The~~ temperature during
153 ~~the~~ campaign was between 17 and 33°C with an average of 24°C and RH was between
154 27 and 97% with an average of 70%.

155 2.2 FIGAERO-I-CIMS

156 2.2.1 Experimental setup

157 Our instrument consists of a Filter Inlet for Gases and AEROSols (FIGAERO)
158 and a time-of-flight chemical ionization mass spectrometer coupled with ~~an~~ iodide
159 ionization source (Bertram et al., 2011; Lee et al., 2014; Lopez-Hilfiker et al., 2014).
160 The FIGAERO is a multi-port inlet assembly following a two-step procedure
161 alternating between gas mode in which online measurements of gases and semi-
162 continuous sampling of particle-phase species are conducted, and particle mode in
163 which particulate composition is investigated via thermal~~ly~~ desorption (Lopez-Hilfiker
164 et al., 2014; Thornton et al., 2020). Iodide ~~reagent ions provide source is~~ a ~~very~~ “soft”
165 ionization technique with little ionization-induced fragmentation and selective
166 detection towards multi-functional organic compounds, ~~providing elemental~~

167 ~~compositions making it suitable for chemical speciation of for~~ thousands of ~~complicated~~
168 oxygenated compounds in the atmosphere (Hyttinen et al., 2018; Iyer et al., 2016; Lee
169 et al., 2014; Riva et al., 2019).

170 The sample air was drawn into the ion molecule reaction (IMR) chamber where
171 it intersected and reacted with ~~the~~ iodide ions generated by flowing 2 mL/min 1000
172 ppm methyl iodide in 2.4 L/min N₂ through an X-ray source. The pressure in the IMR
173 chamber was maintained at 370–390 mbar. Equipped with a long time-of-flight mass
174 analyzer, our instrument was configured to measure singularly charged ions up to 603
175 Th with a mass resolving power of 10000–11000 ($m/\Delta m$ at 50% height) during the
176 campaign (~~see~~ Fig. S2).

177 Ambient air was continuously sampled through two inlets protruding about 1.5
178 meters out of sticking outside the a window on ninth-floor of a building. One was a 3-
179 meter PFA tubing (1/4-inch OD) for gas phase sampling, through which roughly 9
180 L/min air was drawn, and 2 L/min was directly taken into the instrument for gas
181 measurements ~~without removing particles-, resulting in an inlet~~ The residence time ~~was~~
182 of 0.35–24 seconds. The gas sampling line inside the room was covered by heat
183 insulation associated with a heating cable to minimize condensation on the tubing
184 surface. ~~Another~~ The other one inlet for particle phase was a 3.8-meter metal tubing
185 (3/8-inch OD) ~~for particle phase~~ fitted with a PM_{2.5} cyclone and a Nafion dryer (Perma
186 Pure, model PD-07018T-12MSS) to reduce water content in the sampled air. The
187 particle phase inlet was drawn by a laminar flow at about ~10–8 L/min (Reynolds
188 number of ~1500,-), 3.8 L/min of which was collected on PTFE membrane filters
189 (Zefluor[®], Pall Inc., USA). The residence time was 1.3 seconds for the particle phase
190 sampling line. Semi-volatility and low-volatility compounds tend to interact with wall
191 surfaces of both inlet and IMR and thus extend response time (Krechmer et al., 2016).
192 Wall loss also occurs in the IMR and that is why people are trying to improve the
193 designs of the IMR to minimize wall interactions (Palm et al., 2019). Given Asthat
194 accurate estimation correction for wall losses remains poorly understood impossible, we
195 did not no wall loss correction was performed in this study correct wall loss here.-

196 The FIGAERO worked in a cyclical 1-hour pattern with two modes (~~Fig. S3~~):
197 measuring gas for the first 24 minutes while simultaneously collecting particles on the
198 filter; and then analyzing the particle-phase collection for another 36 minutes. ~~Fig. S3~~
199 ~~displays the two sampling setups of the FIGAERO.~~ In every 24-minute gas mode,
200 ambient air was measured for the first 21 minutes, followed by 3-minute gas
201 background by over~~flowing~~ ~~flushing~~ zero air at 5 L/min through a pinhole just in the
202 front of the IMR. ~~The is persistent background measurements for CIMS isare inevitably~~
203 ~~influenced by wall interactions, especially for “sticky” species. Recently, (Palm et al.,~~
204 ~~(2019) proposed a new way to determine gas background (“fast background”) by fast~~
205 ~~switching between ambient air and background, which greatly improves accurate~~
206 ~~determination of CIMS background.~~ In the remaining 36 minutes, the components of
207 ~~the~~ collected particles were thermally desorbed and introduced into the CIMS with 2
208 L/min N₂ carrier gas. ~~The N₂ flow was ramped from ambient temperature to 175°C in~~
209 ~~12 minutes and held for another 20 minutes.~~ Schematic diagram of working modes and
210 temperature profile of FIGAERO heating in a single cycle is shown in Fig. S4. Particle
211 background was determined every 6th 1-hour running cycles ~~in which ambient air~~
212 ~~passed over, during which the particles passed through~~ a filter (Parker Balston, model
213 9922-11-CQ) ~~in front of the FIGAERO filter before being collected on the PTFE~~
214 ~~membrane filter.~~

215 **2.2.2 Calibration experiments**

216 Using various techniques, we calibrated dozens of chemical compounds in the
217 laboratory. Table S1 summarizes the calibrated species and corresponding calibration
218 methods. (1) Gas cylinders are commercially available for a few species (e.g. chlorine,
219 hydrogen cyanide). The gaseous standards were diluted down to different
220 concentrations and then introduced to the CIMS. (2) For those VOCs of which standards
221 are liquid or solid, solutions with known concentrations are made and then vaporized
222 using the liquid calibration unit (LCU, Ionicon Analytic GmbH) to provide gaseous
223 standards. (3) Commercial permeation tubes are available for some species (e.g. nitric
224 acid). (4) Some gaseous chemicals were generated in the laboratory. For example,

225 isocyanic acid was generated from thermal decomposition of cyanuric acid in a
226 diffusion cell (Li et al., 2021; Wang et al., 2020d), and dinitrogen pentoxide was
227 generated via the reaction of ozone with excess nitrogen dioxide in a flow reactor
228 (Bertram et al., 2009). (5) Compounds of low vapor pressure were calibrated through
229 the FIGAERO (Lopez-Hilfiker et al., 2014). Briefly, certain amounts of target species
230 dissolved in organic solvents (e.g. isopropanol or acetone) were ~~injected-deposited~~ onto
231 the PTFE filter of the FIGAERO using a syringe, and the droplet was then subjected to
232 a temperature-programmed thermal desorption by N₂ gas. The sensitivity for particle
233 phase was determined as the ~~peak areas integrated signals~~ under thermogram profiles
234 versus the amount of ~~injected-deposited~~ calibrant.

235 In addition to sensitivity calibration, the effects of humidity on the sensitivity for
236 various species ~~was-were~~ also investigated in the laboratory. ~~The humidity dependence~~
237 ~~curves for~~ some of ~~the calibrated species which~~ are shown in Fig. S5. Considering water
238 vapor pressure in the IMR, Theour humidity-dependent curves results are generally
239 consistent with those reported reported in (Lee et al., (2014) and this work are pretty
240 consistent if considering the water vapor pressure in the IMR (see detailed discussions
241 in Section S3 in the supplement for details). Low-molecular-weight acids, e.g., formic
242 acid and nitric acid, tend to be more sensitive to the humidity changes than multi-
243 functional compounds. Similar tendency of multi-functional compounds associated
244 with less humidity dependence was also reported in previous work (Lee et al., 2014).

245 In the later part of the campaign (after Oct. 22), an isotopically labeled formic
246 acid (DCOOH, Cambridge Isotope Laboratories, Inc.) permeation tube held at constant
247 temperature (65 °C), was mixed with 10 mL/min N₂ and continuously delivered into
248 the entrance of sampling inlet in order to derive a humidity dependence function from
249 ~~the~~ field measurements. ~~Fig. S5 presents that~~ DCOOH signals during the campaign
250 exhibited a consistent humidity-dependent curve consistent with formic acid obtained
251 in the laboratory (Fig. S5). We applied humidity correction to the species with the
252 humidity-dependent curve determined in the laboratory (underlined species in Table
253 S1), including C1-C5 organic acids, catechol, HNCO, Cl₂ and HNO₃. For other
254 compounds, humidity correction was not applied, as there is no universal pattern of

255 humidity dependence for all detected species and multi-functional compounds that
256 comprise the majority of the species measured by FIGAERO-I-CIMS are usually less
257 influenced by humidity.

258 The measured concentration of DCOOH was steady after being applying-applied
259 to humidity correction (Fig. S6g), indicating the stability of our instrument. In addition,
260 we also performed field calibrations throughout the campaign to check the instrument
261 status by spotting a solution mixture of levoglucosan, heptaethylene glycol and
262 octaethylene glycol on the FIGAERO filter every 2---3 days (Fig. S6). Multiple-point
263 calibrations for these organic species were performed in the beginning and the end of
264 the campaign. The concentration of the solution used in the first two calibration
265 experiments was too high, so we prepared a new solution for calibrations after
266 November. The relative changes of the determined calibration factors in November
267 were within 50% for the calibrated species.

268 **2.2.3 Data processing**

269 The TofWare software (version 3.0.3; Tofwerk AG, Switzerland) was used to
270 conduct the high-resolution peak fitting for the mass spectra data of ToF-CIMS,
271 including mass calibration, instrumental parameters optimization (peak shape and peak
272 width) and bunch fitting of high-resolution peaks (Stark et al., 2015). In this study, the
273 signals of ions were normalized to the sum signals of I^- and H_2OI^- at 10^6 cps.
274 Hourly particle-phase data were obtained by integrating the sum-signals of various ionss
275 time series of each ion during each FIGAERO desorption period, i.e., peak areas.
276 Background corrected signals were obtained by subtracting linearly interpolated
277 background signals from ambient signals (and integrated signalspeak areas) for ions in
278 the gas (and particle) phase.

279 In order to determine the sensitivities of uncalibrated species, voltage scanning
280 procedure was performed from time to time throughout the campaign covering different
281 times of the day (Iyer et al., 2016; Lopez-Hilfiker et al., 2016). Here, we selected four
282 representative periods including morning, afternoon, evening and night on polluted
283 days. By performing sigmoidal fitting on the remaining signals as a function of voltages,

284 a dV_{50} value of each ion from each period was determined at which voltage half of one
285 kind of ion dissociated (Lopez-Hilfiker et al., 2016). We observed a positive correlation
286 between the sensitivities of the ions relative to maximum sensitivity and their average
287 dV_{50} values (Fig. S7), consistent with previous studies (Isaacman-VanWertz et al., 2018;
288 Lopez-Hilfiker et al., 2016). This relationship was used to calculate response factors for
289 uncalibrated species, after taking into account the relative transmission efficiency for
290 the ions (see Section S1 in the Supplement for detailed analysis).

291 **3 Results and discussion**

292 **3.1 Overview of detected species in the mass spectra**

293 We identify 1334 ions adducted with iodide from the mass spectra, among which
294 427 are charged closed-shell organic compounds containing only C, H, O elements
295 ($C_xH_yO_zI^-$) and 388 are charged closed-shell organic compounds containing C, H, O
296 and N elements ($C_xH_yN_{1,2}O_zI^-$). For species with the formula of $C_xH_yO_z$, x ranges
297 from 1 to 20; y is an even number and no more than $2x+2$; z is greater than or equal to
298 2. The range of carbon number x for the ions with $C_xH_yN_{1,2}O_z$ is the same as the ions
299 with $C_xH_yO_z$. For species containing one nitrogen ($C_xH_yNO_z$), y is an odd number and
300 less than $2x+2$; z is larger than or equal to 2. For species containing two nitrogen atoms
301 ($C_xH_yN_2O_z$), y is an even number and less than $2x+1$; z is larger than or equal to 4.
302 Table 1 summarizes species discussed in the main text. Although compounds with two
303 nitrogen atoms and zero nitrogen atoms both lie on even/odd masses, they can be
304 separated for certain ions using with the current resolving power, as shown/demonstrated
305 by the peak fitting results of mass spectrum at m/z 311 (Fig. S8).

306 The campaign-averaged mass spectra of detected ions in the both gas and particle
307 phases are shown in Fig. 1. In general, molecules in particle-phase have larger
308 molecular weights compared to gas-phase compounds. Signals in the mass range of 150
309 ~~~~~ 300 Th comprise a large fraction of gas-phase compounds, and concentrations in the
310 gas phase decrease quickly with m/z higher than 250 Th. ~~For~~ In contrast, comparison,
311 the detected signals in the particle phase are mainly distributed within the range of 200
312 ~~~~~ 320 Th.

313 We compare the concentration for various ions between the daytime (10 am -- 6
314 pm) and nighttime (10 pm -- 6 am), by determining concentration ratios between at
315 night and during the daytime (Fig. 2). Most species have higher concentrations during
316 the daytime, especially for relatively volatile compounds in gas-phase, despite the fact
317 that lower boundary layer height at night should increase nighttime mixing ratios, as
318 behaved for many primary gases, e.g. CO (Fig. S1) (Wu et al., 2020). The higher
319 concentrations during the daytime for most species detected by FIGAERO-I-CIMS
320 suggest the dominant role of photochemical induced oxidation in forming these
321 oxidized compounds. In addition to typical nocturnal species including nitryl chloride
322 ($ClNO_2I^-$), chlorine nitrate ($ClONO_2I^-$) and dinitrogen pentoxide ($N_2O_5I^-$), higher
323 concentrations for the ions of $C_6H_{10}O_5I^-$ and $C_6H_{12}O_5I^-$ were also observed, which
324 will be discussed in next section. A large number of particulate N-containing organic
325 compounds increase during the night as well, as shown by mass defect diagrams of
326 $C_xH_yO_z$ and $C_xH_yN_{1,2}O_z$ color coded by the night to day ratios (Fig. S8S9).

327 Based on the mass spectra shown in Fig. 1, we identify a number of ions
328 associated with high concentrations in both gas and particle phases. In the following
329 Section 3.2-3.7, we will perform interpretation of the mass spectra by analyzing
330 variability and correlation of these important ions.~~The ions in the mass spectra of~~
331 ~~FIGAERO-I-CIMS are classified and interpreted in the following Section 3.2-3.7,~~
332 including monosaccharide-derived compounds (with brown tags in Fig. 1), oxygenated
333 aromatics (with purple tags), organic acids (with pink tags), oxidation products of
334 biogenic volatile organic compounds (BVOCs, with green tags), sulfur-containing
335 compounds, and inorganics (with blue tags). After going through detailed analysis in
336 the species level, Section 3.8 will provide an overall picture about bulk chemical
337 characteristics of detected organic compounds in terms of the distributions of average
338 carbon oxidation states, carbon number and oxygen number. Lastly, Section 3.9 will
339 compare our measurement of organic aerosol (OA) with AMS data.

340 **3.2 Monosaccharide-derived compounds**

341 C₆H₁₀O₅ and C₆H₁₂O₅ are highly correlated with each other in aerosol (r=0.92),
342 and they are two of a few C_xH_yO_z compounds with higher concentrations at night,and
343 they are highly correlated with each other in aerosol (r=0.92). Previous work assigned
344 them as monosaccharide derived compounds emitted from biomass burning (Bhattarai
345 et al., 2019; Qi et al., 2019; Reyes-Villegas et al., 2018; Simoneit et al., 1999).—

346 In this campaign, C₆H₁₀O₅ was detected mostly in the particle phase (the fraction
347 in the particle phase F_p=0.~~8381~~±0.0809) with an average concentration of 0.073±0.076
348 μg/m³,and, the-Its diurnal profile started increasing during dusk, reaching a peak at
349 about midnight and then fell off, as shown in Fig. 3. The mass fraction of C₆H₁₀O₅ in
350 OA had a similar diurnal profile, and the ratios of C₆H₁₀O₅ to CO increased at night
351 (from 0.17±0.021.5×10⁻⁴ to 0.5±0.034.1×10⁻⁴ μg·m⁻³/ppbm, Fig. 3c), both suggesting
352 enhanced emissions of this compound were related with combustion activities at
353 nightduring the evening, e.g., residential biofuel burning for cooking as reported by
354 some previous measurements in China (Wang et al., 2020c; Zhang et al., 2015).
355 Furthermore, the time variations of particle-phase C₆H₁₀O₅I⁻ wereas very similar to
356 that ofclosely resembled the m/z 60 fragment in AMS mass spectra (r=0.75)(Fig. 3a),
357 which is an identified tracer of biomass burning OA produced from the decomposition
358 of levoglucosan and similar compounds during detection by AMS (Brege et al., 2018;
359 Cubison et al., 2011; Schneider et al., 2006). Therefore, C₆H₁₀O₅ was probably
360 levoglucosan and its isomers (mannosan and galactosan), and C₆H₁₂O₅ was a similar
361 monosaccharide compound emitted from biomass burning.

362 3.3 Oxygenated aromatic compounds

363 Combustion activities emit a great deal of compounds besides saccharides that
364 the I-CIMS instrument can detect including nitro-aromatics and guaiacol derivatives
365 (Gaston et al., 2016; Kong et al., 2021). Nitro-benzenediols (C₆H₅NO₄I⁻) as well as
366 the highly correlated homologue methyl nitro-benzenediols (C₇H₇NO₄I⁻) (r=0.88 in
367 the particle phase), exhibited double peaks in their diurnal profiles (Fig. 4).
368 Concentrations of C₆H₅NO₄ and C₇H₇NO₄ was-were enhanced in the evening, similar
369 to levoglucosan (C₆H₁₀O₅). Another concentration peaks at noon were-was also

370 observed for $C_6H_5NO_4$ and $C_7H_7NO_4$. The scatterplot of $C_6H_5NO_4$ as the function of
371 $C_6H_{10}O_5$ ~~exhibite~~exhibits two different slopes (Fig. 5): the lower slope at night
372 (0.088 ± 0.005) indicates the contribution of biomass burning, while the higher slope
373 during the daytime (0.26 ± 0.02) suggests there were other important sources for nitro-
374 aromatics, potentially secondary formation from which could be photochemical
375 oxidation of aromatics (Jenkin et al., 2003). ~~at night and during the daytime (Fig. 5).~~
376 ~~This evidence suggests that primary emissions and secondary formation were both~~
377 ~~important contributors to nitro-aromatics during the campaign.~~ Guaiacol derivatives
378 may have similar sources with nitro-aromatics, as implied by the resemblance of the
379 scatterplots of these two chemical classes versus levoglucosan (cf., Fig. ~~S9~~S10 and Fig.
380 5).

381 Nitrophenols ($C_6H_5NO_3I^-$), methyl nitrophenols ($C_7H_7NO_3I^-$) and
382 dinitrophenols ($C_6H_4N_2O_5I^-$) were the most significant components of nitro-aromatics
383 in the gas phase. Despite the fact that nitrated phenols could be formed by
384 photochemical oxidation from their aromatic hydrocarbon precursors (Wang et al.,
385 2020a; Yuan et al., 2016), none of them peaked in the daytime, consistent with
386 photolysis as a dominant chemical loss for these compounds (Chen et al., 2011; Yuan
387 et al., 2016). Nitrophenols and methyl nitrophenols peaked in the evening, suggesting
388 either NO_3 oxidation or primary emissions was important sources. It is interesting to
389 observe that the peak concentration for $C_6H_4N_2O_5$ was later than the nitrophenols, in
390 agreement with dinitrophenols as the oxidation products from nitrophenols (Harrison
391 et al., 2005).

392 Several ions identified as oxidation products of aromatics, including $C_7H_6O_4I^-$,
393 $C_7H_8O_4I^-$ and $C_7H_8O_5I^-$ (Mehra et al., 2020; Schwantes et al., 2017), were detected
394 during the campaign. $C_7H_6O_4$ and $C_7H_8O_4$ correlated well with each other ($r=0.72$).
395 High concentrations of $C_7H_6O_4$ and $C_7H_8O_4$ were mainly observed during the periods
396 with lower NO_x concentration, which ~~is~~was a contrast to the variations of nitrophenols
397 (Fig. ~~S9~~S10). We observed d the concentration ratios of $C_7H_8O_4I^-$ and $C_7H_7NO_3I^-$
398 were lower for higher NO_x concentrations (Fig. 5), consistent with the literature that
399 formation of $C_7H_6O_4$ and $C_7H_8O_4$ is suppressed at high NO_x concentrations (Schwantes

400 et al., 2017). $C_7H_8O_5$ was reported as the ring-retaining oxidation product of $C_7H_8O_4$
401 which is a typical oxidation product of toluene and cresol (Schwantes et al., 2017; Wang
402 et al., 2020b), as well as the ring-scission products of aromatic hydrocarbons with more
403 carbon atoms, e.g. trimethyl benzenes (Mehra et al., 2020). Given that $C_7H_8O_5$ closely
404 followed with $C_7H_8O_4$ ($r=0.93$ in particles), toluene oxidation was probably the main
405 contributor to this ion.

406 **3.4 Organic acids and related compounds**

407 Organic acids were one of the most abundant species classes detected by I-CIMS
408 (Fig. 1). Low-molecular-weight organic acids (e.g., formic, acetic, glycolic and pyruvic
409 acid) constituted a significant fraction of signals in the mass spectra detected from gas
410 phase. As shown in Fig. 6 (and also Fig. [S10S11](#)), they had very similar temporal trends
411 with ~~diel~~-diurnal maxima in the afternoon, indicating photochemical oxidation played
412 a dominant role in their formation (de Gouw et al., 2018; Yuan et al., 2015).

413 In contrast to monocarboxylic acids, dicarboxylic acids partitioned mostly to
414 particle-phase. As the dominant dicarboxylic acids in aerosol (Kawamura and Bikkina,
415 2016; Mellouki et al., 2015), $94\pm 5\%$ and $74\pm 13\%$ (mean \pm one standard deviation of
416 F_p) of $C_2H_2O_4$ and $C_3H_4O_4$, assigned as oxalic and malonic acid, were found in particle-
417 phase, respectively. The concentrations of $C_4H_6O_4$ ~~are~~-were significantly lower
418 compared to that of C2 and C3 homologous series, but $C_5H_8O_4$ and $C_6H_{10}O_4$ had
419 unexpected higher abundances (Fig. 7). $C_5H_8O_4$ and $C_6H_{10}O_4$ had considerable
420 fractions in the gas phase ($45\pm 13\%$ and $43\pm 11\%$), significantly higher than their C2-
421 -C3 homologous series. These two compounds were correlated well with each other in
422 temporal variations ($r=0.97$ and 0.91 in the gas and particle phases, respectively), and
423 their diurnal variations were different from those of oxalic and malonic acid (Fig. 6).
424 Therefore, dicarboxylic acids may not be the dominant contributing species for the two
425 ions. $C_5H_8O_4$ and $C_6H_{10}O_4$ have been observed from previous study on isoprene
426 oxidation (Berndt et al., 2018, 2019), attributing them as epoxy hydroperoxyl carbonyl
427 and accretion product, respectively. However, the relative contributions from these
428 possibilities remain unclear.

429 In addition to the series of $C_nH_{2n-2}O_4$ (i.e. $C_2H_2O_4$, $C_3H_4O_4$), we also observed
430 comparable concentrations of $C_nH_{2n-4}O_4$ ions, especially for carbon number of 4 and
431 5 ($C_4H_4O_4$ and $C_5H_6O_4$). Considering the double bonds in the molecules, $C_nH_{2n-4}O_4$
432 should be more reactive than $C_nH_{2n-2}O_4$, suggesting there were large sources for these
433 compounds. Previous studies have reported photo-oxidation of aromatics can generate
434 $C_nH_{2n-4}O_4$, including $C_4H_4O_4$ and $C_5H_6O_4$ (Brege et al., 2018; Kawamura et al., 1996;
435 Kawamura and Bikkina, 2016). Our measurements ~~during the campaign~~
436 ~~indicateshowed~~ that temporal trends of $C_4H_4O_4$ and $C_5H_6O_4$ followed well with those
437 of aromatic hydrocarbons (Fig. ~~S10bS11b~~). ~~As a result, and thus we attributed oxidation~~
438 ~~of aromatics could be an important contributor to~~ $C_nH_{2n-4}O_4$ ~~ions as oxidation~~
439 ~~products of aromatics~~ in the urban air.

440 3.5 Oxidation products of Biogenic VOCs (BVOCs)

441 In addition to high anthropogenic emissions of aromatics, terrestrial vegetations
442 nearby also released significant amounts of BVOCs (Wu et al., 2020). During the
443 campaign, the concentrations of isoprene at noon were between 0.1 and 1.5 ppb,
444 whereas the range of daily maxima of monoterpenes was 0.05 ~~---~~ 2.5 ppb. Hence, a
445 number of oxidation products of BVOCs were detected (Fig. 8 and Fig. ~~S4S12~~).

446 The ion $C_4H_7NO_5I^-$ was the most abundant N-containing C4 organic ~~ion with~~
447 ~~four or five carbon atoms~~ compounds that were detected in the gas phase. Its daily
448 maxima occurred in the afternoon and correlated moderately with methyl vinyl ketone
449 (MVK) + methacrolein (MACR) measured by PTR-ToF-MS (Fig. 8). We consequently
450 assigned $C_4H_7NO_5$ as MVK ~~methylvinylketone~~ nitrates and MACR ~~methacrolein~~
451 nitrates, which was reported as the second generation of organic nitrates formed from
452 the oxidation of isoprene hydroxynitrates by OH in the presence of NO_x (Fisher et al.,
453 2016; Paulot et al., 2009). Strong correlations were observed between $C_5H_9NO_4I^-$,
454 $C_5H_9NO_5I^-$ and $C_4H_7NO_5I^-$ ($r=0.93$ and 0.80 , respectively), which was in
455 accordance with their similar formation pathways (Jacobs et al., 2014; Wennberg et al.,
456 2018; Xiong et al., 2015). Hence, we expect these three compounds are common
457 oxidation products of isoprene in the polluted atmosphere. While in aerosol, 2-

458 methylglyceric acid ($C_4H_8O_4$) is a commonly reported oxidation product of isoprene
459 formed in high- NO_x conditions (Surratt et al., 2010). We observed the corresponding
460 ion $C_4H_8O_4I^-$ contributing to OA especially in dry conditions with strong sunlight
461 (Fig. [S12S13](#)). This evidence indicates that isoprene oxidation may contributed to
462 $C_4H_8O_4$, but potential contribution from other sources cannot be ruled out in urban areas.

463 ~~In terms~~~~For the oxidaiton~~ of monoterpenes, ~~we observe a~~ reasonable correlation
464 (Fig. [S13aS14a](#), $r=0.63$) ~~was found~~ between the ions $C_{10}H_{16}O_3I^-$ and $C_{10}H_{16}O_2H^+$
465 measured by PTR-ToF-MS. $C_{10}H_{16}O_2H^+$ was attributed to pinonaldehyde formed from
466 the oxidation of monoterpenes (Glasius et al., 2000; Larsen et al., 2001; Mutzel et al.,
467 2016). Therefore, we tentatively assigned $C_{10}H_{16}O_3$ as pinonic acid and its
468 oxocarboxylic acid isomers, which are formed via the oxidation of pinonaldehyde
469 (Fang et al., 2017). $C_8H_{13}NO_6$ also exhibited enhanced gas-phase formation during the
470 day as pinonic acid did. The correlation coefficient of the two compounds (r) was 0.71.
471 In contrast ~~to other monoterpene nitrates~~, ~~particle-phase~~ $C_8H_{11}NO_7$ and $C_{10}H_{15}NO_6$
472 ~~peaked at night and decreased during the daytime~~~~significantly partitioned to the aerosol~~
473 ~~phase ($F_p=0.68\pm 0.19$ and 0.44 ± 0.18 , respectively) with maximums at night~~ (Fig.
474 [S11S12](#)), indicative of the role of NO_3 in producing organic nitrates as reported in the
475 literature (Faxon et al., 2018). ~~However, The time trends of $C_{10}H_{15}NO_6I^-$ in the gas~~
476 ~~phase showed a distinct diurnal profile with peak in both phases did not resemble well~~
477 ~~(Fig. [S13b](#)) before the noon~~. Two possible types of compounds were proposed for
478 $C_{10}H_{15}NO_6$ in previous ~~work~~~~studies~~: peroxyacetyl nitrate from pinonaldehyde (Faxon
479 et al., 2018; Nah et al., 2016; Schwantes et al., 2020), or organic nitrates (Bean and
480 Hildebrandt Ruiz, 2016; Boyd et al., 2015). ~~Given the distinct diurnal profiles of~~
481 ~~$C_{10}H_{15}NO_6I^-$ in the gas and particle phases and the fact that peroxyacetyl nitrate is~~
482 ~~supposed to dissociate during the FIGAERO heating~~ (Slusher et al., 2004). ~~We~~ ~~we~~
483 speculate that both compounds contributed to ~~the~~ ~~this~~ ion ~~$C_{10}H_{15}NO_6I^-$~~ . As shown in
484 Fig. [S14S15](#), $C_8H_{12}O_4$ and $C_9H_{14}O_4$ existed mostly in particle-phase ($F_p=0.63\pm 0.11$ and
485 0.67 ± 0.10 , respectively). We interpreted them as products of monoterpenes via

486 photochemical processes, consistent with the interpretations presented in previous work
487 (Mohr et al., 2013; Mutzel et al., 2015).

488 **3.6 S-containing compounds**

489 Organosulfates are concerned as important components of SOA (Hallquist et al.,
490 2009; Surratt et al., 2007), and they can be detected by iodide anion via proton
491 abstraction (Le Breton et al., 2018b; Lee et al., 2014). We detected the ion $C_2H_3SO_6^-$
492 with peak concentration in the afternoon (Fig. 9). We attributed $C_2H_3SO_6^-$ to glycolic
493 acid sulfate, as suggested by previous work (Galloway et al., 2009; Liao et al., 2015).

494 Abundant SO_3I^- was detected in particles, and it correlated well with the ion
495 $C_2H_3SO_6^-$ (Fig. 9b) and sulfates measured by AMS (Fig. 9b and (Fig. S15S16)).
496 ~~Previous work observed the sulfite ion radical ($\cdot SO_3^-$) during the ionization of~~
497 ~~organosulfates. Previous work indicate that neutral loss of SO_3 during ionization of many~~
498 ~~organosulfates by cleavage of the S-O bond~~ (Huang et al., 2018). As ~~the a~~ result, the
499 SO_3I^- ion from FIGAERO-I-CIMS might be a potential indicator for the total
500 organosulfates. However, more future work is needed for evaluating this possibility.

501 Other sulfate-related ions during gas-phase modes were also detected including
502 HSO_4^- (sulfuric acid), $CH_3SO_3^-$ (methanesulfonic acid) which were enhanced in the
503 gas phase during ~~the~~ daytime, in agreement with the notions of photochemically
504 induced gas-phase oxidation (Brandt and van Eldik, 1995). However, these data were
505 not available for quantification given that these low-volatile species would condense on
506 our long gas sampling inlet. ~~Although~~ ~~But~~ ~~it~~ should ~~still~~ be noted that measuring
507 sulfuric acid in the gas-phase is difficult and generally requires a “wall-less” source
508 design (Eisele and Tanner, 1993).

509 **3.7 Inorganic compounds**

510 There is a growing interest in N_2O_5 and its product nitryl chloride ($ClNO_2$)
511 because $ClNO_2$ is found to serve as a nocturnal reservoir of Cl radical and reactive
512 nitrogen, and hence enhance the ozone formation next day (Osthoff et al., 2008; Wang
513 et al., 2016). Time series of N_2O_5 and $ClNO_2$ exhibited two patterns. During most of
514 the nights, N_2O_5 started to increase quickly at sunset and lasted for only 2–3 hours,

515 and ClNO₂ increased in the meantime and ultimately reached its maximum at night,
516 indicative of local formation of ClNO₂. However, sometimes a high level of N₂O₅ did
517 not lead to an increase in ClNO₂ (tinted background in Fig. 10a), probably due to the
518 lack of chloride salts on the aerosol (Fig. S16). Other nocturnal species including
519 ClONO₂ and Cl₂ were highly correlated with ClNO₂ as we expected (r=0.92 and 0.83,
520 respectively), suggesting they had common formation mechanisms (Liu et al., 2017).

521 *HNO₃I⁻* was observed as one of the most abundant species in the mass spectra
522 of FIGAERO-I-CIMS in both gas and particle phase. In the gas phase, the ion *HNO₃I⁻*
523 from I-CIMS has been used to quantify nitric acid (Lee et al., 2018a). The
524 concentrations of gas-phase nitric acid peaked in the afternoon, suggesting
525 photochemistry in the daytime as the dominant source for gas-phase nitric acid.

526 Previous study suggested that *HNO₃I⁻* from particle-phase measurement by
527 FIGAERO-I-CIMS can be indicative of nitrate in the particle phase (Lee et al., 2016).
528 Here, the concentrations of *HNO₃I⁻* in the particle phase were compared with
529 particulate nitrate measured by AMS (Fig. 11c). Strong correlation was observed
530 (r=0.93), but the concentrations measured by FIGAERO-I-CIMS were higher
531 (slope=1.6), especially for higher concentrations of organic nitrates~~Strong correlation~~
532 ~~was obtained between the two measurements (r=0.93). By separating the dataset around~~
533 Using a threshold of 1 µg/m³ for organic nitrates, the slopes and correlations were
534 higher for ~~However, the concentrations measured by FIGAERO-I-CIMS were higher~~
535 (fitted slope=1.6) than the data points with of particulate organic nitrates larger than 1
536 µg/m³ (slope=1.8, r=0.94) than those with less than 1 µg/m³ vs of organic nitrates
537 (slope=1.1, r=0.90) by AMS, ~~and the discrepancy was larger when organic nitrates~~
538 ~~concentrations measured by FIGAERO-I-CIMS were higher (Fig. 11e). It~~ In short, our
539 measurements suggests that *HNO₃I⁻* in the particle phase from FIGAERO-I-CIMS
540 are formed from thermal-decomposition of both inorganic nitrates (e.g.
541 NH₄NO₃ ammonium nitrate) and organic nitrates.

542 **3.8 Bulk chemical properties of detected organic compounds**

543 The above discussions on individual chemical groups provide insights into the
544 identification of the mass spectra from FIGAERO-I-CIMS, along with sources and
545 chemistry of oxygenated organic compounds in the urban atmosphere. In this section
546 and the following one, we will provide a ~~concise description~~ bulk analysis of the overall
547 ~~picture for these detected organic compounds.~~

548 The composition of organic compounds detected by FIGAERO-I-CIMS was
549 comprehensively characterized with ~~molecular-level details~~ detailed elementary
550 composition by in $\overline{OS}_C - n_C$ space (Fig. 12) which ~~depicting~~ depicts the average
551 oxidation states of carbon for closed-shell $C_xH_yO_z$ and $C_xH_yN_{1,2}O_z$ compounds
552 clustered with iodide as a function of carbon number (~~Fig. 12~~). The details in calculation
553 of \overline{OS}_C can be found in Section S2 in SI. S-containing compounds were omitted given
554 their negligible variety and concentration compared to the former two chemical classes
555 ($C_xH_yO_z$ and $C_xH_yN_{1,2}O_z$). The average \overline{OS}_C in the particle phase was higher than
556 that in the gas phase at the same carbon number, especially for carbon number between
557 2 and 10. This agrees with our expectation that more oxidized compounds would
558 partition more strongly in aerosol, as indicated by larger fractions in particles (Fp) for
559 higher \overline{OS}_C . In addition, the average \overline{OS}_C generally increased for lower carbon
560 number, as a result of functionalization and fragmentation during VOCs aging.
561 However, there was a notable exception in C5 which had a significantly reduced \overline{OS}_C ,
562 probably as the result of ~~augmented primary~~ emissions of isoprene. The analysis of the
563 $\overline{OS}_C - n_C$ space indicates that the large number of organic compounds measured by
564 FIGAERO-I-CIMS are useful to characterize the evolution of organic compounds in
565 the atmosphere.

566 The distributions of carbon number and oxygen number in the organic
567 compounds measured by FIGAERO-I-CIMS were also investigated, as shown in Fig.
568 13. Most abundant organic compounds measured by FIGAERO-I-CIMS were C2–C3
569 compounds, which accounted for about ~~63.66~~ 63.66% of organic compounds in gas-phase and
570 ~~55.56~~ 55.56% in particle-phase. It is unexpected that C2-C3 compounds made up such a
571 significant portion of the particle phase, indicating a non-negligible role of thermal

572 decomposition from very low volatility material compounds such as accretion products
573 or extremely low volatile organic compounds which has been were reported from
574 FIGAERO measurements on SOA (D'Ambro et al., 2018; Lopez-Hilfiker et al., 2014;
575 Stark et al., 2017). Organic compounds with carbon numbers over 5 constituted only
576 39% in the gas phase, while they accounted for 30% in the particle phase. The majority
577 of gaseous organic compounds ~~was were~~ associated with ~~less no more~~ than 4-3 oxygen
578 atoms. Organic compounds containing ~~2 and 3~~ oxygen atoms had the largest
579 contribution in both gas-phase (~~62~~96%) and particle-phase (~~44~~56%). $C_xH_yN_{1,2}O_z$
580 accounted for less than 10% of the total oxygenated organic compounds. In the gas
581 phase, compounds with ~~5 or 6~~ oxygen atoms accounted for 51% of $C_xH_yN_{1,2}O_z$,
582 indicative of the high levels of organic nitrates in the urban atmosphere. Nitrophenols
583 also contributed significantly to $C_xH_yN_{1,2}O_z$ compounds, as they accounted for 74%
584 of $C_xH_yN_{1,2}O_z$ containing 3 oxygen atoms, which in turn accounted for contributed to
585 the fraction of compounds possessing 3 oxygen atoms was 22% of $C_xH_yN_{1,2}O_z$. In
586 contrast, in the particle phase, the oxygen number of $C_xH_yN_{1,2}O_z$ distributed relatively
587 evenly, as the fractions of compounds with ~~3-8~~ oxygen atoms were similar (between
588 ~~14~~12% and 19%). Compared to measurements in a forest in the southeastern United
589 States (cf., Table S1 from Lee et al., 2016), the fractions of N-containing organic
590 compounds with less than 5 oxygen atoms were significantly larger in our
591 measurements as a result of higher concentrations of nitro-aromatics.

592 We further determine the fractions of N-containing organic compounds in total
593 organic compounds as a function of m/z. It is clear that ~~T~~the observed fractions of N-
594 containing organic compounds were are higher for elevated m/z (Fig. 14) and N-
595 containing ions commonly dominate at even nominal masses (Fig. 14 and Fig. S17).
596 The gas-phase CHON ions within the m/z range from 250 to 350 Th accounted for
597 about half of the organic compounds in this range. The fractions of CHON ions in
598 particle-phase are somewhat smaller than those in the gas phase for m/z of 250-350 Th,
599 but are comparable for higher m/z. A possible explanation for this is that functional
600 groups of nitrate and nitro reduce less in vapor pressure for organic compounds than
601 functional groups of carboxylic acid or oxygen-equivalent hydroxyl that without

602 nitrogen atom (Capouet and Müller, 2006; Nannoolal et al., 2008; Pankow and Asher,
603 2008). Consequently, CHON compounds are generally more volatile than CHO
604 compounds with similar molecular weights.

605 In the end, we determined the total concentration of N-containing organic
606 compounds in the particle-phase measured by FIGAERO-I-CIMS and compared it with
607 the particulate organic nitrates derived from AMS (Fig. 15). Good agreement was
608 achieved when the concentrations of inorganic nitrate were relatively lower, ~~(e.g.~~
609 ~~below 8 $\mu\text{g}/\text{m}^3$ inorganic nitrate, $r=0.57$ as shown in Fig. 15b) the period before October~~
610 ~~7, 2018. Moreover/However, ~~the discrepancies of concentrations from these two~~~~
611 ~~methods increased when at higher inorganic nitrate conditions were higher, which can~~
612 ~~affect the determination of organic nitrate from AMS.~~ This encouraging result indicates
613 that FIGAERO-I-CIMS is able to capture the variability of organic nitrates in the urban
614 atmosphere, which can be helpful in understanding the sources and formation
615 mechanism of these organic nitrates.

616 **3.9 Organic aerosol measurements**

617 The total concentrations of organic compounds in the particle phase measured by
618 FIGAERO-I-CIMS were determined and compared with measurements of OA by AMS.
619 The total organic ~~compounds~~ measured by FIGAERO-I-CIMS explained $24 \pm 0.8\%$
620 ~~(fitted slope \pm one standard deviation)~~ of the total OA in average (Fig. 16a), which is
621 lower than the average fractions ($\sim 50\%$) reported previously in boreal and temperate
622 forests (Lopez-Hilfiker et al., 2016; Stark et al., 2017). The lower fractions determined
623 here might be as the result of larger contributions to OA from primary emissions in
624 urban air, which are composed of large number of compounds with little signal in I-
625 CIMS (Zhao et al., 2016). ~~As shown in The-Fig. 16a, organic compounds measured by~~
626 ~~FIGAERO-I-CIMS account for higher fractions in OA concentrations by AMS for more~~
627 ~~aged OA, OA fractions measured by FIGAERO I-CIMS are higher for aged air with~~
628 ~~higher O/C ratios in OA determined by AMS (Fig. 16a) which is,~~ consistent with the
629 fact that I-CIMS are more sensitive to oxygenated organic compounds with multiple
630 functional groups (Lee et al., 2014; Lopez-Hilfiker et al., 2016). Furthermore, we expect

631 this fraction to change with the relative contributions of primary emissions and
632 secondary formation for organic compounds in the atmosphere. Similar trends were
633 found in Le Breton et al. (2019), in which an acetate source was used. Acetate ions have
634 been reported to selectively ionize highly oxygenated organic compoundss as an iodide
635 source does (Aljawhary et al., 2013).

636 Comparison of the Van Krevelen diagram between FIGAERO-I-CIMS and AMS
637 also provides useful insights on the measurement of organic compounds in OA. The
638 Van Krevelen diagram has been used as a tool for analyzing functional groups and OA
639 aging by plotting H/C ratios versus O/C ratios (Heald et al., 2010; Lambe et al., 2012).
640 As shown in Fig. 16a, the data points for bulk OA from FIGAERO-I-CIMS follow the
641 same trend as the data points from AMS. However, the bulk OA measured by
642 FIGAERO-I-CIMS only occupied a much smaller region with the O/C ratio between ~~of~~
643 0.7 and 1.0. We further plot all of the organic compounds in the H/C versus O/C space
644 color-coded with their campaign-average concentrations (Fig. S18a). We observe most
645 particle-phase concentrations measured by FIGAERO-I-CIMS distributed across the
646 zone between the slope of 0 and -1.0. These observations provide additional evidence
647 that FIGAERO-I-CIMS may only measure the more oxidized organic compounds in
648 OA.

649 The correlation coefficients between the particle-phase concentrations at unit
650 masses of various compounds by FIGAERO-I-CIMS and OA mass concentration by
651 AMS are calculated (Fig. S18b). The correlation coefficients are small for ions below
652 m/z 200, as these ions contribute little to organic aerosol. Moderate and strong
653 correlations ($r > 0.7$) were observed for the ions between m/z 200 and m/z 400, implying
654 that organic compounds with molecular weight of 100-300 g/mol may account for
655 significant fractions in organic aerosol. The possible reason for the lower correlations
656 of heavier compounds (m/z >400) with OA mass loadings is that these compounds
657 might be related to specific sources or certain chemical processes, which might not
658 contribute at large fractions to the total OA concentration. ~~The correlation coefficients~~
659 ~~start to decrease for ions above m/z 400, likely due to decomposition during heating or~~
660 ~~partially evaporation from FIGAERO filter for these high-molecular weight compounds.~~

661 **4 ConclusionsSummary**

662 We deployed a FIGAERO-I-CIMS instrument to measure oxygenated organic
663 compounds in both gas phase and particle phase at a representative urban site in China.
664 The mass spectra ~~from the measurements by~~ FIGAERO-I-CIMS ~~from the measurements~~ was
665 systematically interpreted. We detected high concentrations of several monosaccharide
666 species (e.g., levoglucosan) potentially emitted from biomass burning, which also
667 contributed to the enhancement of multiple nitro-aromatic species. Photochemistry was
668 also identified as a strong source of nitro-aromatics. Low-molecular-weight organic
669 acids were mainly observed in the gas phase, and observations support daytime
670 photochemistry as the dominant source. Different diurnal profiles for various BVOC-
671 derived organic nitrates were observed, reflecting their different formation pathways
672 related to NO_x chemistry (i.e. daytime photo-oxidation, nocturnal NO₃ reactions).
673 ~~Various oxidation products of BVOCs were detected in both gas and particle phase,~~
674 ~~reflecting the role of NO_x in the oxidation of BVOC species.~~ Local formation of nitril
675 chloride was observed, highlighting the potential importance of nighttime chemistry in
676 the urban region.

677 Our measurements show that oxygenated organic compounds dominated the
678 majority of detected species by FIGAERO-I-CIMS, in which CHO and CHON
679 compounds both accounted for significant fractions. Nitrogen-containing organic
680 compounds occupied a significant fraction of the total signals in both the gas and
681 particle phases, with elevated fractions at higher molecular weights. The most abundant
682 organic compounds were formic acid and multifunctional organics compounds
683 containing 3--5 oxygen atoms. Organic compounds containing 2 or 3 carbon atoms
684 accounted for over half of the total organic compoundss in both gas- and particle phase
685 measured by FIGAERO-I-CIMS. During the campaign, the FIGAERO-I-CIMS
686 measurements explained $24 \pm 0.8\%$ of OA measured by AMS, but the fractions are
687 higher for measurements of more aged organic aerosol in the urban atmosphere. This
688 evidence, along with the analysis of the Van Krevelen plot, indicate that FIGAERO-I-
689 CIMS were measuring the more oxidized fraction of OA in the urban air.

690

691 **Acknowledgement**

692 This work was supported by the National Key R&D Plan of China (grant No.
693 2019YFE0106300, 2018YFC0213904, 2016YFC0202206), the National Natural
694 Science Foundation of China (grant No. 41877302), Guangdong Natural Science
695 Funds for Distinguished Young Scholar (grant No. 2018B030306037), Guangdong
696 Provincial Key R&D Plan (grant No. 2019B110206001), Guangdong Soft Science
697 Research Program (grant No. 2019B101001005) and Guangdong Innovative and
698 Entrepreneurial Research Team Program (grant No. 2016ZT06N263). This work was
699 also supported by Special Fund Project for Science and Technology Innovation Strategy
700 of Guangdong Province (Grant No.2019B121205004). Weiwei Hu and Wei Chen were
701 supported by National Natural Science Foundation of China (41875156).

702 **Data availability**

703 The more detailed data can be provided by contacting the corresponding authors.

704 **Author contributions**

705 BY and MS designed the research. CSY, YL, ZLW, TGL, WWH, WC, CHW,
706 CMW, SH, JPQ, BLW, CW, WS, XMW, ZYZ, XMW contributed to data collection.
707 CSY performed the data analysis with contributions from WWH and WC. CSY and
708 BY prepared the manuscript with contributions from JEK and other authors. All the
709 authors reviewed the manuscript.

710 **Competing interest**

711 The authors declare that they have no conflicts of interest.

712

713

714 **References**

715 Aiken, A. C., DeCarlo, P. F. and Jimenez, J. L.: Elemental Analysis of Organic
716 Species with Electron Ionization High-Resolution Mass Spectrometry, *Anal. Chem.*,
717 79(21), 8350–8358, doi:10.1021/ac071150w, 2007.

718 Aljawhary, D., Lee, A. K. Y. and Abbatt, J. P. D.: High-resolution chemical
719 ionization mass spectrometry (ToF-CIMS): Application to study SOA composition
720 and processing, *Atmos. Meas. Tech.*, 6(11), 3211–3224, doi:10.5194/amt-6-3211-
721 2013, 2013.

722 Bean, J. K. and Hildebrandt Ruiz, L.: Gas-particle partitioning and hydrolysis of
723 organic nitrates formed from the oxidation of alpha-pinene in environmental chamber
724 experiments, *Atmos. Chem. Phys.*, 16(4), 2175–2184, doi:10.5194/acp-16-2175-2016,
725 2016.

726 Berndt, T., Scholz, W., Mentler, B., Fischer, L., Herrmann, H., Kulmala, M. and
727 Hansel, A.: Accretion Product Formation from Self- and Cross-Reactions of RO₂
728 Radicals in the Atmosphere, *Angew. Chemie Int. Ed.*, 57(14), 3820–3824,
729 doi:10.1002/anie.201710989, 2018.

730 Berndt, T., Hyttinen, N., Herrmann, H. and Hansel, A.: First oxidation products from
731 the reaction of hydroxyl radicals with isoprene for pristine environmental conditions,
732 *Commun. Chem.*, 2(1), 1–10, doi:10.1038/s42004-019-0120-9, 2019.

733 Bertram, T. H., Thornton, J. A. and Riedel, T. P.: An experimental technique for the
734 direct measurement of N₂O₅ reactivity on ambient particles, *Atmos. Meas. Tech.*,
735 2(1), 231–242, doi:10.5194/amt-2-231-2009, 2009.

736 Bertram, T. H., Kimmel, J. R., Crisp, T. A., Ryder, O. S., Yatavelli, R. L. N.,
737 Thornton, J. A., Cubison, M. J., Gonin, M. and Worsnop, D. R.: A field-deployable,
738 chemical ionization time-of-flight mass spectrometer, *Atmos. Meas. Tech.*, 4(7),
739 1471–1479, doi:10.5194/amt-4-1471-2011, 2011.

740 Bhattarai, H., Saikawa, E., Wan, X., Zhu, H., Ram, K., Gao, S., Kang, S., Zhang, Q.,
741 Zhang, Y., Wu, G., Wang, X., Kawamura, K., Fu, P. and Cong, Z.: Levoglucosan as a
742 tracer of biomass burning: Recent progress and perspectives, *Atmos. Res.*,
743 220(November 2018), 20–33, doi:10.1016/j.atmosres.2019.01.004, 2019.

744 Boyd, C. M., Sanchez, J., Xu, L., Eugene, A. J., Nah, T., Tuet, W. Y., Guzman, M. I.

745 and Ng, N. L.: Secondary organic aerosol formation from the β -pinene+NO₃ system:
746 effect of humidity and peroxy radical fate, *Atmos. Chem. Phys.*, 15(13), 7497–7522,
747 doi:10.5194/acp-15-7497-2015, 2015.

748 Brandt, C. and van Eldik, R.: Transition Metal-Catalyzed Oxidation of Sulfur(IV)
749 Oxides. Atmospheric-Relevant Processes and Mechanisms, *Chem. Rev.*, 95(1), 119–
750 190, doi:10.1021/cr00033a006, 1995.

751 Brege, M., Paglione, M., Gilardoni, S., Decesari, S., Cristina Facchini, M. and
752 Mazzoleni, L. R.: Molecular insights on aging and aqueous-phase processing from
753 ambient biomass burning emissions-influenced Po Valley fog and aerosol, *Atmos.*
754 *Chem. Phys.*, 18(17), 13197–13214, doi:10.5194/acp-18-13197-2018, 2018.

755 Le Breton, M., Hallquist, A. M., Pathak, R. K., Simpson, D., Wang, Y., Johansson, J.,
756 Zheng, J., Yang, Y., Shang, D., Wang, H., Liu, Q., Chan, C., Wang, T., Bannan, T. J.,
757 Priestley, M., Percival, C. J., Shallcross, D. E., Lu, K., Guo, S., Hu, M. and Hallquist,
758 M.: Chlorine oxidation of VOCs at a semi-rural site in Beijing: significant chlorine
759 liberation from ClNO₂ and subsequent gas- and particle-phase Cl-VOC production,
760 *Atmos. Chem. Phys.*, 18(17), 13013–13030, doi:10.5194/acp-18-13013-2018, 2018a.

761 Le Breton, M., Wang, Y., Hallquist, Å. M., Pathak, R. K., Zheng, J., Yang, Y., Shang,
762 D., Glasius, M., Bannan, T. J., Liu, Q., Chan, C. K., Percival, C. J., Zhu, W., Lou, S.,
763 Topping, D., Wang, Y., Yu, J., Lu, K., Guo, S., Hu, M. and Hallquist, M.: Online gas-
764 and particle-phase measurements of organosulfates, organosulfonates and nitrooxy
765 organosulfates in Beijing utilizing a FIGAERO ToF-CIMS, *Atmos. Chem. Phys.*,
766 18(14), 10355–10371, doi:10.5194/acp-18-10355-2018, 2018b.

767 Le Breton, M., Psichoudaki, M., Hallquist, M., Watne, Å. K., Lutz, A. and Hallquist,
768 Å. M.: Application of a FIGAERO ToF CIMS for on-line characterization of real-
769 world fresh and aged particle emissions from buses, *Aerosol Sci. Technol.*, 53(3),
770 244–259, doi:10.1080/02786826.2019.1566592, 2019.

771 Canagaratna, M. R., Jimenez, J. L., Kroll, J. H., Chen, Q., Kessler, S. H., Massoli, P.
772 and Ruiz, L. H.: Elemental ratio measurements of organic compounds using aerosol
773 mass spectrometry: characterization, improved calibration, and implications, *Atmos.*
774 *Chem. Phys.*, 15, 253–272, doi:10.5194/acp-15-253-2015, 2015.

775 Capouet, M. and Müller, J. F.: A group contribution method for estimating the vapour
776 pressures of α -pinene oxidation products, *Atmos. Chem. Phys.*, 6(6), 1455–1467,
777 doi:10.5194/acp-6-1455-2006, 2006.

778 Carlton, A. G., Turpin, B. J., Altieri, K. E., Seitzinger, S., Reff, A., Lim, H.-J. and
779 Ervens, B.: Atmospheric oxalic acid and SOA production from glyoxal: Results of
780 aqueous photooxidation experiments, *Atmos. Environ.*, 41(35), 7588–7602,
781 doi:10.1016/j.atmosenv.2007.05.035, 2007.

782 Carslaw, N.: A mechanistic study of limonene oxidation products and pathways
783 following cleaning activities, *Atmos. Environ.*, 80, 507–513,
784 doi:https://doi.org/10.1016/j.atmosenv.2013.08.034, 2013.

785 Chen, H. and Finlayson-Pitts, B. J.: New Particle Formation from Methanesulfonic
786 Acid and Amines/Ammonia as a Function of Temperature, *Environ. Sci. Technol.*,
787 51(1), 243–252, doi:10.1021/acs.est.6b04173, 2017.

788 Chen, J., Wenger, J. C. and Venables, D. S.: Near-Ultraviolet Absorption Cross
789 Sections of Nitrophenols and Their Potential Influence on Tropospheric Oxidation
790 Capacity, *J. Phys. Chem. A*, 115(44), 12235–12242, doi:10.1021/jp206929r, 2011.

791 Cubison, M. J., Ortega, A. M., Hayes, P. L., Farmer, D. K., Day, D., Lechner, M. J.,
792 Brune, W. H., Apel, E., Diskin, G. S., Fisher, J. A., Fuelberg, H. E., Hecobian, A.,
793 Knapp, D. J., Mikoviny, T., Riemer, D., Sachse, G. W., Sessions, W., Weber, R. J.,
794 Weinheimer, A. J., Wisthaler, A. and Jimenez, J. L.: Effects of aging on organic
795 aerosol from open biomass burning smoke in aircraft and laboratory studies, *Atmos.*
796 *Chem. Phys.*, 11(23), 12049–12064, doi:10.5194/acp-11-12049-2011, 2011.

797 D'Ambro, E. L., Lee, B. H., Liu, J., Shilling, J. E., Gaston, C. J., Lopez-Hilfiker, F.
798 D., Schobesberger, S., Zaveri, R. A., Mohr, C., Lutz, A., Zhang, Z., Gold, A., Surratt,
799 J. D., Rivera-Rios, J. C., Keutsch, F. N. and Thornton, J. A.: Molecular composition
800 and volatility of isoprene photochemical oxidation secondary organic aerosol under
801 low- and high-NO_x conditions, *Atmos. Chem. Phys.*, 17(1), 159–174,
802 doi:10.5194/acp-17-159-2017, 2017.

803 D'Ambro, E. L., Schobesberger, S., Zaveri, R. A., Shilling, J. E., Lee, B. H., Lopez-
804 Hilfiker, F. D., Mohr, C. and Thornton, J.: Isothermal evaporation of α -pinene

805 ozonolysis SOA: volatility, phase state, and oligomeric composition, ACS Earth Sp.
806 Chem., acsearthspacechem.8b00084, doi:10.1021/acsearthspacechem.8b00084, 2018.
807 Edwards, P. M., Brown, S. S., Roberts, J. M., Ahmadov, R., Banta, R. M., DeGouw,
808 J. A., Dubé, W. P., Field, R. A., Flynn, J. H., Gilman, J. B., Graus, M., Helmig, D.,
809 Koss, A., Langford, A. O., Lefer, B. L., Lerner, B. M., Li, R., Li, S. M., McKeen, S.
810 A., Murphy, S. M., Parrish, D. D., Senff, C. J., Soltis, J., Stutz, J., Sweeney, C.,
811 Thompson, C. R., Trainer, M. K., Tsai, C., Veres, P. R., Washenfelder, R. A.,
812 Warneke, C., Wild, R. J., Young, C. J., Yuan, B. and Zamora, R.: High winter ozone
813 pollution from carbonyl photolysis in an oil and gas basin, Nature, 514(7522), 351–
814 354, doi:10.1038/nature13767, 2014.

815 Eger, P. G., Schuladen, J., Sobanski, N., Fischer, H., Karu, E., Williams, J., Riva, M.,
816 Zha, Q., Ehn, M., Quéléver, L. L. J., Schallhart, S., Lelieveld, J. and Crowley, J. N.:
817 Pyruvic acid in the boreal forest: gas-phase mixing ratios and impact on radical
818 chemistry, Atmos. Chem. Phys., 20(6), 3697–3711, doi:10.5194/acp-20-3697-2020,
819 2020.

820 Eisele, F. L. and Tanner, D. J.: Measurement of the gas phase concentration of
821 H₂SO₄ and methane sulfonic acid and estimates of H₂SO₄ production and loss in the
822 atmosphere, J. Geophys. Res. Atmos., 98(D5), 9001–9010, doi:10.1029/93JD00031,
823 1993.

824 Fang, W., Gong, L. and Sheng, L.: Online analysis of secondary organic aerosols
825 from OH-initiated photooxidation and ozonolysis of α -pinene, β -pinene, Δ 3-carene
826 and d-limonene by thermal desorption-photoionisation aerosol mass spectrometry,
827 Environ. Chem., 14(2), 75–90, doi:10.1071/EN16128, 2017.

828 Faxon, C., Hammes, J., Pathak, R. K. and Hallquist, M.: Characterization of organic
829 nitrate constituents of secondary organic aerosol (SOA) from nitrate-radical-initiated
830 oxidation of limonene using High-Resolution Chemical Ionization Mass
831 Spectrometry, Atmos. Chem. Phys., 18, 5467–5481, doi:10.5194/acp-2017-584, 2018.

832 Fisher, J. A., Jacob, D. J., Travis, K. R., Kim, P. S., Marais, E. A., Chan Miller, C.,
833 Yu, K., Zhu, L., Yantosca, R. M. and Sulprizio, M. P.: Organic Nitrate Chemistry and
834 its Implications for Nitrogen Budgets in an Isoprene- and Monoterpene-Rich

835 Atmosphere: Constraints from Aircraft (SEAC4RS) and Ground-Based (SOAS)
836 Observations in the Southeast US, *Atmos. Chem. Phys.*, 16, 5969 [online] Available
837 from: <https://www.atmos-chem-phys.net/16/5969/2016/acp-16-5969-2016.pdf>, 2016.
838 Fountoukis, C. and Nenes, A.: ISORROPIA II: a computationally efficient
839 thermodynamic equilibrium model for K^+ – Ca^{2+} – Mg^{2+} – NH_4^+ – Na^+ – SO_4^{2-} – NO_3^- –
840 Cl^- – H_2O aerosols, *Atmos. Chem. Phys.*, 7(17), 4639–4659, doi:10.5194/acp-7-
841 4639-2007, 2007.

842 Fry, J. L., Draper, D. C., Zarzana, K. J., Campuzano-Jost, P., Day, D. A., Jimenez, J.
843 L., Brown, S. S., Cohen, R. C., Kaser, L., Hansel, A., Cappellin, L., Karl, T., Hodzic
844 Roux, A., Turnipseed, A., Cantrell, C., Lefer, B. L., Grossberg, N., Farmer, D. K. and
845 Jimenez, J. L.: Observations of gas- and aerosol-phase organic nitrates at BEACHON-
846 RoMBAS 2011, *Atmos. Chem. Phys.*, 13(17), 8585–8605, doi:10.5194/acp-13-8585-
847 2013, 2013.

848 Galloway, M. M., Chhabra, P. S., Chan, A. W. H., Surratt, J. D., Flagan, R. C.,
849 Seinfeld, J. H. and Keutsch, F. N.: Glyoxal uptake on ammonium sulphate seed
850 aerosol: reaction products and reversibility of uptake under dark and irradiated
851 conditions, *Atmos. Chem. Phys.*, 9(10), 3331–3345, doi:10.5194/acp-9-3331-2009,
852 2009.

853 Gaston, C. J., Lopez-Hilfiker, F. D., Whybrew, L. E., Hadley, O., McNair, F., Gao,
854 H., Jaffe, D. A. and Thornton, J. A.: Online molecular characterization of fine
855 particulate matter in Port Angeles, WA: Evidence for a major impact from residential
856 wood smoke, *Atmos. Environ.*, 138, 99–107, doi:10.1016/j.atmosenv.2016.05.013,
857 2016.

858 Glasius, M., Lahaniati, M., Calogirou, A., Di Bella, D., Jensen, N. R., Hjorth, J.,
859 Kotzias, D. and Larsen, B. R.: Carboxylic acids in secondary aerosols from oxidation
860 of cyclic monoterpenes by ozone, *Environ. Sci. Technol.*, 34(6), 1001–1010,
861 doi:10.1021/es990445r, 2000.

862 Gondwe, M., Krol, M., Gieskes, W., Klaassen, W. and de Baar, H.: The contribution
863 of ocean-leaving DMS to the global atmospheric burdens of DMS, MSA, SO_2 , and
864 $NSS\ SO_4^{2-}$, *Global Biogeochem. Cycles*, 17(2), doi:10.1029/2002GB001937, 2003.

865 de Gouw, J. A., Middlebrook, A. M., Warneke, C., Goldan, P. D., Kuster, W. C.,
866 Roberts, J. M., Fehsenfeld, F. C., Worsnop, D. R., Canagaratna, M. R., Pszenny, A.
867 A. P., Keene, W. C., Marchewka, M., Bertman, S. B. and Bates, T. S.: Budget of
868 organic carbon in a polluted atmosphere: Results from the New England Air Quality
869 Study in 2002, *J. Geophys. Res. D Atmos.*, 110(16), 1–22,
870 doi:10.1029/2004JD005623, 2005.

871 de Gouw, J. A., Gilman, J. B., Kim, S. W., Alvarez, S. L., Dusanter, S., Graus, M.,
872 Griffith, S. M., Isaacman-VanWertz, G., Kuster, W. C., Lefer, B. L., Lerner, B. M.,
873 McDonald, B. C., Rappenglück, B., Roberts, J. M., Stevens, P. S., Stutz, J., Thalman,
874 R., Veres, P. R., Volkamer, R., Warneke, C., Washenfelder, R. A. and Young, C. J.:
875 Chemistry of Volatile Organic Compounds in the Los Angeles Basin: Formation of
876 Oxygenated Compounds and Determination of Emission Ratios, *J. Geophys. Res.*
877 *Atmos.*, 123(4), 2298–2319, doi:10.1002/2017JD027976, 2018.

878 Guo, H., Xu, L., Bougiatioti, A., Cerully, K. M., Capps, S. L., Hite, J. R., Carlton, A.
879 G., Lee, S. H., Bergin, M. H., Ng, N. L., Nenes, A. and Weber, R. J.: Fine-particle
880 water and pH in the southeastern United States, *Atmos. Chem. Phys.*, 15(9), 5211–
881 5228, doi:10.5194/acp-15-5211-2015, 2015.

882 Hallquist, M., Wenger, J. C., Baltensperger, U., Rudich, Y., Simpson, D., Claeys, M.,
883 Dommen, J., Donahue, N. M., George, C., Goldstein, a. H., Hamilton, J. F.,
884 Herrmann, H., Hoffmann, T., Iinuma, Y., Jang, M., Jenkin, M. E., Jimenez, J. L.,
885 Kiendler-Scharr, a., Maenhaut, W., McFiggans, G., Mentel, T. F., Monod, a.,
886 Prévôt, a. S. H., Seinfeld, J. H., Surratt, J. D., Szmigielski, R. and Wildt, J.: The
887 formation, properties and impact of secondary organic aerosol: current and emerging
888 issues, *Atmos. Chem. Phys.*, 9(14), 5155–5236, doi:10.5194/acp-9-5155-2009, 2009.

889 Hammes, J., Lutz, A., Mentel, T., Faxon, C. and Hallquist, M.: Carboxylic acids from
890 limonene oxidation by ozone and hydroxyl radicals: insights into mechanisms derived
891 using a FIGAERO-CIMS, *Atmos. Chem. Phys.*, 19(20), 13037–13052,
892 doi:10.5194/acp-19-13037-2019, 2019.

893 Harrison, M. A. J., Barra, S., Borghesi, D., Vione, D., Arsene, C. and Iulian Olariu,
894 R.: Nitrated phenols in the atmosphere: a review, *Atmos. Environ.*, 39(2), 231–248,

895 doi:<https://doi.org/10.1016/j.atmosenv.2004.09.044>, 2005.

896 He, Q.-F., Ding, X., Wang, X.-M., Yu, J.-Z., Fu, X.-X., Liu, T.-Y., Zhang, Z., Xue, J.,
897 Chen, D.-H., Zhong, L.-J. and Donahue, N. M.: Organosulfates from Pinene and
898 Isoprene over the Pearl River Delta, South China: Seasonal Variation and Implication
899 in Formation Mechanisms, *Environ. Sci. Technol.*, 48(16), 9236–9245,
900 doi:10.1021/es501299v, 2014.

901 Heald, C. L., Kroll, J. H., Jimenez, J. L., Docherty, K. S., Decarlo, P. F., Aiken, A. C.,
902 Chen, Q., Martin, S. T., Farmer, D. K. and Artaxo, P.: A simplified description of the
903 evolution of organic aerosol composition in the atmosphere, *Geophys. Res. Lett.*,
904 37(8), doi:10.1029/2010GL042737, 2010.

905 Hodzic, A., Jimenez, J. L., Madronich, S., Canagaratna, M. R., Decarlo, P. F.,
906 Kleinman, L. and Fast, J.: Modeling organic aerosols in a megacity: Potential
907 contribution of semi-volatile and intermediate volatility primary organic compounds
908 to secondary organic aerosol formation, *Atmos. Chem. Phys.*, 10(12), 5491–5514,
909 doi:10.5194/acp-10-5491-2010, 2010.

910 Hu, W., Hu, M., Hu, W., Jimenez, J. L., Yuan, B., Chen, W., Wang, M., Wu, Y.,
911 Chen, C., Wang, Z., Peng, J., Zeng, L. and Shao, M.: Chemical composition, sources,
912 and aging process of submicron aerosols in Beijing: Contrast between summer and
913 winter, *J. Geophys. Res. Atmos.*, 121(4), 1955–1977,
914 doi:10.1002/2015JD024020.Received, 2016.

915 Hu, W., Day, D. A., Campuzano-Jost, P., Nault, B. A., Park, T., Lee, T., Croteau, P.,
916 Canagaratna, M. R., Jayne, J. T., Worsnop, D. R. and Jimenez, J. L.: Evaluation of the
917 new capture vaporizer for aerosol mass spectrometers: Characterization of organic
918 aerosol mass spectra, *Aerosol Sci. Technol.*, 52(7), 725–739,
919 doi:10.1080/02786826.2018.1454584, 2018.

920 Huang, R.-J., Cao, J., Chen, Y., Yang, L., Shen, J., You, Q., Wang, K., Lin, C., Xu,
921 W., Gao, B., Li, Y., Chen, Q., Hoffmann, T., O’Dowd, C. D., Bilde, M. and Glasius,
922 M.: Organosulfates in atmospheric aerosol: synthesis and quantitative analysis of
923 PM_{2.5} from Xi’an, northwestern China, *Atmos. Meas. Tech.*, 11(6), 3447–3456,
924 doi:10.5194/amt-11-3447-2018, 2018.

925 Huang, R. J., Zhang, Y., Bozzetti, C., Ho, K. F., Cao, J. J., Han, Y., Daellenbach, K.
926 R., Slowik, J. G., Platt, S. M., Canonaco, F., Zotter, P., Wolf, R., Pieber, S. M., Bruns,
927 E. A., Crippa, M., Ciarelli, G., Piazzalunga, A., Schwikowski, M., Abbaszade, G.,
928 Schnelle-Kreis, J., Zimmermann, R., An, Z., Szidat, S., Baltensperger, U., El Haddad,
929 I. and Prévôt, A. S. H.: High secondary aerosol contribution to particulate pollution
930 during haze events in China, *Nature*, 514(7521), 218–222, doi:10.1038/nature13774,
931 2015.

932 Huang, W., Saathoff, H., Shen, X., Ramisetty, R., Leisner, T. and Mohr, C.: Chemical
933 Characterization of Highly Functionalized Organonitrates Contributing to Night-Time
934 Organic Aerosol Mass Loadings and Particle Growth, *Environ. Sci. Technol.*, 53(3),
935 1165–1174, doi:10.1021/acs.est.8b05826, 2019.

936 Hunter, J. F., Day, D. A., Palm, B. B., Yatavelli, R. L. N., Chan, A. W. H., Kaser, L.,
937 Cappellin, L., Hayes, P. L., Cross, E. S., Carrasquillo, A. J., Campuzano-Jost, P.,
938 Stark, H., Zhao, Y., Hohaus, T., Smith, J. N., Hansel, A., Karl, T., Goldstein, A. H.,
939 Guenther, A., Worsnop, D. R., Thornton, J. A., Heald, C. L., Jimenez, J. L. and Kroll,
940 J. H.: Comprehensive characterization of atmospheric organic carbon at a forested
941 site, *Nat. Geosci.*, 10(10), 748–753, doi:10.1038/NGEO3018, 2017.

942 Hyttinen, N., Otkjær, R. V., Iyer, S., Kjaergaard, H. G., Rissanen, M. P., Wennberg,
943 P. O. and Kurtén, T.: Computational Comparison of Different Reagent Ions in the
944 Chemical Ionization of Oxidized Multifunctional Compounds, *J. Phys. Chem. A*,
945 122(1), 269–279, doi:10.1021/acs.jpca.7b10015, 2018.

946 Isaacman-VanWertz, G., Massoli, P., O'Brien, R., Lim, C., Franklin, J., Moss, J.,
947 Hunter, J., Nowak, J., Canagaratna, M., Misztal, P., Arata, C., Roscioli, J., Herndon,
948 S., Onasch, T., Lambe, A., Jayne, J., Su, L., Knopf, D., Goldstein, A., Worsnop, D.
949 and Kroll, J.: Chemical evolution of atmospheric organic carbon over multiple
950 generations of oxidation, *Nat. Chem.*, 10(4), 462–468, doi:10.1038/s41557-018-0002-
951 2, 2018.

952 Iyer, S., Lopez-Hilfiker, F., Lee, B. H., Thornton, J. A. and Kurtén, T.: Modeling the
953 Detection of Organic and Inorganic Compounds Using Iodide-Based Chemical
954 Ionization, *J. Phys. Chem. A*, 120(4), 576–587, doi:10.1021/acs.jpca.5b09837, 2016.

955 Jacobs, M. I., Burke, W. J. and Elrod, M. J.: Kinetics of the Reactions of Isoprene-
956 Derived Hydroxynitrates: Gas Phase Epoxide Formation and Solution Phase
957 Hydrolysis, *Atmos. Chem. Phys.*, 14, 8933, 2014.

958 Jenkin, M. E., Saunders, S. M., Wagner, V. and Pilling, M. J.: Protocol for the
959 development of the Master Chemical Mechanism, MCM v3 (Part B): tropospheric
960 degradation of aromatic volatile organic compounds, *Atmos. Chem. Phys.*, 3(1), 181–
961 193, doi:10.5194/acp-3-181-2003, 2003.

962 Karl, T., Striednig, M., Graus, M., Hammerle, A. and Wohlfahrt, G.: Urban flux
963 measurements reveal a large pool of oxygenated volatile organic compound
964 emissions, *Proc. Natl. Acad. Sci.*, 201714715, doi:10.1073/pnas.1714715115, 2018.

965 Kawamura, K. and Bikkina, S.: A review of dicarboxylic acids and related
966 compounds in atmospheric aerosols: Molecular distributions, sources and
967 transformation, *Atmos. Res.*, 170, 140–160,
968 doi:https://doi.org/10.1016/j.atmosres.2015.11.018, 2016.

969 Kawamura, K., Kasukabe, H. and Barrie, L. A.: Source and reaction pathways of
970 dicarboxylic acids, ketoacids and dicarbonyls in arctic aerosols: One year of
971 observations, *Atmos. Environ.*, 30(10), 1709–1722, doi:https://doi.org/10.1016/1352-
972 2310(95)00395-9, 1996.

973 Kong, X., Salvador, C. M., Carlsson, S., Pathak, R., Davidsson, K. O., Le Breton, M.,
974 Gaita, S. M., Mitra, K., Hallquist, Å. M., Hallquist, M. and Pettersson, J. B. C.:
975 Molecular characterization and optical properties of primary emissions from a
976 residential wood burning boiler, *Sci. Total Environ.*, 754, 142143,
977 doi:https://doi.org/10.1016/j.scitotenv.2020.142143, 2021.

978 Krechmer, J. E., Pagonis, D., Ziemann, P. J. and Jimenez, J. L.: Quantification of Gas-
979 Wall Partitioning in Teflon Environmental Chambers Using Rapid Bursts of Low-
980 Volatility Oxidized Species Generated in Situ, *Environ. Sci. Technol.*, 50(11), 5757–
981 5765, doi:10.1021/acs.est.6b00606, 2016.

982 Kroll, J. H. and Seinfeld, J. H.: Chemistry of secondary organic aerosol: Formation
983 and evolution of low-volatility organics in the atmosphere, *Atmos. Environ.*, 42(16),
984 3593–3624, doi:10.1016/j.atmosenv.2008.01.003, 2008.

985 Lambe, A. T., Onasch, T. B., Croasdale, D. R., Wright, J. P., Martin, A. T., Franklin,
986 J. P., Massoli, P., Kroll, J. H., Canagaratna, M. R., Brune, W. H., Worsnop, D. R. and
987 Davidovits, P.: Transitions from functionalization to fragmentation reactions of
988 laboratory Secondary Organic Aerosol (SOA) generated from the OH oxidation of
989 alkane precursors, *Environ. Sci. Technol.*, 46(10), 5430–5437,
990 doi:10.1021/es300274t, 2012.

991 Larsen, B. R., Di Bella, D., Glasius, M., Winterhalter, R., Jensen, N. R. and Hjorth, J.:
992 Gas-phase OH oxidation of monoterpenes: Gaseous and particulate products, *J.*
993 *Atmos. Chem.*, 38(3), 231–276, doi:10.1023/A:1006487530903, 2001.

994 Lee, B. H., Lopez-Hilfiker, F. D., Mohr, C., Kurtén, T., Worsnop, D. R. and
995 Thornton, J. A.: An iodide-adduct high-resolution time-of-flight chemical-ionization
996 mass spectrometer: Application to atmospheric inorganic and organic compounds,
997 *Environ. Sci. Technol.*, 48(11), 6309–6317, doi:10.1021/es500362a, 2014.

998 Lee, B. H., Mohr, C., Lopez-Hilfiker, F. D., Lutz, A., Hallquist, M., Lee, L., Romer,
999 P., Cohen, R. C., Iyer, S., Kurtén, T., Hu, W., Day, D. A., Campuzano-Jost, P.,
1000 Jimenez, J. L., Xu, L., Ng, N. L., Guo, H., Weber, R. J., Wild, R. J., Brown, S. S.,
1001 Koss, A., de Gouw, J., Olson, K., Goldstein, A. H., Seco, R., Kim, S., McAvey, K.,
1002 Shepson, P. B., Starn, T., Baumann, K., Edgerton, E. S., Liu, J., Shilling, J. E., Miller,
1003 D. O., Brune, W., Schobesberger, S., D’Ambro, E. L. and Thornton, J. A.: Highly
1004 functionalized organic nitrates in the southeast United States: Contribution to
1005 secondary organic aerosol and reactive nitrogen budgets, *Proc. Natl. Acad. Sci.*,
1006 113(6), 1516–1521, doi:10.1073/pnas.1508108113, 2016.

1007 Lee, B. H., Lopez-hilfiker, F. D., Veres, P. R., Mcduffie, E. E., Fibiger, D. L.,
1008 Tamara, L. and Thornton, J. A.: Flight deployment of a high-resolution time-of-flight
1009 chemical ionization mass spectrometer : observations of reactive halogen and nitrogen
1010 oxide species, , doi:10.1029/2017JD028082, 2018a.

1011 Lee, B. H., Lopez-Hilfiker, F. D., D’Ambro, E. L., Zhou, P., Boy, M., Petäjä, T., Hao,
1012 L., Virtanen, A. and Thornton, J. A.: Semi-volatile and highly oxygenated gaseous
1013 and particulate organic compounds observed above a boreal forest canopy, *Atmos.*
1014 *Chem. Phys.*, 18(15), 11547–11562, doi:10.5194/acp-18-11547-2018, 2018b.

1015 Li, T., Wang, Z., Yuan, B., Ye, C., Lin, Y., Wang, S., Sha, Q., Yuan, Z., Zheng, J. and
1016 Shao, M.: Emissions of carboxylic acids, hydrogen cyanide (HCN) and isocyanic acid
1017 (HNCO) from vehicle exhaust, *Atmos. Environ.*, 247, 118218,
1018 doi:<https://doi.org/10.1016/j.atmosenv.2021.118218>, 2021.

1019 Liao, J., Froyd, K. D., Murphy, D. M., Keutsch, F. N., Yu, G., Wennberg, P. O., St
1020 Clair, J. M., Crouse, J. D., Wisthaler, A., Mikoviny, T., Jimenez, J. L., Campuzano-
1021 Jost, P., Day, D. A., Hu, W., Ryerson, T. B., Pollack, I. B., Peischl, J., Anderson, B.
1022 E., Ziemba, L. D., Blake, D. R., Meinardi, S. and Diskin, G.: Airborne measurements
1023 of organosulfates over the continental U.S, *J. Geophys. Res. Atmos.* JGR, 120(7),
1024 2990–3005, doi:[10.1002/2014JD022378](https://doi.org/10.1002/2014JD022378), 2015.

1025 Lim, H.-J., Carlton, A. G. and Turpin, B. J.: Isoprene Forms Secondary Organic
1026 Aerosol through Cloud Processing: Model Simulations, *Environ. Sci. Technol.*,
1027 39(12), 4441–4446, doi:[10.1021/es048039h](https://doi.org/10.1021/es048039h), 2005.

1028 Liu, C., Deng, X., Zhu, B. and Yin, C.: Characteristics of GSR of China’s three major
1029 economic regions in the past 10 years and its relationship with O₃ and PM_{2.5}, *China*
1030 *Environ. Sci.*, 38(08), 2820–2829, doi:[10.19674/j.cnki.issn1000-6923.2018.0295](https://doi.org/10.19674/j.cnki.issn1000-6923.2018.0295),
1031 2018.

1032 Liu, X., Qu, H., Huey, L. G., Wang, Y., Sjostedt, S., Zeng, L., Lu, K., Wu, Y., Hu,
1033 M., Shao, M., Zhu, T. and Zhang, Y.: High Levels of Daytime Molecular Chlorine
1034 and Nitryl Chloride at a Rural Site on the North China Plain, *Environ. Sci. Technol.*,
1035 51(17), 9588–9595, doi:[10.1021/acs.est.7b03039](https://doi.org/10.1021/acs.est.7b03039), 2017.

1036 Liu, Z., Wang, Y., Gu, D., Zhao, C., Huey, L. G., Stickel, R., Liao, J., Shao, M., Zhu,
1037 T., Zeng, L., Amoroso, A., Costabile, F., Chang, C. C. and Liu, S. C.: Summertime
1038 photochemistry during CAREBeijing-2007: ROxbudgets and O₃ formation, *Atmos.*
1039 *Chem. Phys.*, 12(16), 7737–7752, doi:[10.5194/acp-12-7737-2012](https://doi.org/10.5194/acp-12-7737-2012), 2012.

1040 Lopez-Hilfiker, F. D., Mohr, C., Ehn, M., Rubach, F., Kleist, E., Wildt, J., Mentel, T.
1041 F., Lutz, A., Hallquist, M., Worsnop, D. and Thornton, J. A.: A novel method for
1042 online analysis of gas and particle composition: description and evaluation of a Filter
1043 Inlet for Gases and AEROSols (FIGAERO), *Atmos. Meas. Tech.*, 7(4), 983–1001,
1044 doi:[10.5194/amt-7-983-2014](https://doi.org/10.5194/amt-7-983-2014), 2014.

1045 Lopez-Hilfiker, F. D., Mohr, C., Ehn, M., Rubach, F., Kleist, E., Wildt, J., Mentel, T.
1046 F. and Carrasquillo, A. J.: Phase partitioning and volatility of secondary organic
1047 aerosol components formed from α -pinene ozonolysis and OH oxidation : the
1048 importance of accretion products and other low volatility compounds, *Atmos. Chem.*
1049 *Phys.*, 15, 7765–7776, doi:10.5194/acp-15-7765-2015, 2015.

1050 Lopez-Hilfiker, F. D., Iyer, S., Mohr, C., Lee, B. H., Ambro, E. L. D., Kurtén, T. and
1051 Thornton, J. A.: Constraining the sensitivity of iodide adduct chemical ionization
1052 mass spectrometry to multifunctional organic molecules using the collision limit and
1053 thermodynamic stability of iodide ion adducts, *Atmos. Meas. Tech.*, 9, 1505–1512,
1054 doi:10.5194/amt-9-1505-2016, 2016.

1055 Massoli, P., Stark, H., Canagaratna, M. R., Krechmer, J. E., Xu, L., Ng, N. L.,
1056 Mauldin, R. L., Yan, C., Kimmel, J., Misztal, P. K., Jimenez, J. L., Jayne, J. T. and
1057 Worsnop, D. R.: Ambient Measurements of Highly Oxidized Gas-Phase Molecules
1058 during the Southern Oxidant and Aerosol Study (SOAS) 2013, *ACS Earth Sp. Chem.*,
1059 2(7), 653–672, doi:10.1021/acsearthspacechem.8b00028, 2018.

1060 Mattila, J. M., Brophy, P., Kirkland, J., Hall, S., Ullmann, K., Fischer, E. V., Brown,
1061 S., McDuffie, E., Tevlin, A. and Farmer, D. K.: Tropospheric sources and sinks of
1062 gas-phase acids in the Colorado Front Range, *Atmos. Chem. Phys.*, 18(16), 12315–
1063 12327, doi:10.5194/acp-18-12315-2018, 2018.

1064 Mehra, A., Wang, Y., Krechmer, J. E., Lambe, A., Majluf, F., Morris, M. A.,
1065 Priestley, M., Bannan, T. J., Bryant, D. J., Pereira, K. L., Hamilton, J. F., Rickard, A.
1066 R., Newland, M. J., Stark, H., Croteau, P., Jayne, J. T., Worsnop, D. R., Canagaratna,
1067 M. R., Wang, L. and Coe, H.: Evaluation of the chemical composition of gas- and
1068 particle-phase products of aromatic oxidation, *Atmos. Chem. Phys.*, 20(16), 9783–
1069 9803, doi:10.5194/acp-20-9783-2020, 2020.

1070 Mellouki, A., Wallington, T. J. and Chen, J.: Atmospheric Chemistry of Oxygenated
1071 Volatile Organic Compounds: Impacts on Air Quality and Climate, *Chem. Rev.*,
1072 115(10), 3984–4014, doi:10.1021/cr500549n, 2015.

1073 Mohr, C., Lopez-Hilfiker, F. D., Zotter, P., Prévôt, A. S. H., Xu, L., Ng, N. L.,
1074 Herndon, S. C., Williams, L. R., Franklin, J. P., Zahniser, M. S., Worsnop, D. R.,

1075 Knighton, W. B., Aiken, A. C., Gorkowski, K. J., Dubey, M. K., Allan, J. D. and
1076 Thornton, J. A.: Contribution of Nitrated Phenols to Wood Burning Brown Carbon
1077 Light Absorption in Detling, United Kingdom during Winter Time, *Environ. Sci.*
1078 *Technol.*, 47(12), 6316–6324, doi:10.1021/es400683v, 2013.

1079 Mutzel, A., Poulain, L., Berndt, T., Iinuma, Y., Rodigast, M., Böge, O., Richters, S.,
1080 Spindler, G., Sipilä, M., Jokinen, T., Kulmala, M. and Herrmann, H.: Highly
1081 Oxidized Multifunctional Organic Compounds Observed in Tropospheric Particles: A
1082 Field and Laboratory Study, *Environ. Sci. Technol.*, 49(13), 7754–7761,
1083 doi:10.1021/acs.est.5b00885, 2015.

1084 Mutzel, A., Rodigast, M., Iinuma, Y., Böge, O. and Herrmann, H.: Monoterpene SOA
1085 - Contribution of first-generation oxidation products to formation and chemical
1086 composition, *Atmos. Environ.*, 130, 136–144, doi:10.1016/j.atmosenv.2015.10.080,
1087 2016.

1088 Nah, T., Sanchez, J., Boyd, C. M. and Ng, N. L.: Photochemical Aging of α -pinene
1089 and β -pinene Secondary Organic Aerosol formed from Nitrate Radical Oxidation,
1090 *Environ. Sci. Technol.*, 50(1), 222–231, doi:10.1021/acs.est.5b04594, 2016.

1091 Nannoolal, Y., Rarey, J. and Ramjugernath, D.: Estimation of pure component
1092 properties Part 3. Estimation of the vapor pressure of non-electrolyte organic
1093 compounds via group contributions and group interactions, *Fluid Phase Equilib.*,
1094 269(1–2), 117–133, doi:10.1016/j.fluid.2008.04.020, 2008.

1095 Ng, N. L., Brown, S. S., Archibald, A. T., Atlas, E., Cohen, R. C., Crowley, J. N.,
1096 Day, D. A., Donahue, N. M., Fry, J. L., Fuchs, H., Griffin, R. J., Guzman, M. I.,
1097 Herrmann, H., Hodzic, A., Iinuma, Y., Jimenez, J. L., Kiendler-Scharr, A., Lee, B. H.,
1098 Luecken, D. J., Mao, J., McLaren, R., Mutzel, A., Osthoff, H. D., Ouyang, B.,
1099 Picquet-Varrault, B., Platt, U., Pye, H. O. T., Rudich, Y., Schwantes, R. H., Shiraiwa,
1100 M., Stutz, J., Thornton, J. A., Tilgner, A., Williams, B. J. and Zaveri, R. A.: Nitrate
1101 radicals and biogenic volatile organic compounds: oxidation, mechanisms, and
1102 organic aerosol, *Atmos. Chem. Phys.*, 17(3), 2103–2162, doi:10.5194/acp-17-2103-
1103 2017, 2017.

1104 Noelscher, A. C., Yanez-Serrano, A. M., Wolff, S., de Araujo, A. C., Lavric, J. V,

1105 Kesselmeier, J. and Williams, J.: Unexpected seasonality in quantity and composition
1106 of Amazon rainforest air reactivity, *Nat. Commun.*, 7, doi:10.1038/ncomms10383,
1107 2016.

1108 Osthoff, H. D., Roberts, J. M., Ravishankara, A. R., Williams, E. J., Lerner, B. M.,
1109 Sommariva, R., Bates, T. S., Coffman, D., Quinn, P. K., Dibb, J. E., Stark, H.,
1110 Burkholder, J. B., Talukdar, R. K., Meagher, J., Fehsenfeld, F. C. and Brown, S. S.:
1111 High levels of nitryl chloride in the polluted subtropical marine boundary layer, *Nat.*
1112 *Geosci.*, 1(5), 324–328, doi:10.1038/ngeo177, 2008.

1113 Palm, B. B., Liu, X., Jimenez, J. L. and Thornton, J. A.: Performance of a new coaxial
1114 ion-molecule reaction region for low-pressure chemical ionization mass spectrometry
1115 with reduced instrument wall interactions, *Atmos. Meas. Tech.*, 12(11), 5829–5844,
1116 doi:10.5194/amt-12-5829-2019, 2019.

1117 Pankow, J. F. and Asher, W. E.: SIMPOL.1: A simple group contribution method for
1118 predicting vapor pressures and enthalpies of vaporization of multifunctional organic
1119 compounds, *Atmos. Chem. Phys.*, 8(10), 2773–2796, doi:10.5194/acp-8-2773-2008,
1120 2008.

1121 Paulot, F., Crouse, J. D., Kjaergaard, H. G., Kroll, J. H., Seinfeld, J. H. and
1122 Wennberg, P. O.: Isoprene photooxidation: New insights into the production of acids
1123 and organic nitrates, *Atmos. Chem. Phys.*, 9(4), 1479–1501, doi:10.5194/acp-9-1479-
1124 2009, 2009.

1125 Qi, L., Chen, M., Stefenelli, G., Pospisilova, V., Tong, Y., Bertrand, A., Hueglin, C.,
1126 Ge, X., Baltensperger, U., Prévôt, A. S. H. and Slowik, J. G.: Organic aerosol source
1127 apportionment in Zurich using an extractive electrospray ionization time-of-flight
1128 mass spectrometer (EESI-TOF-MS) – Part 2: Biomass burning influences in winter,
1129 *Atmos. Chem. Phys.*, 19(12), 8037–8062, doi:10.5194/acp-19-8037-2019, 2019.

1130 Reyes-Villegas, E., Bannan, T., Le Breton, M., Mehra, A., Priestley, M., Percival, C.,
1131 Coe, H. and Allan, J. D.: Online Chemical Characterization of Food-Cooking Organic
1132 Aerosols: Implications for Source Apportionment, *Environ. Sci. Technol.*, 52(9),
1133 5308–5318, doi:10.1021/acs.est.7b06278, 2018.

1134 Riva, M., Rantala, P., Krechmer, J. E., Peräkylä, O., Zhang, Y., Heikkinen, L.,

1135 Garmash, O., Yan, C., Kulmala, M., Worsnop, D. and Ehn, M.: Evaluating the
1136 performance of five different chemical ionization techniques for detecting gaseous
1137 oxygenated organic species, *Atmos. Meas. Tech.*, 2018(4), 1–39, doi:10.5194/amt-
1138 2018-407, 2019.

1139 Sander, R. and Crutzen, P. J.: Model study indicating halogen activation and ozone
1140 destruction in polluted air masses transported to the sea, *J. Geophys. Res. Atmos.*,
1141 101(D4), 9121–9138, doi:10.1029/95JD03793, 1996.

1142 Schneider, J., Weimer, S., Drewnick, F., Borrmann, S., Helas, G., Gwaze, P., Schmid,
1143 O., Andreae, M. O. and Kirchner, U.: Mass spectrometric analysis and aerodynamic
1144 properties of various types of combustion-related aerosol particles, *Int. J. Mass
1145 Spectrom.*, 258(1), 37–49, doi:https://doi.org/10.1016/j.ijms.2006.07.008, 2006.

1146 Schwantes, R. H., Teng, A. P., Nguyen, T. B., Coggon, M. M., Crouse, J. D., St
1147 Clair, J. M., Zhang, X., Schilling, K. A., Seinfeld, J. H. and Wennberg, P. O.:
1148 Isoprene NO₃ Oxidation Products from the RO₂ + HO₂ Pathway, *J. Phys. Chem. A*,
1149 119, 10158, 2015.

1150 Schwantes, R. H., Schilling, K. A., McVay, R. C., Lignell, H., Coggon, M. M.,
1151 Zhang, X., Wennberg, P. O. and Seinfeld, J. H.: Formation of highly oxygenated low-
1152 volatility products from cresol oxidation, *Atmos. Chem. Phys.*, 17(5), 3453–3474,
1153 doi:10.5194/acp-17-3453-2017, 2017.

1154 Schwantes, R. H., Emmons, L. K., Orlando, J. J., Barth, M. C., Tyndall, G. S., Hall, S.
1155 R., Ullmann, K., St. Clair, J. M., Blake, D. R., Wisthaler, A. and Paul V. Bui, T.:
1156 Comprehensive isoprene and terpene gas-phase chemistry improves simulated surface
1157 ozone in the southeastern US, *Atmos. Chem. Phys.*, 20(6), 3739–3776,
1158 doi:10.5194/acp-20-3739-2020, 2020.

1159 Shrivastava, M., Andreae, M. O., Artaxo, P., Barbosa, H. M. J., Berg, L. K., Brito, J.,
1160 Ching, J., Easter, R. C., Fan, J., Fast, J. D., Feng, Z., Fuentes, J. D., Glasius, M.,
1161 Goldstein, A. H., Alves, E. G., Gomes, H., Gu, D., Guenther, A., Jathar, S. H., Kim,
1162 S., Liu, Y., Lou, S., Martin, S. T., McNeill, V. F., Medeiros, A., de Sá, S. S., Shilling,
1163 J. E., Springston, S. R., Souza, R. A. F., Thornton, J. A., Isaacman-VanWertz, G.,
1164 Yee, L. D., Ynoue, R., Zaveri, R. A., Zelenyuk, A. and Zhao, C.: Urban pollution

1165 greatly enhances formation of natural aerosols over the Amazon rainforest, *Nat.*
1166 *Commun.*, 10(1), doi:10.1038/s41467-019-08909-4, 2019.

1167 Simoneit, B. R. T., Schauer, J. J., Nolte, C. G., Oros, D. R., Elias, V. O., Fraser, M.
1168 P., Rogge, W. F. and Cass, G. R.: Levoglucosan, a tracer for cellulose in biomass
1169 burning and atmospheric particles, *Atmos. Environ.*, 33(2), 173–182,
1170 doi:[https://doi.org/10.1016/S1352-2310\(98\)00145-9](https://doi.org/10.1016/S1352-2310(98)00145-9), 1999.

1171 Slusher, D. L., Huey, L. G., Tanner, D. J., Flocke, F. M. and Roberts, J. M.: A thermal
1172 dissociation–chemical ionization mass spectrometry (TD-CIMS) technique for the
1173 simultaneous measurement of peroxyacyl nitrates and dinitrogen pentoxide, *J.*
1174 *Geophys. Res. Atmos.*, 109(D19), doi:10.1029/2004JD004670, 2004.

1175 Stark, H., Yatavelli, R. L. N., Thompson, S. L., Kimmel, J. R., Cubison, M. J.,
1176 Chhabra, P. S., Canagaratna, M. R., Jayne, J. T., Worsnop, D. R. and Jimenez, J. L.:
1177 Methods to extract molecular and bulk chemical information from series of complex
1178 mass spectra with limited mass resolution, *Int. J. Mass Spectrom.*, 389, 26–38,
1179 doi:10.1016/j.ijms.2015.08.011, 2015.

1180 Stark, H., Yatavelli, R. L. N., Thompson, S. L., Kang, H., Krechmer, J. E., Kimmel, J.
1181 R., Palm, B. B., Hu, W., Hayes, P. L., Day, D. A., Campuzano-Jost, P., Canagaratna,
1182 M. R., Jayne, J. T., Worsnop, D. R. and Jimenez, J. L.: Impact of Thermal
1183 Decomposition on Thermal Desorption Instruments: Advantage of Thermogram
1184 Analysis for Quantifying Volatility Distributions of Organic Species, *Environ. Sci.*
1185 *Technol.*, 51(15), 8491–8500, doi:10.1021/acs.est.7b00160, 2017.

1186 Stolzenburg, D., Fischer, L., Vogel, A. L., Heinritzi, M., Schervish, M., Simon, M.,
1187 Wagner, A. C., Dada, L., Ahonen, L. R., Amorim, A., Baccarini, A., Bauer, P. S.,
1188 Baumgartner, B., Bergen, A., Bianchi, F., Breitenlechner, M., Brilke, S., Buenrostro
1189 Mazon, S., Chen, D., Dias, A., Draper, D. C., Duplissy, J., El Haddad, I.,
1190 Finkenzeller, H., Frege, C., Fuchs, C., Garmash, O., Gordon, H., He, X., Helm, J.,
1191 Hofbauer, V., Hoyle, C. R., Kim, C., Kirkby, J., Kontkanen, J., Kürten, A.,
1192 Lampilahti, J., Lawler, M., Lehtipalo, K., Leiminger, M., Mai, H., Mathot, S.,
1193 Mentler, B., Molteni, U., Nie, W., Nieminen, T., Nowak, J. B., Ojdanic, A., Onnela,
1194 A., Passananti, M., Petäjä, T., Quéléver, L. L. J., Rissanen, M. P., Sarnela, N.,

1195 Schallhart, S., Tauber, C., Tomé, A., Wagner, R., Wang, M., Weitz, L., Wimmer, D.,
1196 Xiao, M., Yan, C., Ye, P., Zha, Q., Baltensperger, U., Curtius, J., Dommen, J., Flagan,
1197 R. C., Kulmala, M., Smith, J. N., Worsnop, D. R., Hansel, A., Donahue, N. M.,
1198 Winkler, P. M., Nie, W., Passananti, M., Leiminger, M., Stolzenburg, D., Yan, C.,
1199 Wimmer, D., Buenrostro Mazon, S., Kontkanen, J., Wang, M., Garmash, O., Kulmala,
1200 M., Petäjä, T., Bianchi, F., Chen, D., Nieminen, T., Brilke, S., Nowak, J. B., Duplissy,
1201 J., El Haddad, I., Simon, M., Wagner, A. C., Kürten, A., Smith, J. N., Kim, C., et al.:
1202 Rapid growth of organic aerosol nanoparticles over a wide tropospheric temperature
1203 range, *Proc. Natl. Acad. Sci.*, 115(37), 201807604, doi:10.1073/pnas.1807604115,
1204 2018.

1205 Surratt, J. D., Murphy, S. M., Kroll, J. H., Ng, N. L., Hildebrandt, L., Sorooshian, A.,
1206 Szmigielski, R., Vermeylen, R., Maenhaut, W., Claeys, M., Flagan, R. C. and
1207 Seinfeld, J. H.: Chemical Composition of Secondary Organic Aerosol Formed from
1208 the Photooxidation of Isoprene, *J. Phys. Chem. A*, 110(31), 9665–9690,
1209 doi:10.1021/jp061734m, 2006.

1210 Surratt, J. D., Kroll, J. H., Kleindienst, T. E., Edney, E. O., Claeys, M., Sorooshian,
1211 A., Ng, N. L., Offenberg, J. H., Lewandowski, M., Jaoui, M., Flagan, R. C. and
1212 Seinfeld, J. H.: Evidence for Organosulfates in Secondary Organic Aerosol, *Environ.*
1213 *Sci. Technol.*, 41(2), 517–527, doi:10.1021/es062081q, 2007.

1214 Surratt, J. D., Chan, A. W. H., Eddingsaas, N. C., Chan, M., Loza, C. L., Kwan, A. J.,
1215 Hersey, S. P., Flagan, R. C., Wennberg, P. O. and Seinfeld, J. H.: Reactive
1216 intermediates revealed in secondary organic aerosol formation from isoprene, *Proc.*
1217 *Natl. Acad. Sci.*, 107(15), 6640–6645, doi:10.1073/pnas.0911114107, 2010.

1218 Thornton, J. A., Mohr, C., Schobesberger, S., D’Ambro, E. L., Lee, B. H. and Lopez-
1219 Hilfiker, F. D.: Evaluating Organic Aerosol Sources and Evolution with a Combined
1220 Molecular Composition and Volatility Framework Using the Filter Inlet for Gases and
1221 Aerosols (FIGAERO), *Acc. Chem. Res.*, 53(8), 1415–1426,
1222 doi:10.1021/acs.accounts.0c00259, 2020.

1223 Volkamer, R., Jimenez, J. L., San Martini, F., Dzepina, K., Zhang, Q., Salcedo, D.,
1224 Molina, L. T., Worsnop, D. R. and Molina, M. J.: Secondary organic aerosol

1225 formation from anthropogenic air pollution: Rapid and higher than expected,
1226 *Geophys. Res. Lett.*, 33(17), doi:10.1029/2006GL026899, 2006.

1227 Wang, H., Gao, Y., Wang, S., Wu, X., Liu, Y., Li, X., Huang, D., Lou, S., Wu, Z.,
1228 Guo, S., Jing, S., Li, Y., Huang, C., Tyndall, G. S., Orlando, J. J. and Zhang, X.:
1229 Atmospheric Processing of Nitrophenols and Nitrocresols from Biomass Burning
1230 Emissions, *J. Geophys. Res. Atmos.*, 0–3, doi:10.1029/2020JD033401, 2020a.

1231 Wang, M., Chen, D., Xiao, M., Ye, Q., Stolzenburg, D., Hofbauer, V., Ye, P., Vogel,
1232 A. L., Mauldin, R. L., Amorim, A., Baccarini, A., Baumgartner, B., Brilke, S., Dada,
1233 L., Dias, A., Duplissy, J., Finkenzeller, H., Garmash, O., He, X.-C., Hoyle, C. R.,
1234 Kim, C., Kvashnin, A., Lehtipalo, K., Fischer, L., Molteni, U., Petäjä, T., Pospisilova,
1235 V., Quéléver, L. L. J., Rissanen, M., Simon, M., Tauber, C., Tomé, A., Wagner, A. C.,
1236 Weitz, L., Volkamer, R., Winkler, P. M., Kirkby, J., Worsnop, D. R., Kulmala, M.,
1237 Baltensperger, U., Dommen, J., El-Haddad, I. and Donahue, N. M.: Photo-oxidation
1238 of Aromatic Hydrocarbons Produces Low-Volatility Organic Compounds, *Environ.*
1239 *Sci. Technol.*, 54(13), 7911–7921, doi:10.1021/acs.est.0c02100, 2020b.

1240 Wang, Q., He, X., Zhou, M., Huang, D. D., Qiao, L., Zhu, S., Ma, Y., Wang, H., Li,
1241 L., Huang, C., Huang, X. H. H., Xu, W., Worsnop, D., Goldstein, A. H., Guo, H. and
1242 Yu, J. Z.: Hourly Measurements of Organic Molecular Markers in Urban Shanghai,
1243 China: Primary Organic Aerosol Source Identification and Observation of Cooking
1244 Aerosol Aging, *ACS Earth Sp. Chem.*, 4(9), 1670–1685,
1245 doi:10.1021/acsearthspacechem.0c00205, 2020c.

1246 Wang, T., Tham, Y. J., Xue, L., Li, Q., Zha, Q., Wang, Z., Poon, S. C. N., Dube, W.
1247 P., Blake, D. R., Louie, P. K. K., Luk, C. W. Y., Tsui, W., Brown, S. S., Osthoff, H.
1248 D., Roberts, J. M., Ravishankara, A. R., Williams, E. J., Lerner, B. M., Sommariva,
1249 R., Bates, T. S., Coffman, D., Quinn, P. K., Dibb, J. E., Stark, H., Burkholder, J. B.,
1250 Talukdar, R. K., Meagher, J., Fehsenfeld, F. C. and Brown, S. S.: Observations of
1251 nitryl chloride and modeling its source and effect on ozone in the planetary boundary
1252 layer of southern China, *J. Geophys. Res.*, 121(5), 2476–2489,
1253 doi:10.1002/2015JD024556, 2016.

1254 Wang, X., Jacob, D. J., Eastham, S. D., Sulprizio, M. P., Zhu, L., Chen, Q.,

1255 Alexander, B., Sherwen, T., Evans, M. J., Lee, B. H., Haskins, J. D., Lopez-Hilfiker,
1256 F. D., Thornton, J. A., Huey, G. L. and Liao, H.: The role of chlorine in global
1257 tropospheric chemistry, *Atmos. Chem. Phys.*, 19(6), 3981–4003, doi:10.5194/acp-19-
1258 3981-2019, 2019.

1259 Wang, Z., Yuan, B., Ye, C., Roberts, J., Wisthaler, A., Lin, Y., Li, T., Wu, C., Peng,
1260 Y., Wang, C., Wang, S., Yang, S., Wang, B., Qi, J., Wang, C., Song, W., Hu, W.,
1261 Wang, X., Xu, W., Ma, N., Kuang, Y., Tao, J., Zhang, Z., Su, H., Cheng, Y., Wang,
1262 X. and Shao, M.: High Concentrations of Atmospheric Isocyanic Acid (HNCO)
1263 Produced from Secondary Sources in China, *Environ. Sci. Technol.*, 11818–11826,
1264 doi:10.1021/acs.est.0c02843, 2020d.

1265 Wennberg, P. O., Bates, K. H., Crounse, J. D., Dodson, L. G., McVay, R. C., Mertens,
1266 L. A., Nguyen, T. B., Praske, E., Schwantes, R. H., Smarte, M. D., St Clair, J. M.,
1267 Teng, A. P., Zhang, X. and Seinfeld, J. H.: Gas-Phase Reactions of Isoprene and Its
1268 Major Oxidation Products, *Chem. Rev.*, 118(7), 3337–3390,
1269 doi:10.1021/acs.chemrev.7b00439, 2018.

1270 Wu, C., Wang, C., Wang, S., Wang, W., Yuan, B., Qi, J., Wang, B., Wang, H., Wang,
1271 C., Song, W., Wang, X., Hu, W., Lou, S., Ye, C., Peng, Y., Wang, Z., Huangfu, Y.,
1272 Xie, Y., Zhu, M., Zheng, J., Wang, X., Jiang, B., Zhang, Z. and Shao, M.:
1273 Measurement report: Important contributions of oxygenated compounds to emissions
1274 and chemistry of VOCs in urban air, *Atmos. Chem. Phys.*, 14769–14785,
1275 doi:10.5194/acp-2020-152, 2020.

1276 Xiong, F., McAvey, K. M., Pratt, K. A., Groff, C. J., Hostetler, M. A., Lipton, M. A.,
1277 Starn, T. K., Seeley, J. V, Bertman, S. B. and Teng, A. P.: Observation of Isoprene
1278 Hydroxynitrates in the Southeastern United States and Implications for the Fate of
1279 NO_x, *Atmos. Chem. Phys.*, 15, 11257, 2015.

1280 Xue, L., Gu, R., Wang, T., Wang, X., Saunders, S., Blake, D., Louie, P. K. K., Luk,
1281 C. W. Y., Simpson, I., Xu, Z., Wang, Z., Gao, Y., Lee, S., Mellouki, A. and Wang,
1282 W.: Oxidative capacity and radical chemistry in the polluted atmosphere of Hong
1283 Kong and Pearl River Delta region: analysis of a severe photochemical smog episode,
1284 *Atmos. Chem. Phys.*, 16(15), 9891–9903, doi:10.5194/acp-16-9891-2016, 2016.

1285 Yang, Y., Shao, M., Wang, X., Nölscher, A. C., Kessel, S., Guenther, A. and
1286 Williams, J.: Towards a quantitative understanding of total OH reactivity: A review,
1287 *Atmos. Environ.*, 134(2), 147–161, doi:10.1016/j.atmosenv.2016.03.010, 2016.

1288 Yang, Y., Shao, M., Keßel, S., Li, Y., Lu, K., Lu, S., Williams, J., Zhang, Y., Zeng,
1289 L., Nölscher, A. C., Wu, Y., Wang, X. and Zheng, J.: How the OH reactivity affects
1290 the ozone production efficiency: case studies in Beijing and Heshan, China, *Atmos.*
1291 *Chem. Phys.*, 17(11), 7127–7142, doi:10.5194/acp-17-7127-2017, 2017.

1292 Yasmeen, F., Szmigielski, R., Vermeylen, R., Gomez-Gonzalez, Y., Surratt, J. D.,
1293 Chan, A. W. H., Seinfeld, J. H., Maenhaut, W. and Claeys, M.: Mass spectrometric
1294 characterization of isomeric terpenoic acids from the oxidation of alpha-pinene, beta-
1295 pinene, d-limonene, and Delta(3)-carene in fine forest aerosol, *J. MASS Spectrom.*,
1296 46(4), 425–442, doi:10.1002/jms.1911, 2011.

1297 Yatavelli, R. L. N., Lopez-Hilfiker, F., Wargo, J. D., Kimmel, J. R., Cubison, M. J.,
1298 Bertram, T. H., Jimenez, J. L., Gonin, M., Worsnop, D. R. and Thornton, J. A.: A
1299 Chemical Ionization High-Resolution Time-of-Flight Mass Spectrometer Coupled to a
1300 Micro Orifice Volatilization Impactor (MOVI-HRToF-CIMS) for Analysis of Gas and
1301 Particle-Phase Organic Species, *Aerosol Sci. Technol.*, 46(12), 1313–1327,
1302 doi:10.1080/02786826.2012.712236, 2012.

1303 Yuan, B., Veres, P. R., Warneke, C., Roberts, J. M., Gilman, J. B., Koss, A., Edwards,
1304 P. M., Graus, M., Kuster, W. C., Li, S. M., Wild, R. J., Brown, S. S., Dubé, W. P.,
1305 Lerner, B. M., Williams, E. J., Johnson, J. E., Quinn, P. K., Bates, T. S., Lefer, B.,
1306 Hayes, P. L., Jimenez, J. L., Weber, R. J., Zamora, R., Ervens, B., Millet, D. B.,
1307 Rappenglück, B. and De Gouw, J. A.: Investigation of secondary formation of formic
1308 acid: Urban environment vs. oil and gas producing region, *Atmos. Chem. Phys.*,
1309 15(4), 1975–1993, doi:10.5194/acp-15-1975-2015, 2015.

1310 Yuan, B., Liggio, J., Wentzell, J., Li, S. M., Stark, H., Roberts, J. M., Gilman, J.,
1311 Lerner, B., Warneke, C., Li, R., Leithead, A., Osthoff, H. D., Wild, R., Brown, S. S.
1312 and De Gouw, J. A.: Secondary formation of nitrated phenols: Insights from
1313 observations during the Uintah Basin Winter Ozone Study (UBWOS) 2014, *Atmos.*
1314 *Chem. Phys.*, 16(4), 2139–2153, doi:10.5194/acp-16-2139-2016, 2016.

1315 Yuan, B., Koss, A. R., Warneke, C., Coggon, M., Sekimoto, K. and De Gouw, J. A.:
1316 Proton-Transfer-Reaction Mass Spectrometry: Applications in Atmospheric Sciences,
1317 Chem. Rev., 117(21), 13187–13229, doi:10.1021/acs.chemrev.7b00325, 2017.

1318 Zhang, Q., Yuan, B., Shao, M., Wang, X., Lu, S., Lu, K., Wang, M., Chen, L., Chang,
1319 C.-C. and Liu, S. C.: Variations of ground-level O₃ and its precursors in Beijing in
1320 summertime between 2005 and 2011, Atmos. Chem. Phys., 14(12), 6089–6101,
1321 doi:10.5194/acp-14-6089-2014, 2014.

1322 Zhang, Y. J., Tang, L. L., Wang, Z., Yu, H. X., Sun, Y. L., Liu, D., Qin, W.,
1323 Canonaco, F., Prévôt, A. S. H., Zhang, H. L. and Zhou, H. C.: Insights into
1324 characteristics, sources, and evolution of submicron aerosols during harvest seasons in
1325 the Yangtze River delta region, China, Atmos. Chem. Phys., 15(3), 1331–1349,
1326 doi:10.5194/acp-15-1331-2015, 2015.

1327 Zhao, R.: The Recent Development and Application of Chemical Ionization Mass
1328 Spectrometry in Atmospheric Chemistry., 2018.

1329 Zhao, Y., Nguyen, N. T., Presto, A. A., Hennigan, C. J., May, A. A. and Robinson, A.
1330 L.: Intermediate Volatility Organic Compound Emissions from On-Road Gasoline
1331 Vehicles and Small Off-Road Gasoline Engines, Environ. Sci. Technol., 50(8), 4554–
1332 4563, doi:10.1021/acs.est.5b06247, 2016.

1333 Zhou, Y., Huang, X. H., Bian, Q., Griffith, S. M., Louie, P. K. K. and Yu, J. Z.:
1334 Sources and atmospheric processes impacting oxalate at a suburban coastal site in
1335 Hong Kong: Insights inferred from 1 year hourly measurements, J. Geophys. Res.
1336 Atmos., 120(18), 9772–9788, doi:10.1002/2015JD023531, 2015.

1337

1338 **Table 1.** The detected ions discussed in the text.

Ion formula	m/z	Assigned compounds	Possible formation pathways	References
$C_6H_{10}O_5I^-$	288.96	Levoglucozan, mannosan and galactosan	Biomass burning or cooking emissions	(Gaston et al., 2016; Reyes-Villegas et al., 2018)
$C_6H_{12}O_5I^-$	290.97	Fucose	Biomass burning emissions	(Qi et al., 2019)
$C_6H_5NO_3I^-$	265.93	Nitro-phenols	Direct emissions, oxidation of aromatics in the presence of NO _x	(Gaston et al., 2016; Yuan et al., 2016)
$C_6H_5NO_4I^-$	281.93	Nitro-benzenediols	Direct emissions, oxidation of aromatics in the presence of NO _x	(Gaston et al., 2016; Yuan et al., 2016)
$C_6H_4N_2O_5I^-$	310.92	Dinitro-phenols	Direct emissions, oxidation of aromatics in the presence of NO _x	(Gaston et al., 2016; Yuan et al., 2016)
$C_7H_7NO_3I^-$	279.95	Methyl nitro-phenols	Direct emissions, oxidation of aromatics in the presence of NO _x	(Gaston et al., 2016; Yuan et al., 2016)
$C_7H_7NO_4I^-$	295.94	Methyl nitro-benzenediols	Direct emissions, oxidation of aromatics in the presence of NO _x	(Gaston et al., 2016; Yuan et al., 2016)
$C_7H_6O_4I^-$	280.93	Dihydroxy methyl benzoquinone	Aromatics + OH	(Schwantes et al., 2017; Wang et al., 2020b)
$C_7H_8O_4I^-$	282.95	Tetrahydroxy toluene	Aromatics + OH	(Schwantes et al., 2017; Wang et al., 2020b)
$C_7H_8O_5I^-$	298.94	Pentahydroxy toluene, fragments of C9 aromatics	Aromatics + OH	(Mehra et al., 2020; Schwantes et al., 2017)

$CH_2O_2I^-$	172.91	Formic acid	Oxidation of VOCs	(Lee et al., 2014; Yuan et al., 2015)
$C_2H_4O_2I^-$	186.93	Acetic acid	Oxidation of VOCs	(Lee et al., 2014; Mattila et al., 2018)
$C_5H_{10}O_2I^-$	228.97	Pentanoic acid	Traffic emissions, secondary formation	(Mattila et al., 2018)
$C_2H_4O_3I^-$	202.92	Glycolic acid	Oxidation of VOCs	(Lee et al., 2014; Lim et al., 2005)
$C_3H_4O_3I^-$	214.92	Pyruvic acid	Photolysis of methylglyoxal, BVOCs+OH, photo-oxidation of aromatics in the presence of NO _x	(Eger et al., 2020; Mattila et al., 2018)
$C_2H_2O_4I^-$	216.90	Oxalic acid	Aqueous-phase photooxidation of glyoxal, photo-oxidation of VOCs	(Carlton et al., 2007; Lee et al., 2014; Zhou et al., 2015)
$C_3H_4O_4I^-$	230.92	Malonic acid, hydroxypyruvic acid	Oxidation of VOCs	(Kawamura and Bikkina, 2016; Lee et al., 2014)
$C_4H_4O_4I^-$	242.92	Maleic acid, fumaric acid	Oxidation of aromatics	(Brege et al., 2018; Kawamura et al., 1996)
$C_5H_6O_4I^-$	256.93	Unsaturated dicarboxylic acid	Oxidation of aromatics	(Brege et al., 2018; Kawamura et al., 1996)
$C_5H_8O_4I^-$	258.95		Photo-oxidation of VOCs	(Berndt et al., 2019; Kawamura and Bikkina, 2016)
$C_6H_{10}O_4I^-$	272.96		Photo-oxidation of VOCs	(Berndt et al., 2019; Kawamura and Bikkina, 2016)

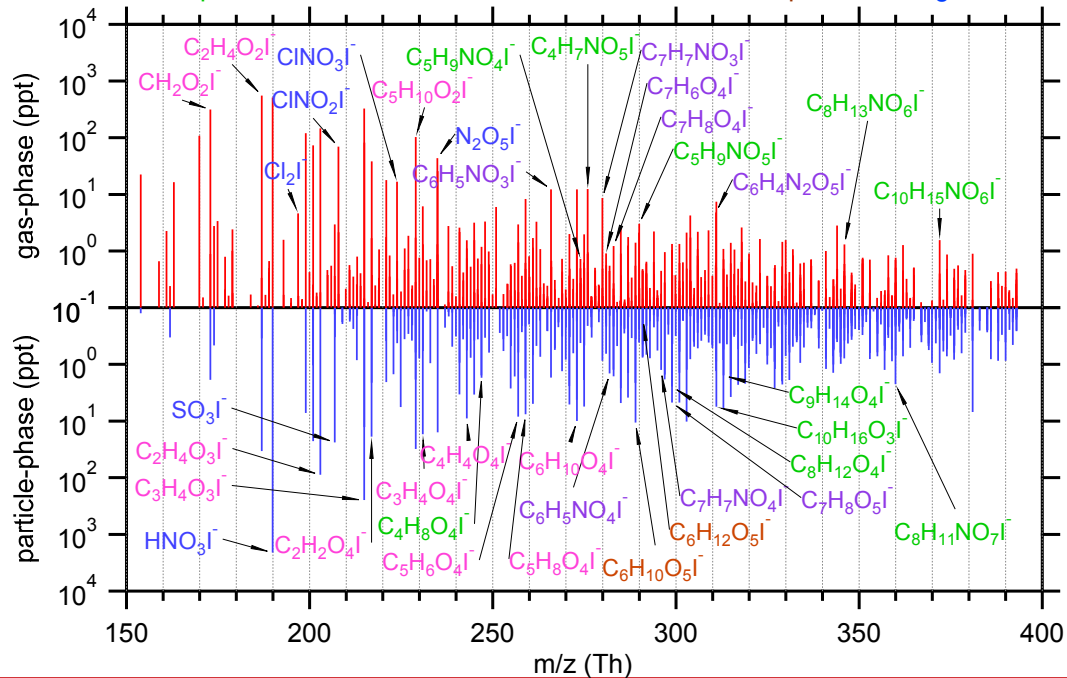
$C_4H_8O_4I^-$	246.95	2-methylglyceric acid	Isoprene SOA component under high NO _x conditions	(Surratt et al., 2006, 2010)
$C_5H_9NO_4I^-$	273.96	IHN (isoprene hydroxy nitrates)	1st-generation organic nitrates from reaction: isoprene+OH+NO _x , isoprene+NO ₃	(Jacobs et al., 2014; Xiong et al., 2015)
$C_4H_7NO_5I^-$	275.94	MVKN/MACRN	2nd-generation organic nitrates from oxidation of IHN in the presence of NO _x	(Fisher et al., 2016; Paulot et al., 2009)
$C_5H_9NO_5I^-$	289.95	C5 nitrooxy hydroperoxide, C5 nitrooxy hydroxyepoxide, C5 dihydroxy nitrate	isoprene+NO ₃ , isoprene+OH+NO _x	(Ng et al., 2017; Schwantes et al., 2015; Wennberg et al., 2018)
$C_8H_{12}O_4I^-$	298.98	Dicarboxylic and oxocarboxylic acids like norpinic acid, terpenylic acid	Monoterpenes+OH, monoterpenes O ₃	(Fang et al., 2017; Mutzel et al., 2016; Yasmeen et al., 2011)
$C_9H_{14}O_4I^-$	312.99	Dicarboxylic and oxocarboxylic acids like pinic acid, homoterpenylic acid, caric acid	Monoterpenes+OH, monoterpenes O ₃	(Fang et al., 2017; Mutzel et al., 2016; Yasmeen et al., 2011)
$C_{10}H_{16}O_3I^-$	311.02	Oxocarboxylic acids like	Monoterpenes+OH, monoterpenes O ₃	(Fang et al., 2017; Glasius et al.,

		pinonic acid, caronic acid		2000; Yasmeen et al., 2011)
$C_8H_{13}NO_6I^-$	345.98	Organic nitrates from monoterpenes	Monoterpenes+OH+NO _x , monoterpenes +NO ₃	(Lee et al., 2016; Nah et al., 2016)
$C_8H_{11}NO_7I^-$	359.96	Organic nitrates from monoterpenes	Monoterpenes+OH+NO _x , monoterpenes O ₃ +NO ₃	(Carslaw, 2013; Lee et al., 2016)
$C_{10}H_{15}NO_6I^-$	372.00	Organic nitrates from monoterpenes, peroxyacetyl nitrate from pinonaldehyde	Monoterpenes+OH+NO _x , monoterpenes O ₃ +NO ₃	(Boyd et al., 2015; Massoli et al., 2018; Schwantes et al., 2020)
HSO_4^-	96.96	Sulfuric acid	Oxidation of SO ₂ etc.	(Le Breton et al., 2018b)
SO_3I^-	206.86	Sulfur trioxide, Fragment of organosulfates	Oxidation of SO ₂ , decomposition of organosulfates	(Surratt et al., 2007)
$C_2H_3SO_6^-$	154.96	Glycolic acid sulfate	Aqueous reaction of glycolic acid and sulfuric acid	(Galloway et al., 2009; Huang et al., 2018)
$CH_3SO_3^-$	94.98	Methanesulfonic acid	Oxidation of dimethyl sulfide	(Chen and Finlayson-Pitts, 2017; Gondwe et al., 2003)
$N_2O_5I^-$	234.89	Dinitrogen pentoxide	NO ₃ + NO ₂ + M	(Le Breton et al., 2018a; Wang et al., 2016)
$ClNO_2I^-$	207.87	Nitryl chloride	N ₂ O ₅ (g) + Cl ⁻ (aq)	(Le Breton et al., 2018a; Wang et al., 2016)

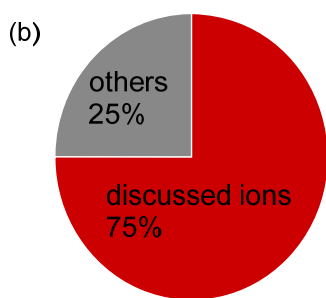
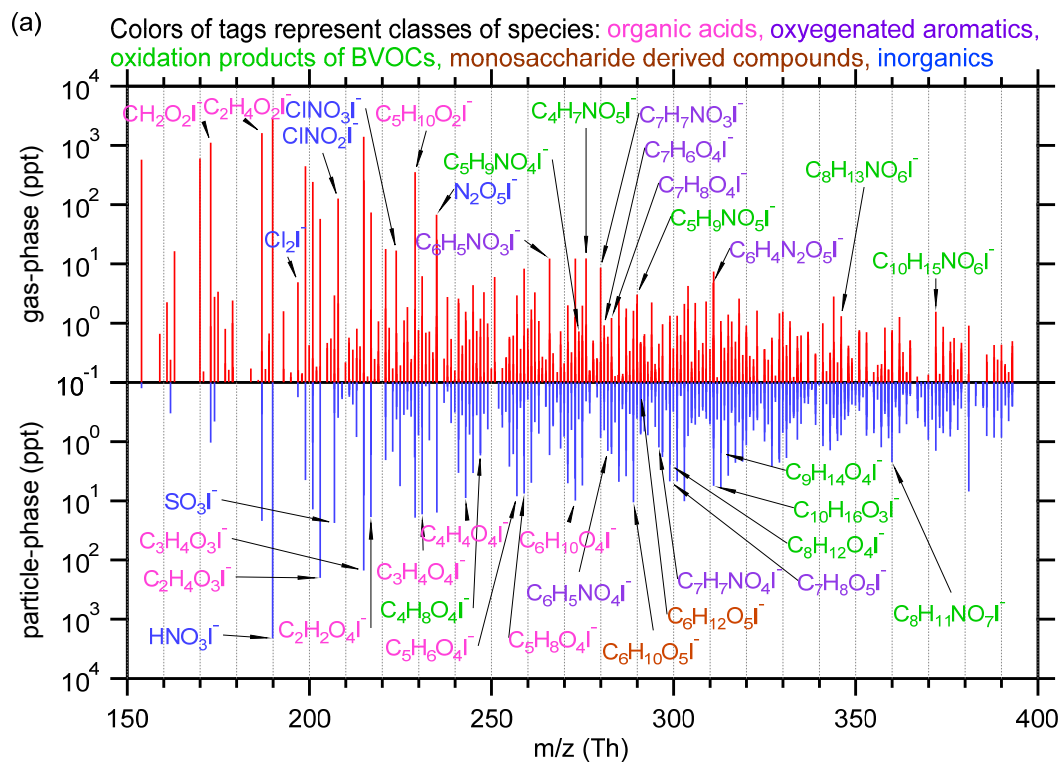
$ClNO_3I^-$	223.86	Chlorine nitrate	$ClO + NO_2 + M$	(Liu et al., 2017; Sander and Crutzen, 1996)
Cl_2I^-	196.84	Chlorine	Heterogeneous reactions of Cl^- and reactive chlorine like HOCl, $ClNO_2$ etc.	(Le Breton et al., 2018a; Liu et al., 2017; Wang et al., 2019)
HNO_3I^-	189.90	Nitric acid	$NO_x + OH$, hydrolysis of organic nitrates and N_2O_5	(Fisher et al., 2016; Wang et al., 2016)

1339

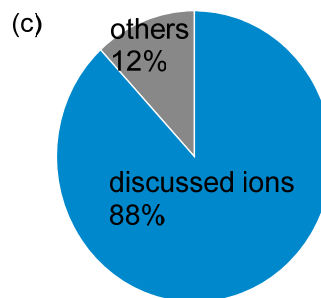
Colors of tags represent classes of species: organic acids, oxygenated aromatics, oxidation products of BVOCs, monosaccharide derived compounds, inorganics



1340



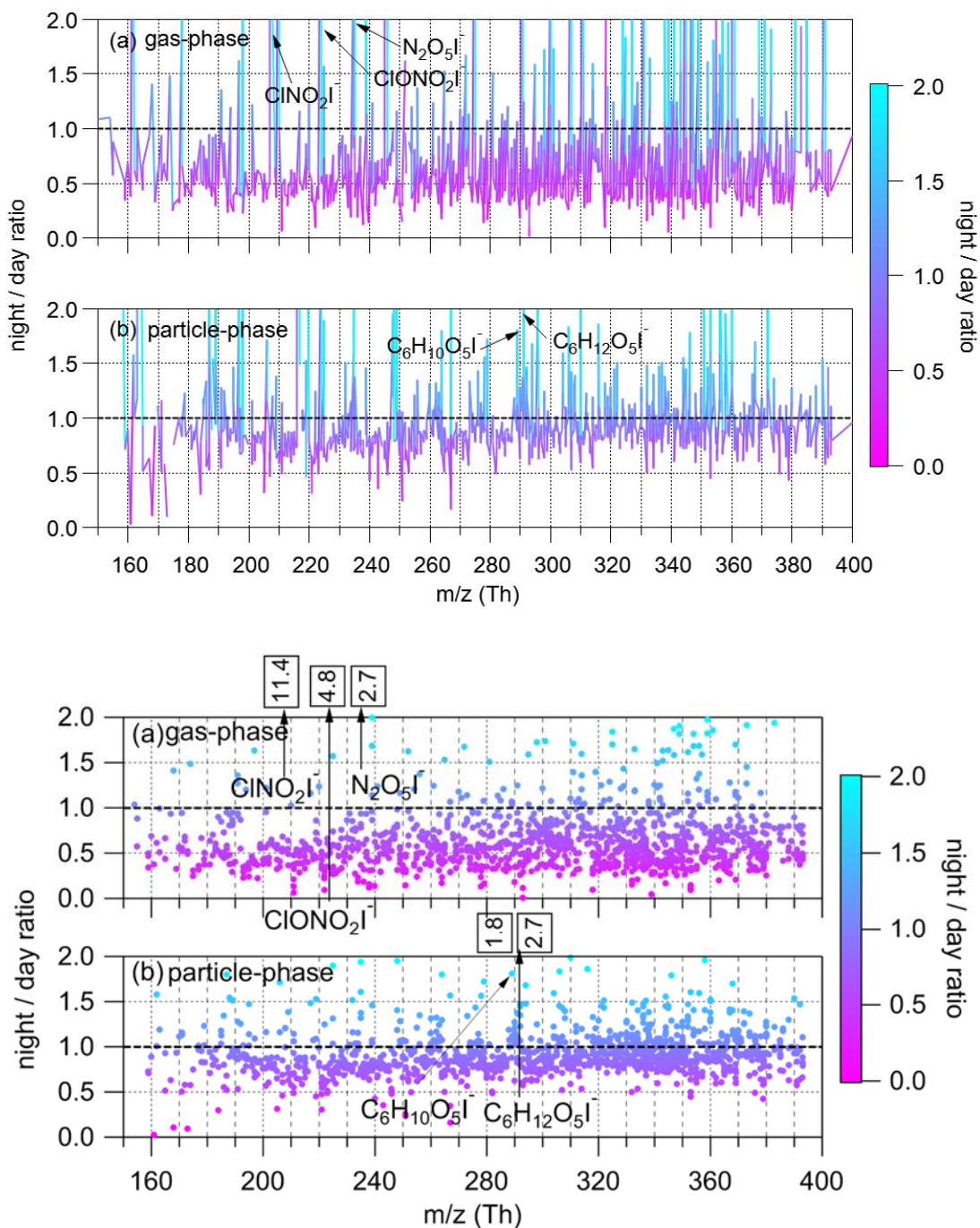
gas-phase



particle-phase

1341

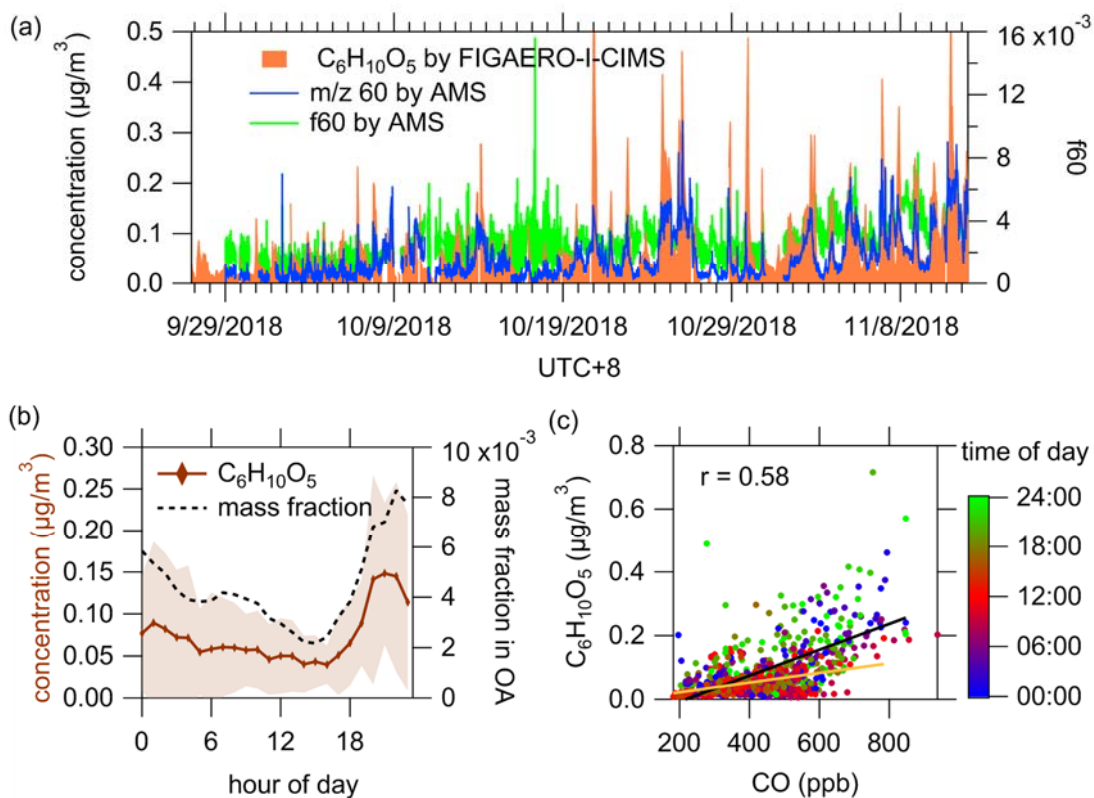
1342 **Figure 1.** (a) Mass spectra of iodide charged ion within m/z 150–400 Th in gas-phase
 1343 (red) and particle-phase (blue), respectively. Humidity correction was not applied when
 1344 calculating the averaged concentrations in mass spectra. (b and c) The fractions of I-
 1345 clusters adduct ions discussed in the main text (Table 1) in the total ion signals for I-
 1346 adduct ions measured in gas-phase (b) and I-clusters. (c) The fraction of I-clusters
 1347 discussed in the text in the total particle-phase (c), respectively I-clusters.



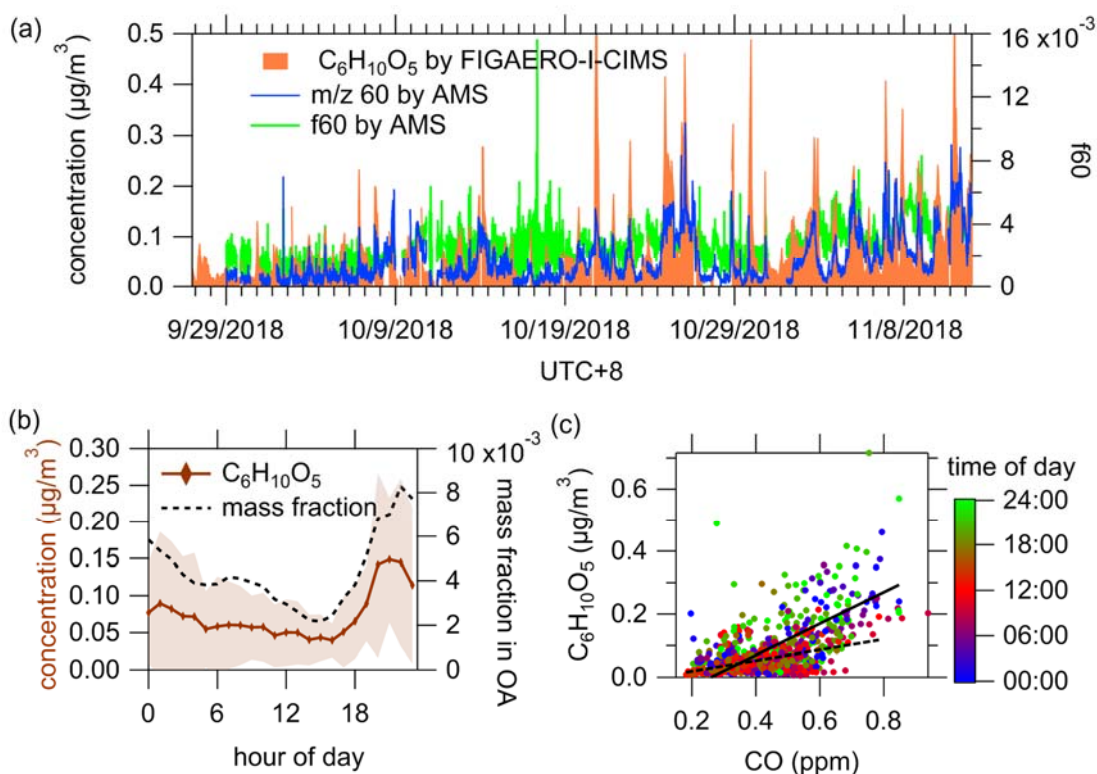
1348

1349

1350 **Figure 2.** The ratios of concentrations at night (10 pm – 6 am) to concentrations during
 1351 the day (10 am – 6 pm) for ions ranging from 150 to ~~500~~ 400 Th in gas-phase (a) and
 1352 particle-phase (b). The range of y-axis is set between 0 and 2 for clarity, although the
 1353 ratios of some compounds are larger than 2. The numbers in boxes ~~are~~ indicate the
 1354 night/day ratios of tagged ions that exceed the y-axis ranges.



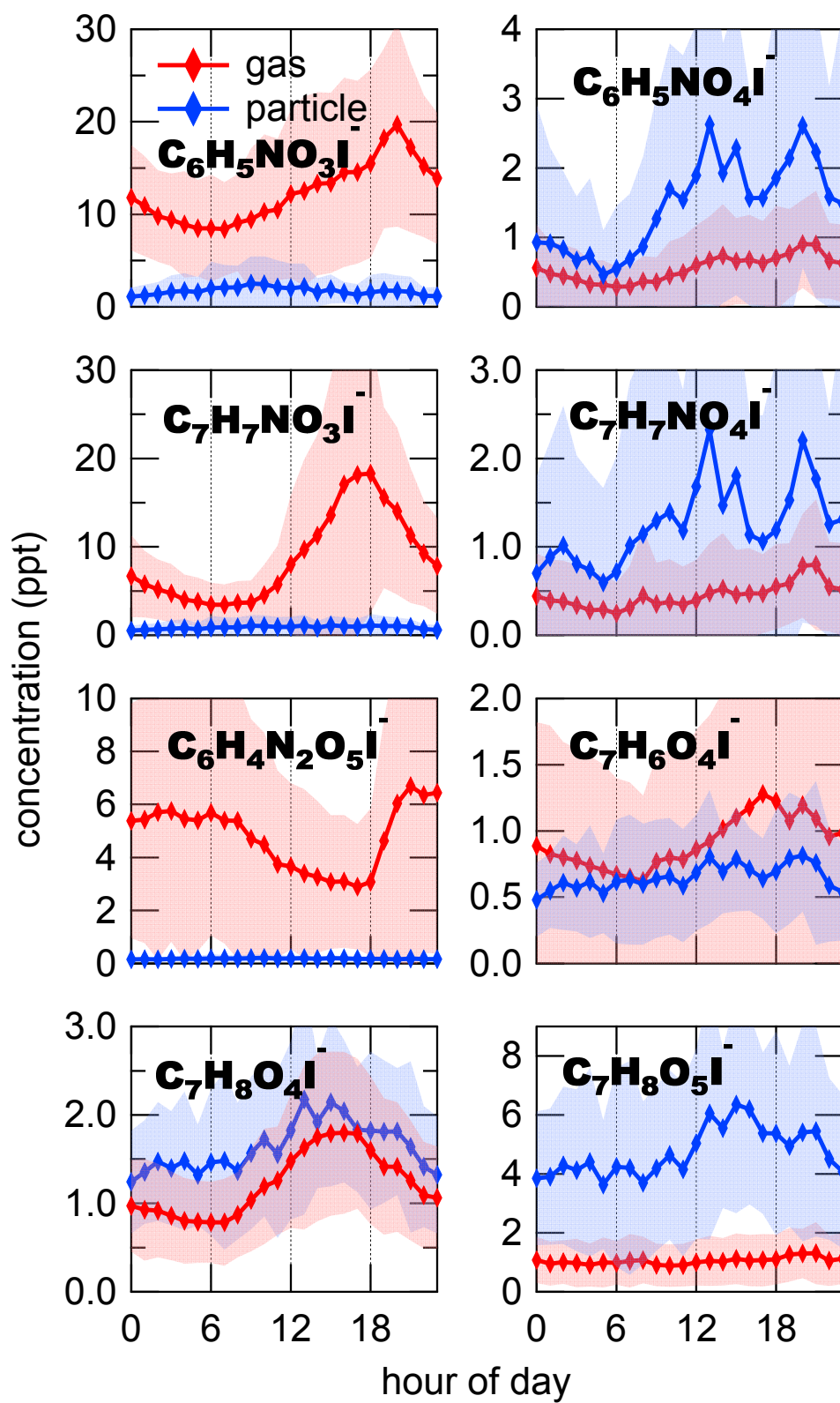
1355

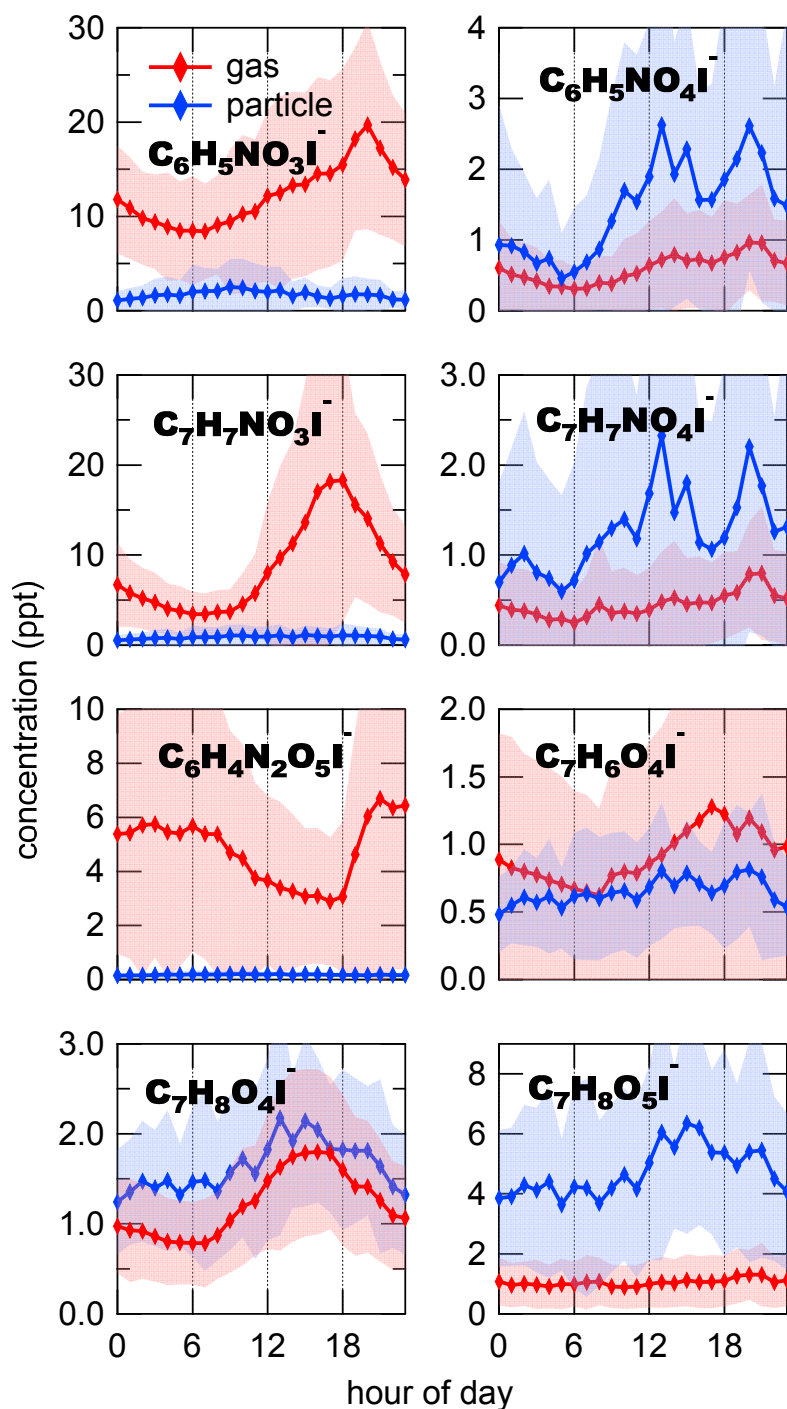


1356

1357 **Figure 3.** (a) Time series of particulate $C_6H_{10}O_5$ measured by FIGAERO-I-CIMS, m/z
 1358 60 fragment and f60 measured by AMS. Background f60=0.3% and background m/z
 1359 60=0.3% \times OA were subtracted from f60 and m/z 60 (Cubison et al., 2011; Hu et al.,

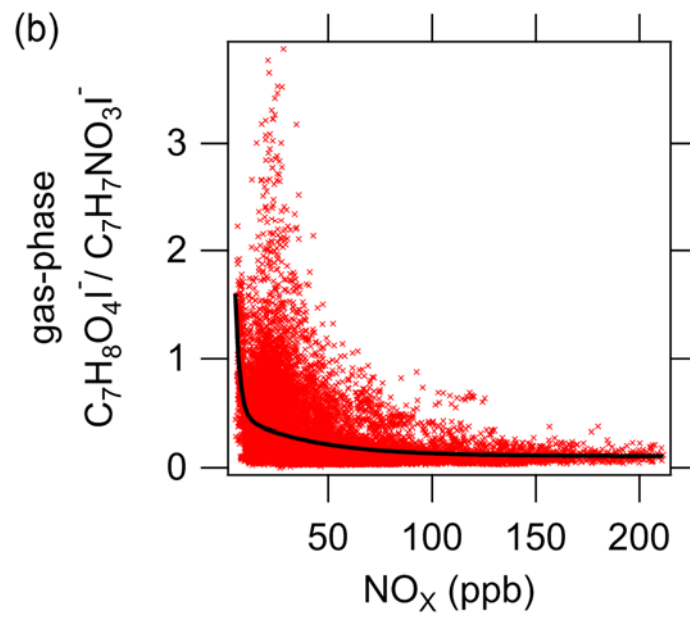
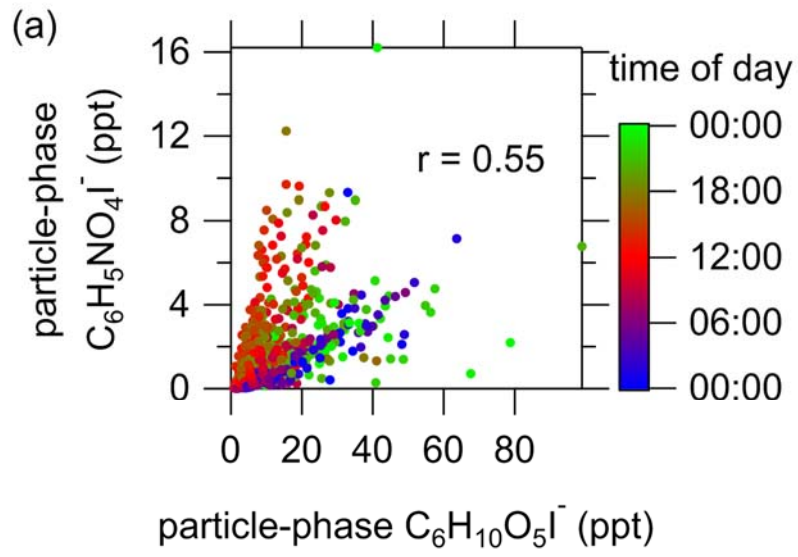
1360 2016). (b) Diurnal variations of particulate C₆H₁₀O₅ and its mass fraction in OA. (c)
1361 Correlation between CO and particulate C₆H₁₀O₅. The ~~orange-dash~~ and ~~black-solid~~ lines
1362 indicate the ratios during daytime (10 am ~~~~~ 6 pm, 0.17±0.02 μg·m⁻³/ppm) and
1363 nighttime (10 pm ~~~~~ 6 am), ~~which are 1.5×10⁻⁴ and 0.50±0.03 4.1×10⁻⁴ (μg·m⁻³/~~
1364 ~~ppbppm)~~, respectively, ~~respectively~~.

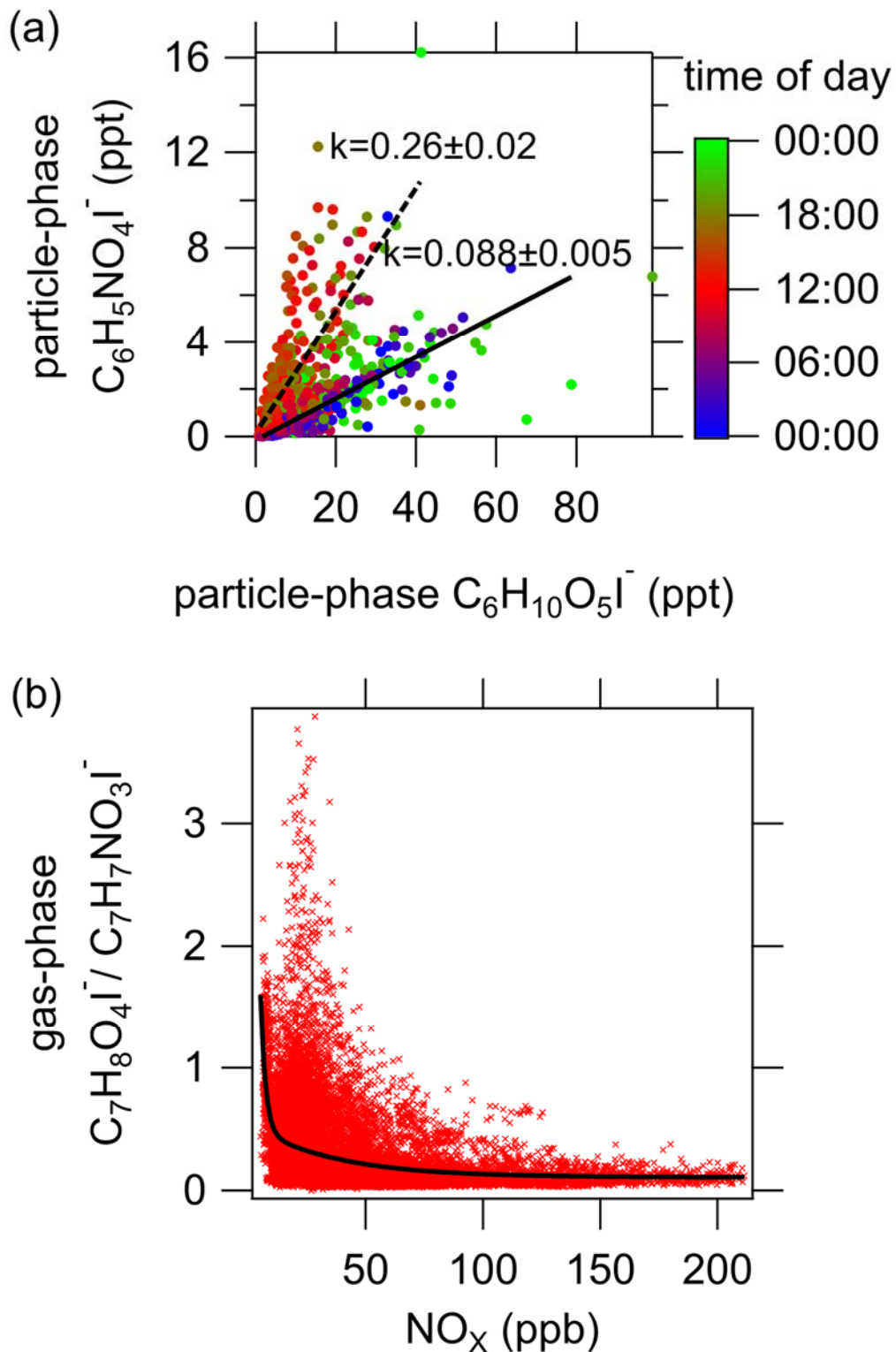




1366

1367 **Figure 4.** Diurnal variations of oxidized aromatics in both phases including nitro-
 1368 phenols ($C_6H_5NO_3I^-$), nitro-benzenediols ($C_6H_5NO_4I^-$), methyl nitro-phenols
 1369 ($C_7H_7NO_3I^-$), methyl nitro-benzenediols ($C_7H_7NO_4I^-$), dinitro-phenols
 1370 ($C_6H_4N_2O_5I^-$), dihydroxy methyl benzoquinone ($C_7H_6O_4I^-$), tetrahydroxy toluene
 1371 ($C_7H_8O_4I^-$), pentahydroxy toluene and fragments of C9 aromatics ($C_7H_8O_5I^-$). The
 1372 shaded areas indicates one standard deviations.

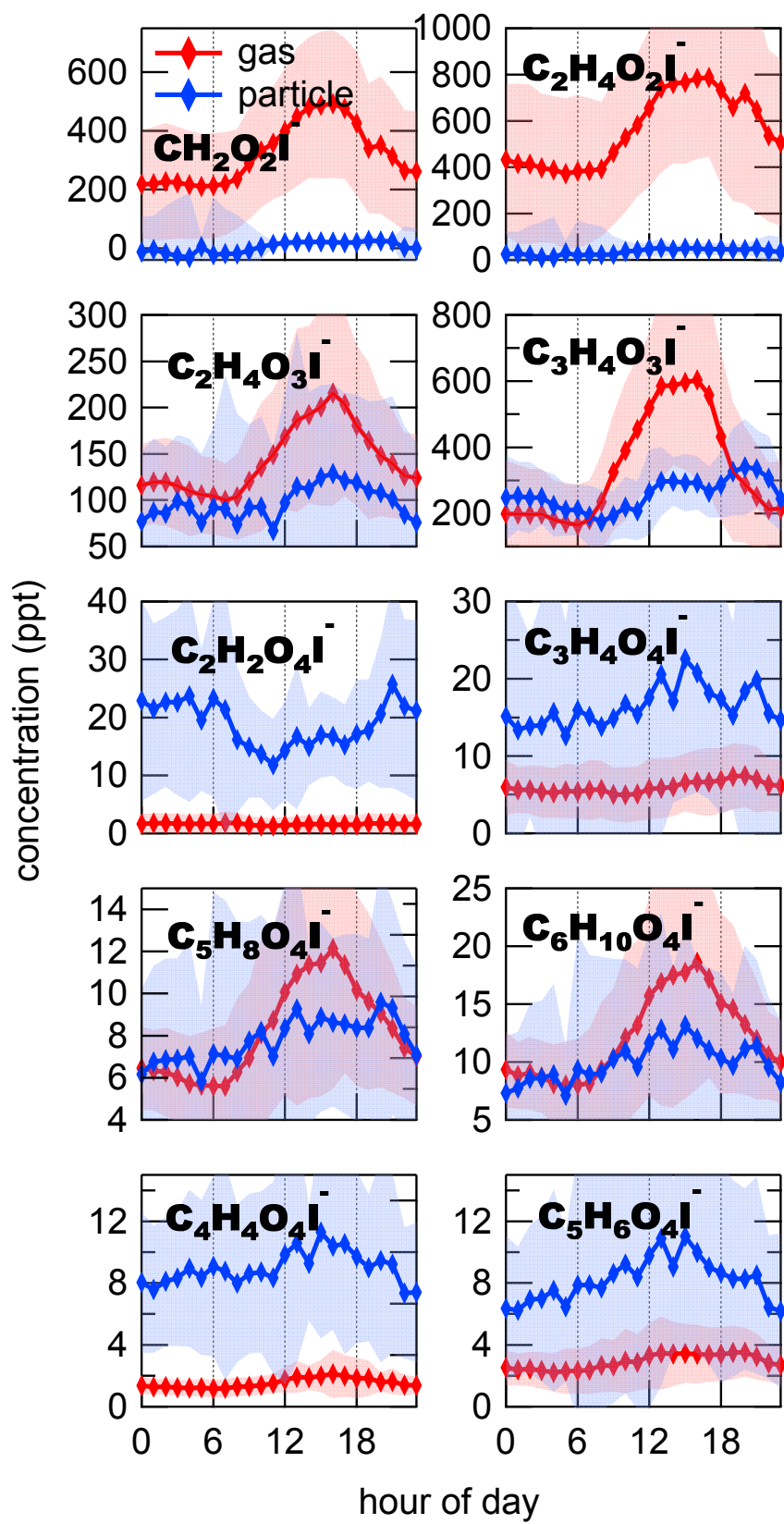


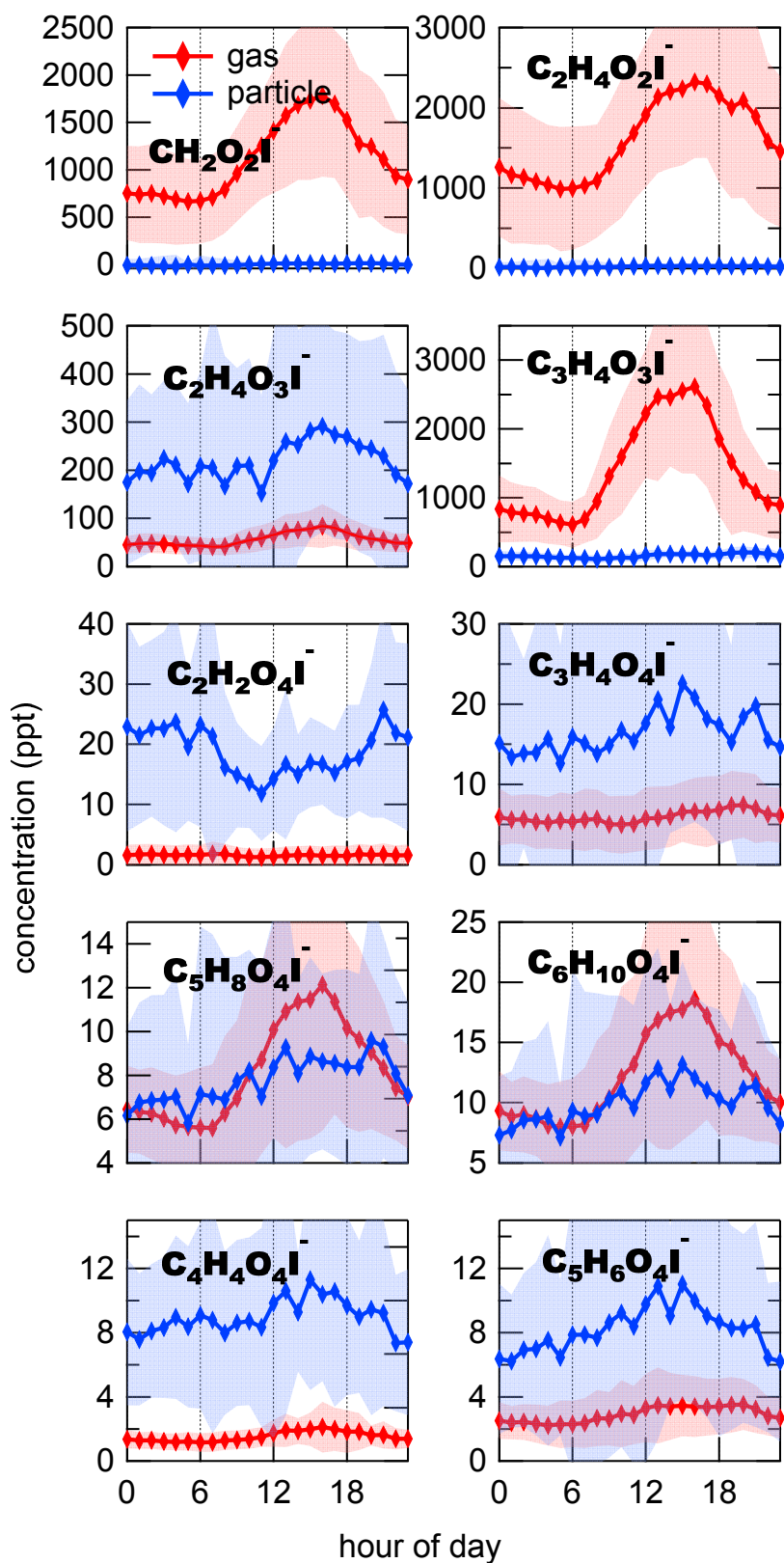


1374

1375 **Figure 5.** (a) Correlation between particle-phase $C_6H_5NO_4I^-$ and $C_6H_{10}O_5I^-$. The
 1376 data points are color-coded using the time of the day. Solid and dash lines represent the
 1377 slopes during the nighttime and daytime, respectively. (b) Relative concentration of

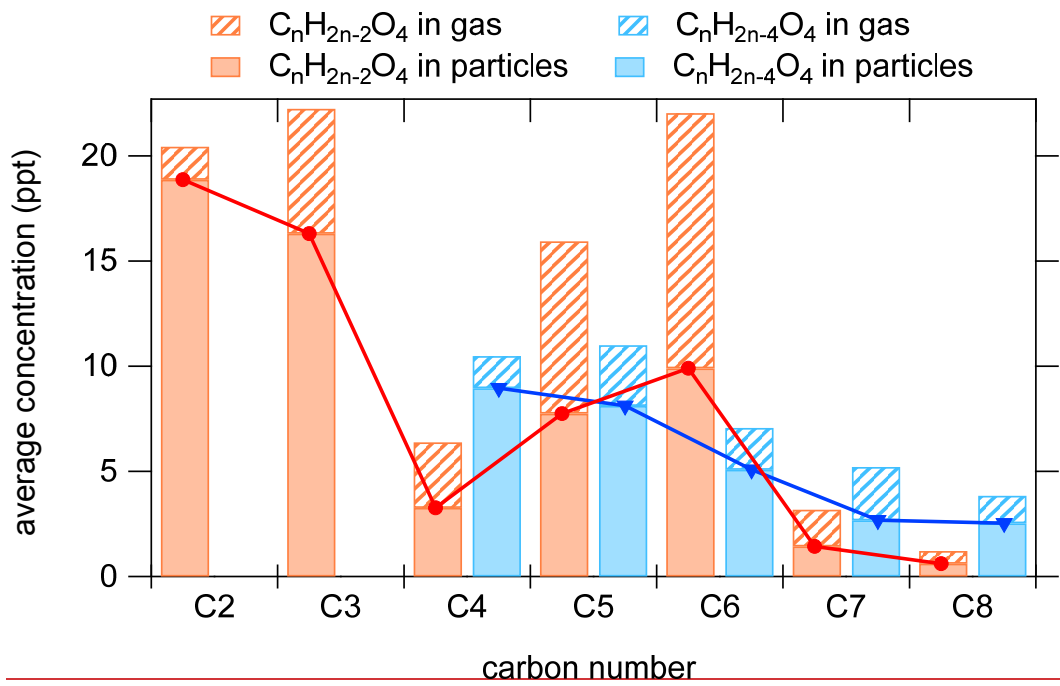
- 1378 $C_7H_8O_4I^-$ and $C_7H_7NO_3I^-$ in the gas phase as a function of NO_x concentration. The
1379 black line is the fitted curve using a double exponential function.



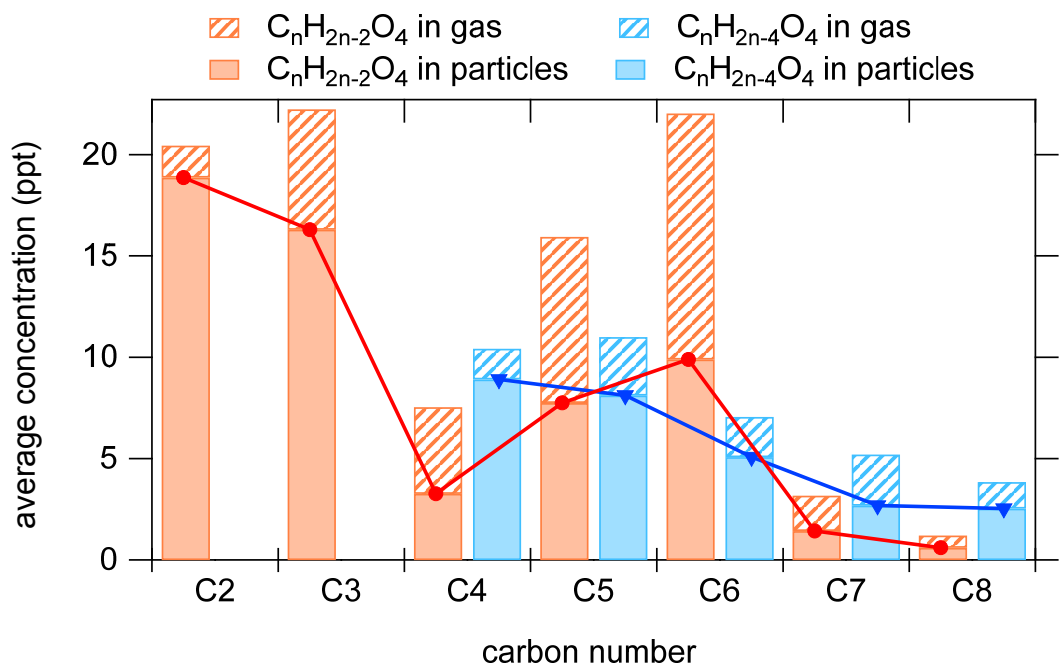


1381

1382 **Figure 6.** Diurnal variations of organic acids in the gas phase (red) and particle phase
 1383 (blue). The shaded area indicates one standard deviations.

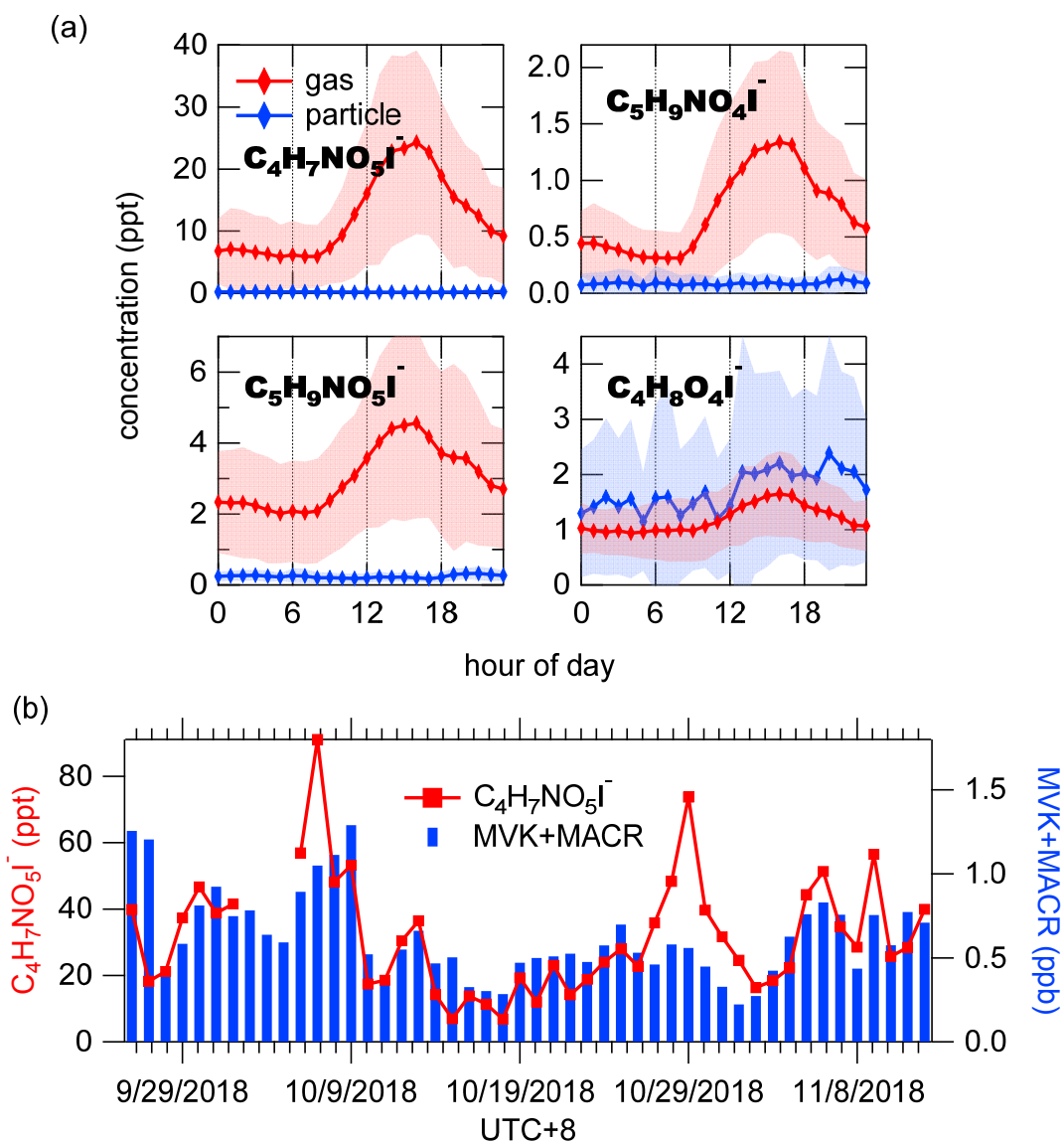


1384



1385

1386 **Figure 7.** Average concentrations of compounds with the formulas of $C_nH_{2n-2}O_4$
 1387 and $C_nH_{2n-4}O_4$.



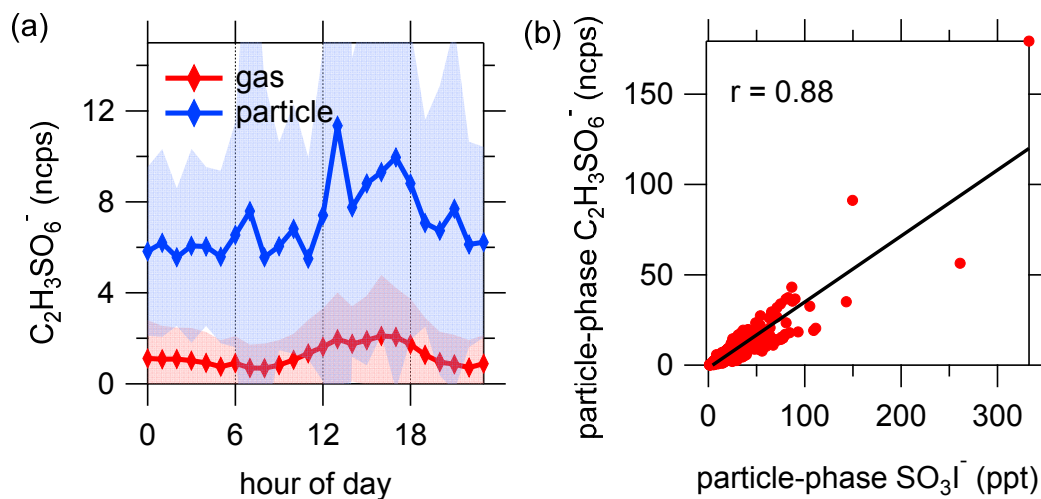
1388

1389 **Figure 8.** (a) Diurnal variations of isoprene oxidation products in the gas phase (red)

1390 and particle phase (blue). The shaded area indicates one standard deviations. (b) Time

1391 series of daily maximum concentrations of gaseous $C_4H_7NO_5I^-$ and MVK+MACR

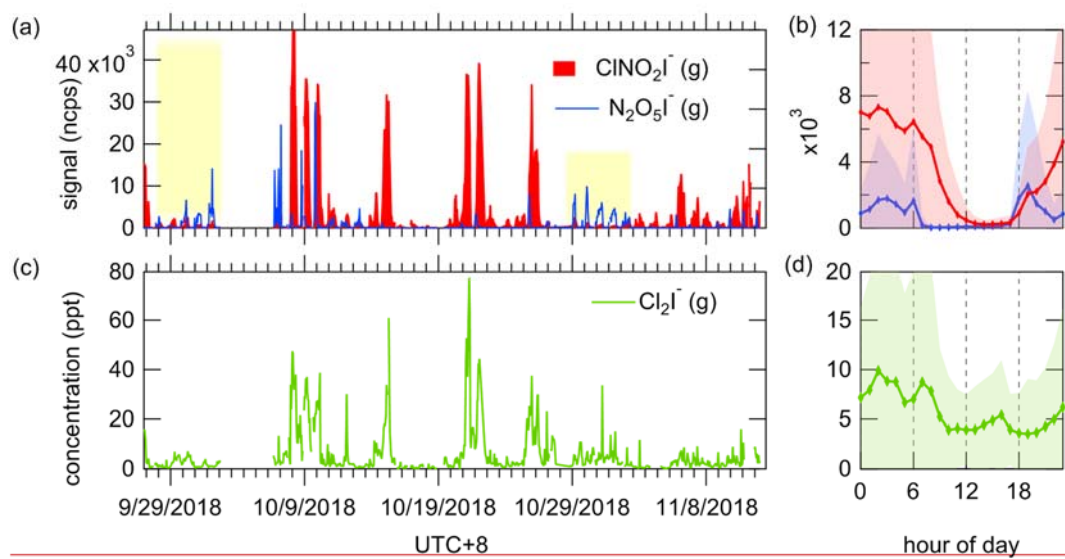
1392 ($C_4H_6OH^+$, m/z 71.05) measured by PTR-ToF-MS.



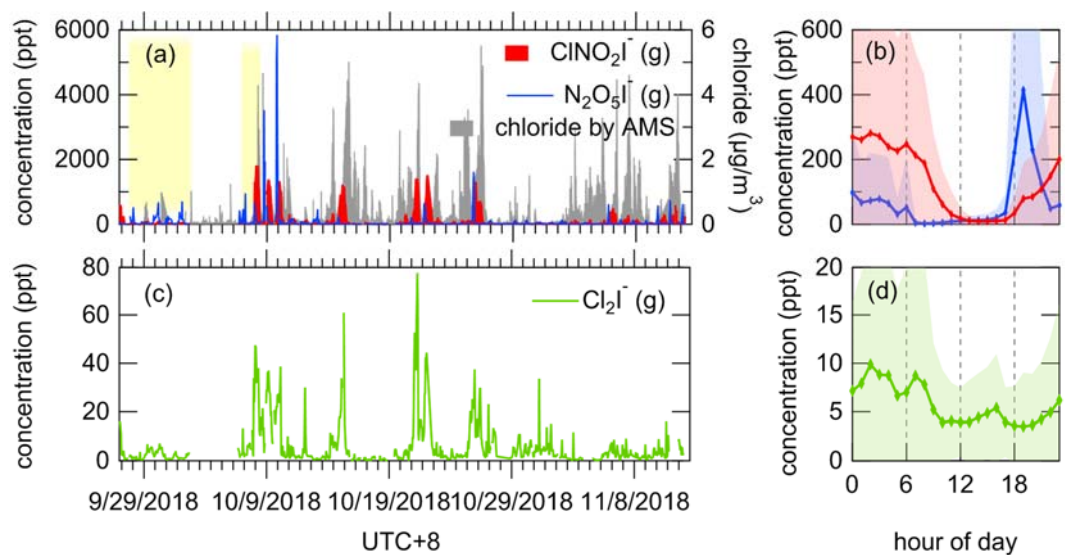
1393

1394 **Figure 9.** (a) Diurnal variation of $C_2H_3SO_6^-$. The shaded areas indicate one standard

1395 deviation. (b) Correlation between particle-phase $C_2H_3SO_6^-$ and SO_3I^- .

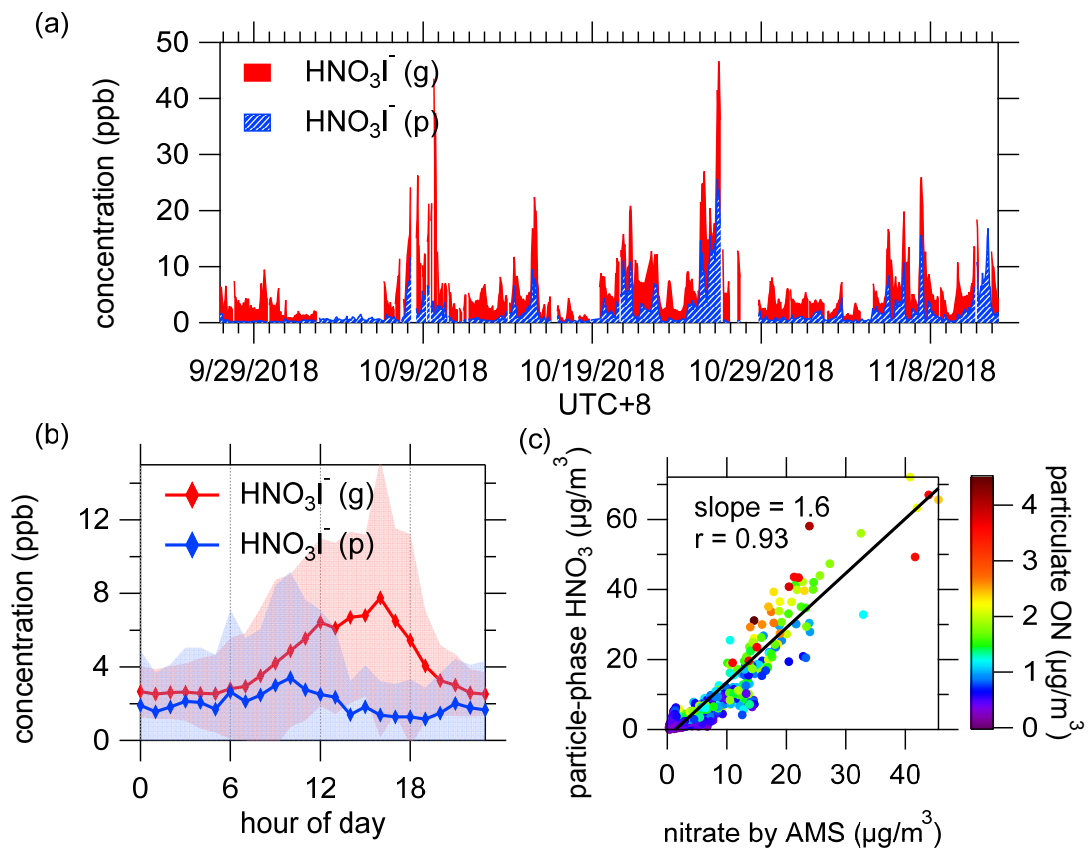


1396

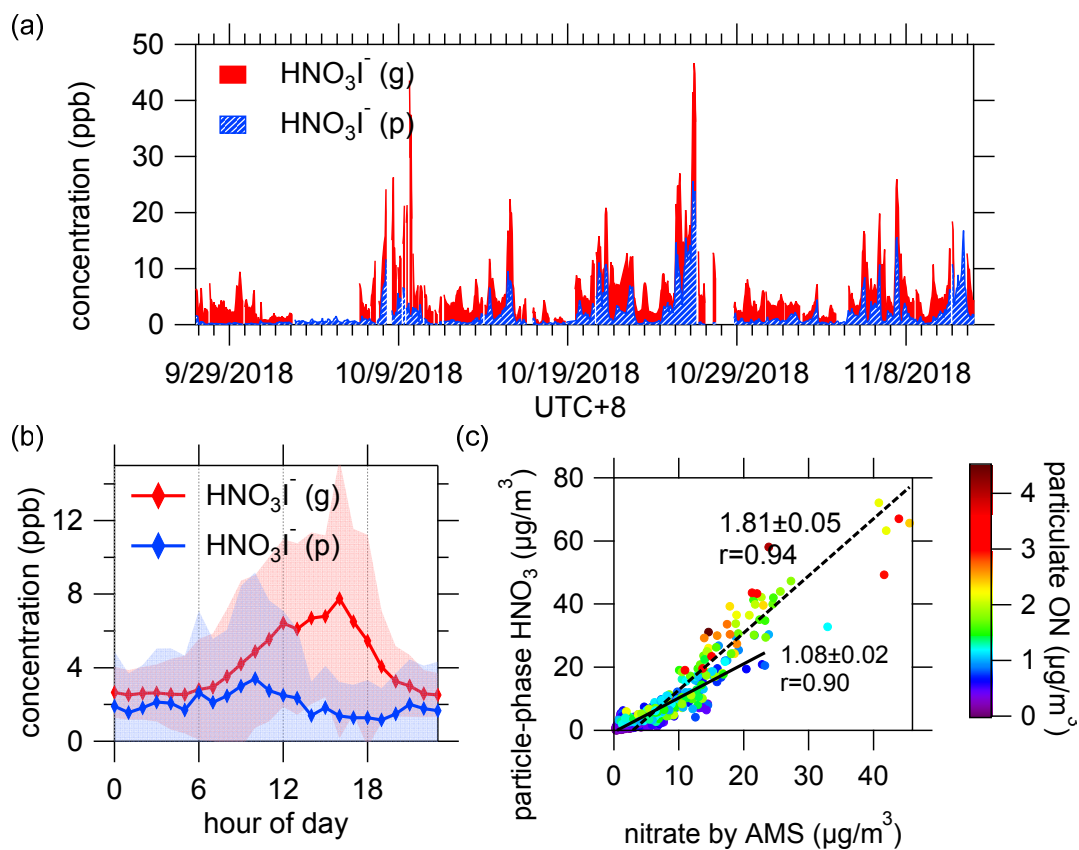


1397

1398 **Figure 10.** Time series and diurnal variations of humidity-corrected concentrations of
 1399 N_2O_5 and ClNO_2 (a, b) and Cl_2 (c, d). The gray profile is the time series of chloride
 1400 measured by AMS (mainly non-sea salt). The tinted background indicates the days with
 1401 high concentrations of N_2O_5 but low concentrations of ClNO_2 . The shaded areas
 1402 indicate one standard deviations. The humidity dependence of the sensitivity of chlorine
 1403 was experimentally determined and thus humidity correction was applied to chlorine.
 1404 The tinted background indicates the days with high concentrations of N_2O_5 but low
 1405 concentrations of ClNO_2 . The shaded areas indicate standard deviations.



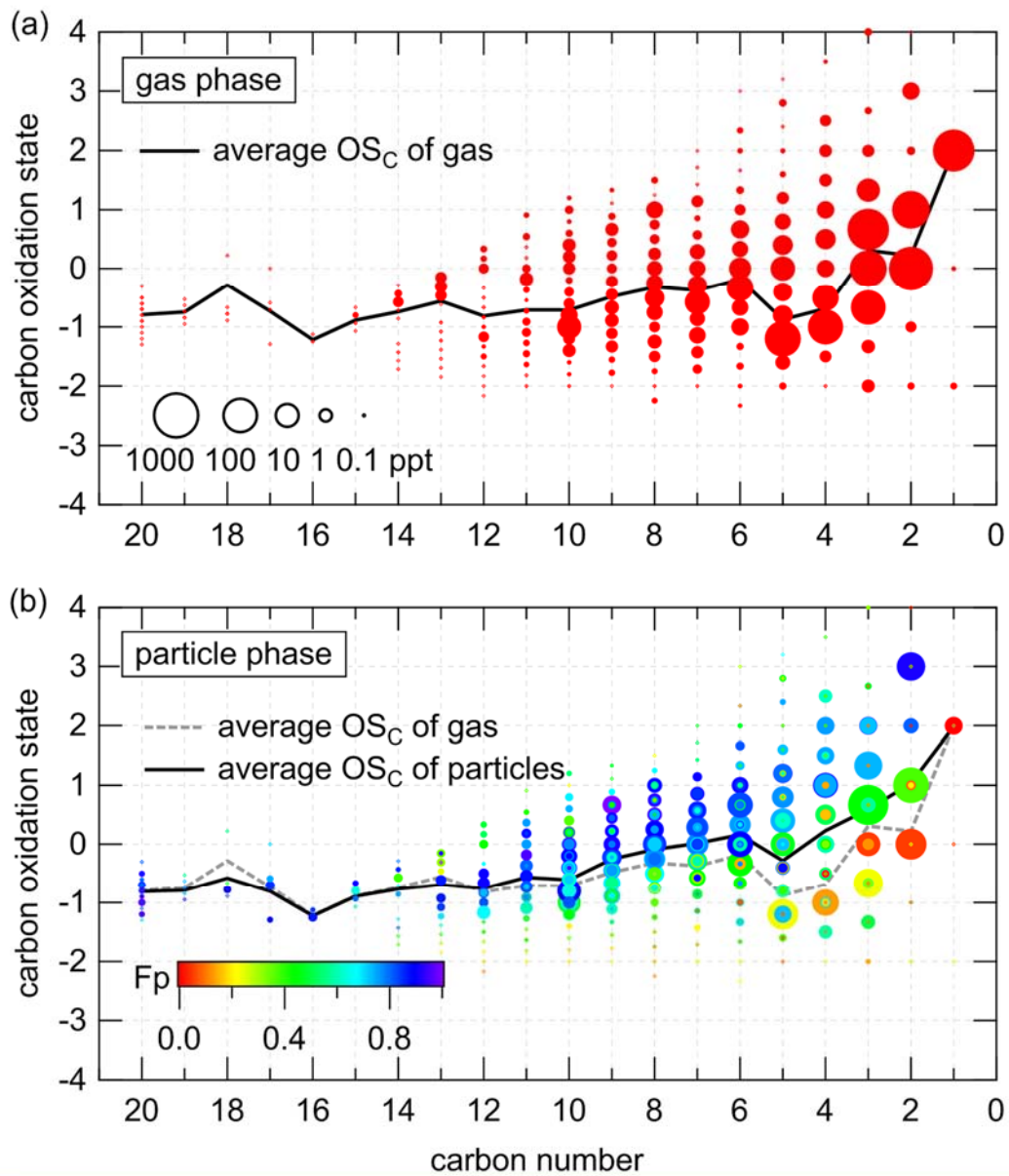
1406



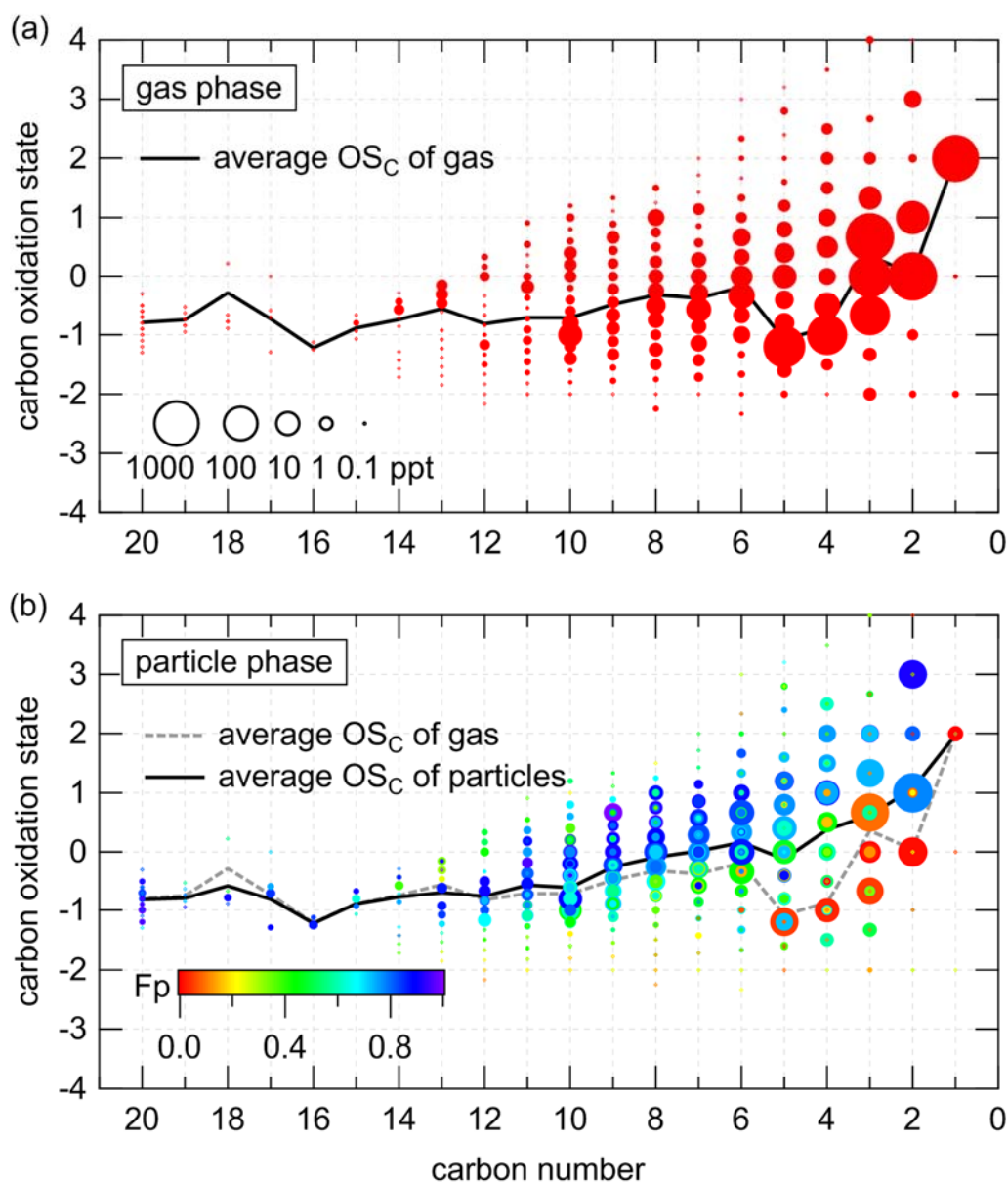
1407

1408 **Figure 11.** (a) Time series of humidity-corrected HNO_3I^- in both phases. (b) Diurnal
 1409 variation of humidity-corrected HNO_3I^- . The shaded areas indicate one standard

1410 deviations. (c) Comparison of particle-phase HNO_3I^- and nitrate measured by AMS.
1411 The color scale denotes particulate N-containing organic nitrates-compounds measured
1412 by FIGAERO-I-CIMS (pON). The solid and dash lines show the correlations fitted
1413 results for the dataset of pON less than $1 \mu\text{g}/\text{m}^3$ and more than $1 \mu\text{g}/\text{m}^3$, respectively.
1414 The concentration of gaseous HNO_3I^- shown here only included the last 5-minute of
1415 every gas-phase working mode, as high level of HNO_3 came out of aerosol which then
1416 passed through the CIMS in a short time during particle analysis and a substantial
1417 amount would subsequently accumulate on the inner surfaces, leading to a persistent
1418 carried over signal that was long enough to disturb the next gas measurement cycle
1419 (Palm et al., 2019).

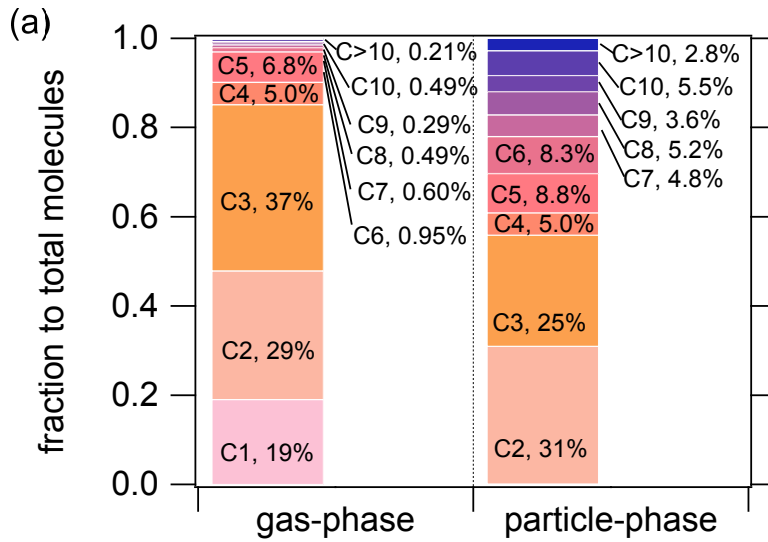


1420

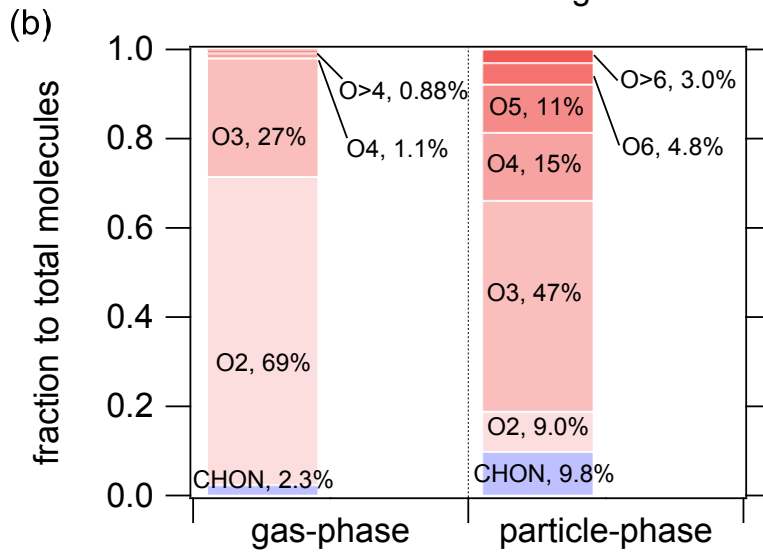


1421

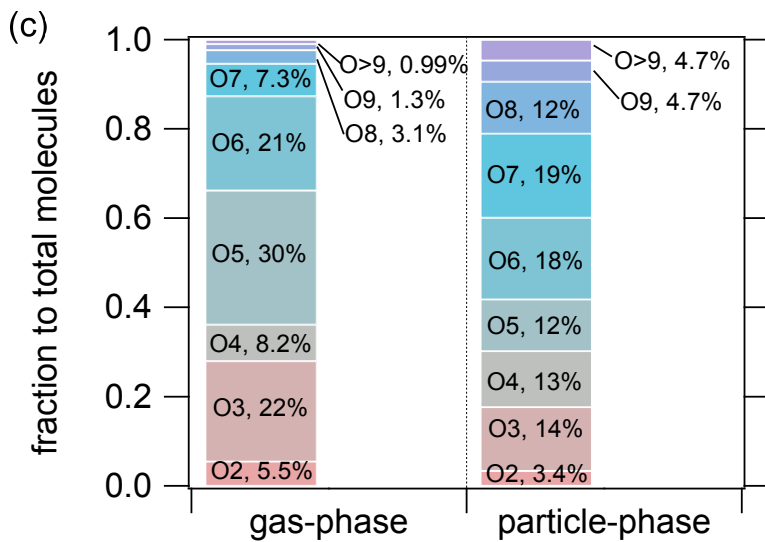
1422 **Figure 12.** $\overline{OS}_C - n_C$ spaces for $C_xH_yO_z$ and $C_xH_yN_{1,2}O_z$ compounds in gas-phase
 1423 (a) and particle-phase (b). The diameters of circles are proportional to the logarithmic
 1424 average concentrations. The black lines are the average \overline{OS}_C of each carbon number
 1425 for compounds in gas-phase and particle-phase, respectively. The compounds in Fig. (b)
 1426 are color-coded by their fractions in particles.



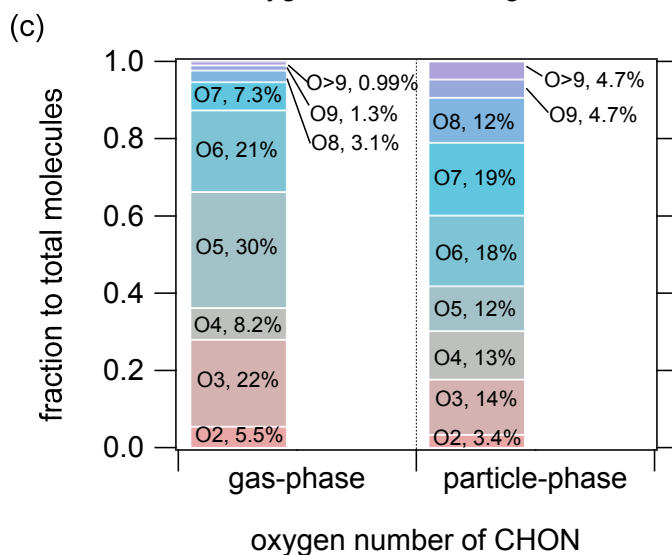
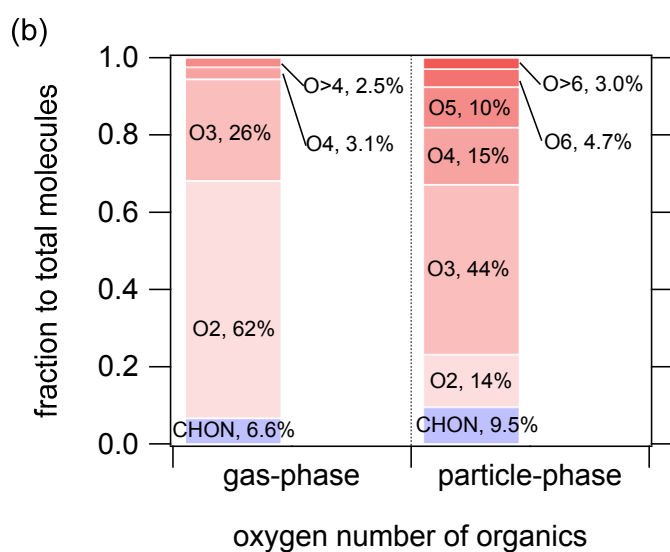
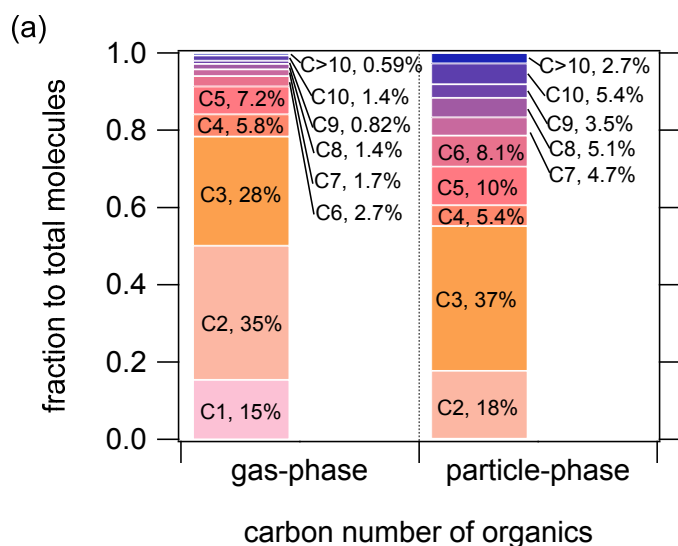
carbon number of organics



oxygen number of organics



oxygen number of CHON



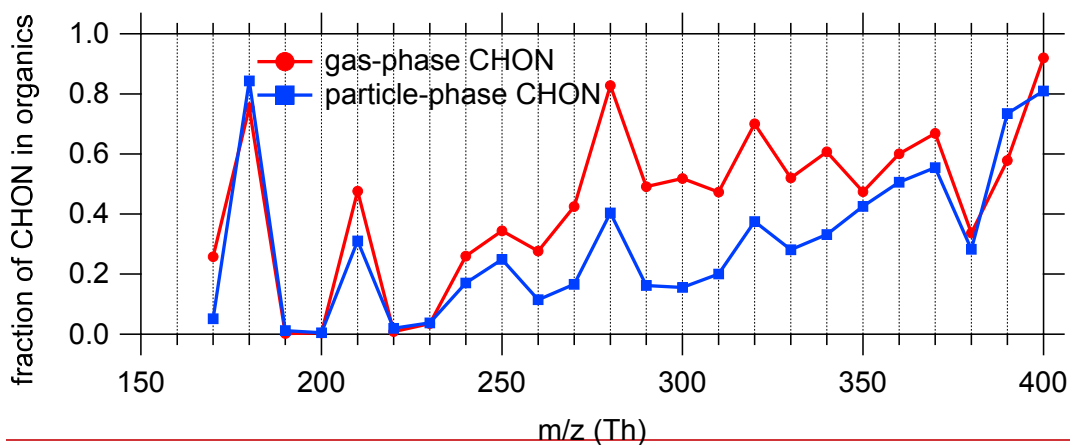
1428

1429

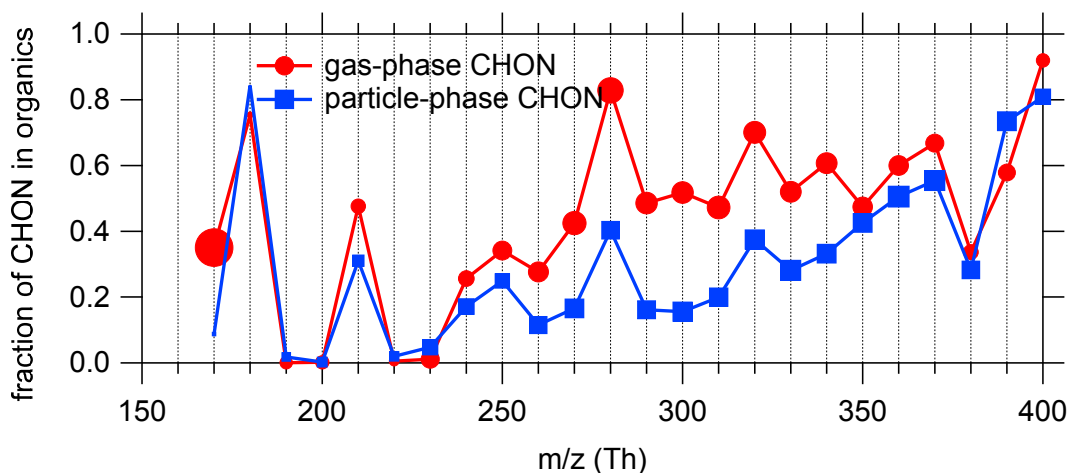
1430

1431

Figure 13. Carbon number distribution (a) and oxygen number distribution of total $C_xH_yO_z$ and $C_xH_yN_{1,2}O_z$ compounds (b), and oxygen number distribution of $C_xH_yN_{1,2}O_z$ compounds (c).

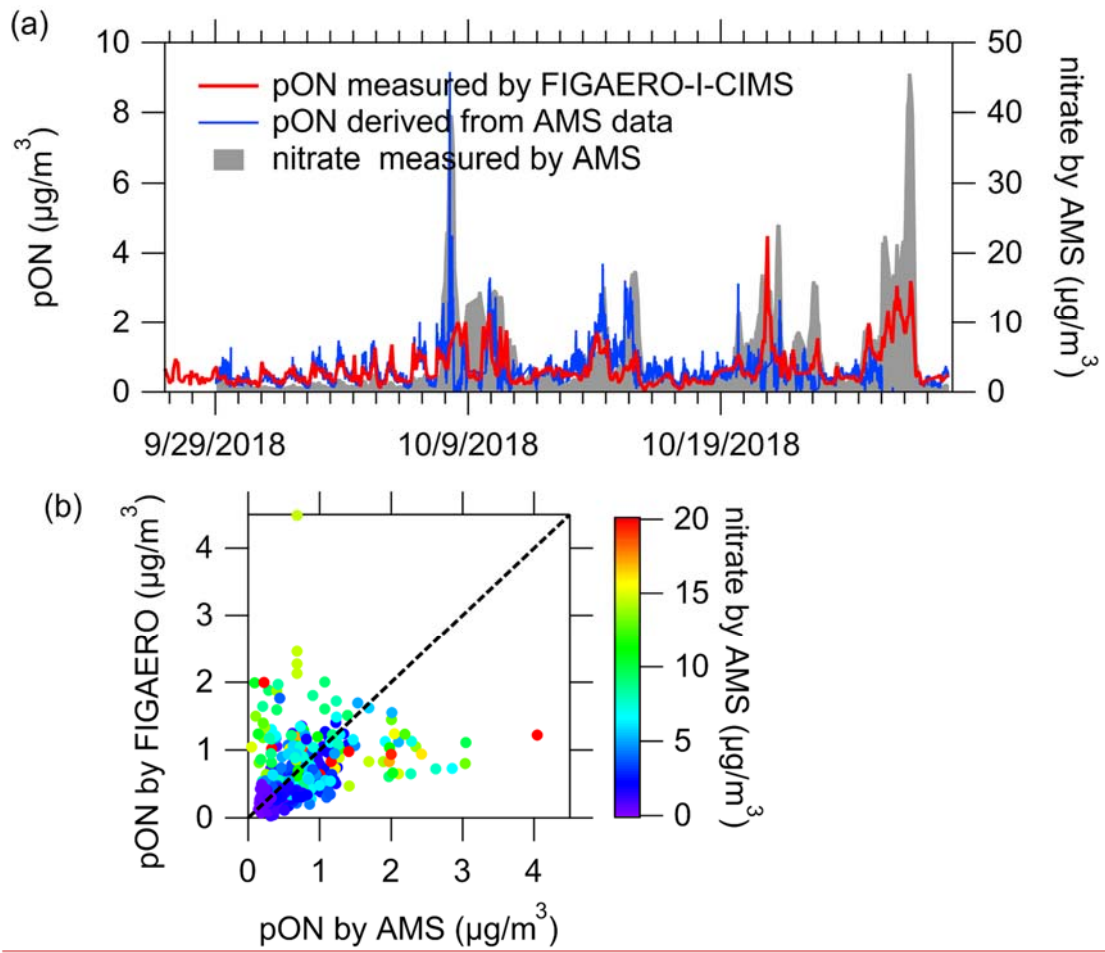


1432

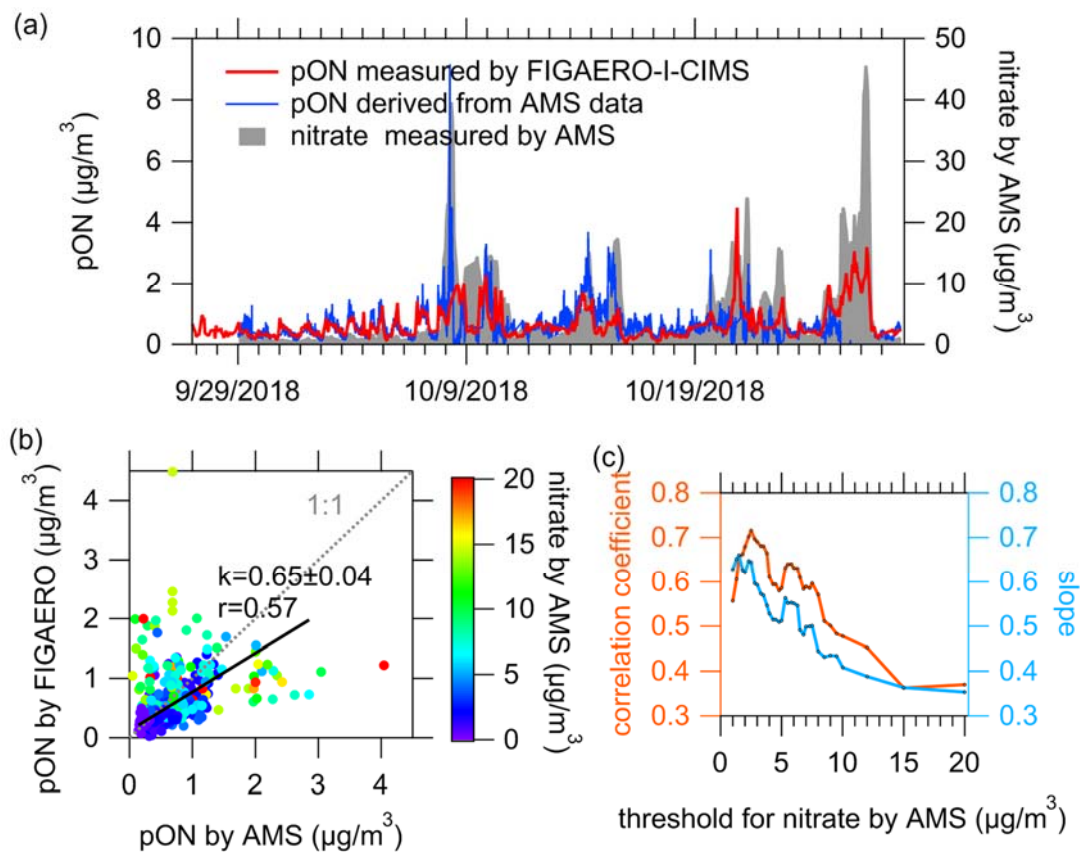


1433

1434 **Figure 14.** The average fractions of CHON to total organic compounds (CHO +
 1435 CHON + CHOS + CHONS) of every 10 Th in both phases. See Fig. S16 for the overall
 1436 distribution of the contributions of species classes to the total concentrations. Marker
 1437 sizes indicate the total concentration level in each m/z bin. High ambient concentration
 1438 of HNCO resulted in the large marker around m/z 170 in the gas phase (Wang et al.,
 1439 2020d).

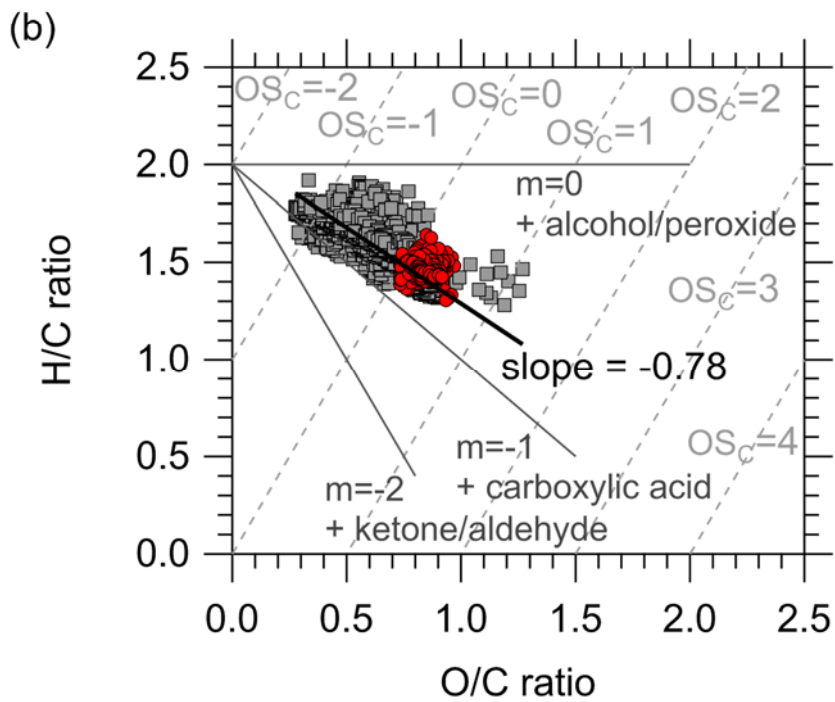
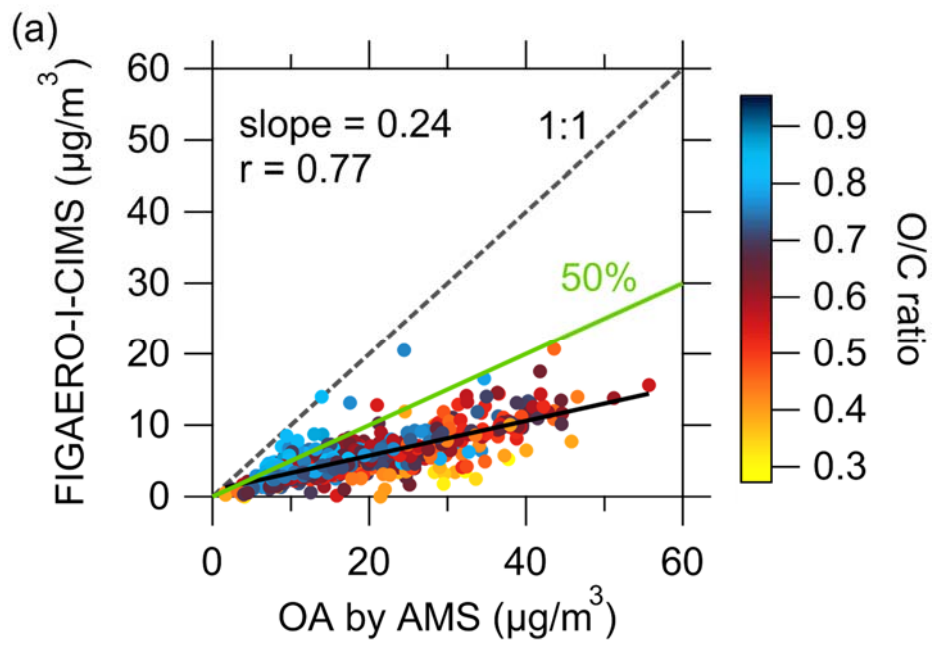


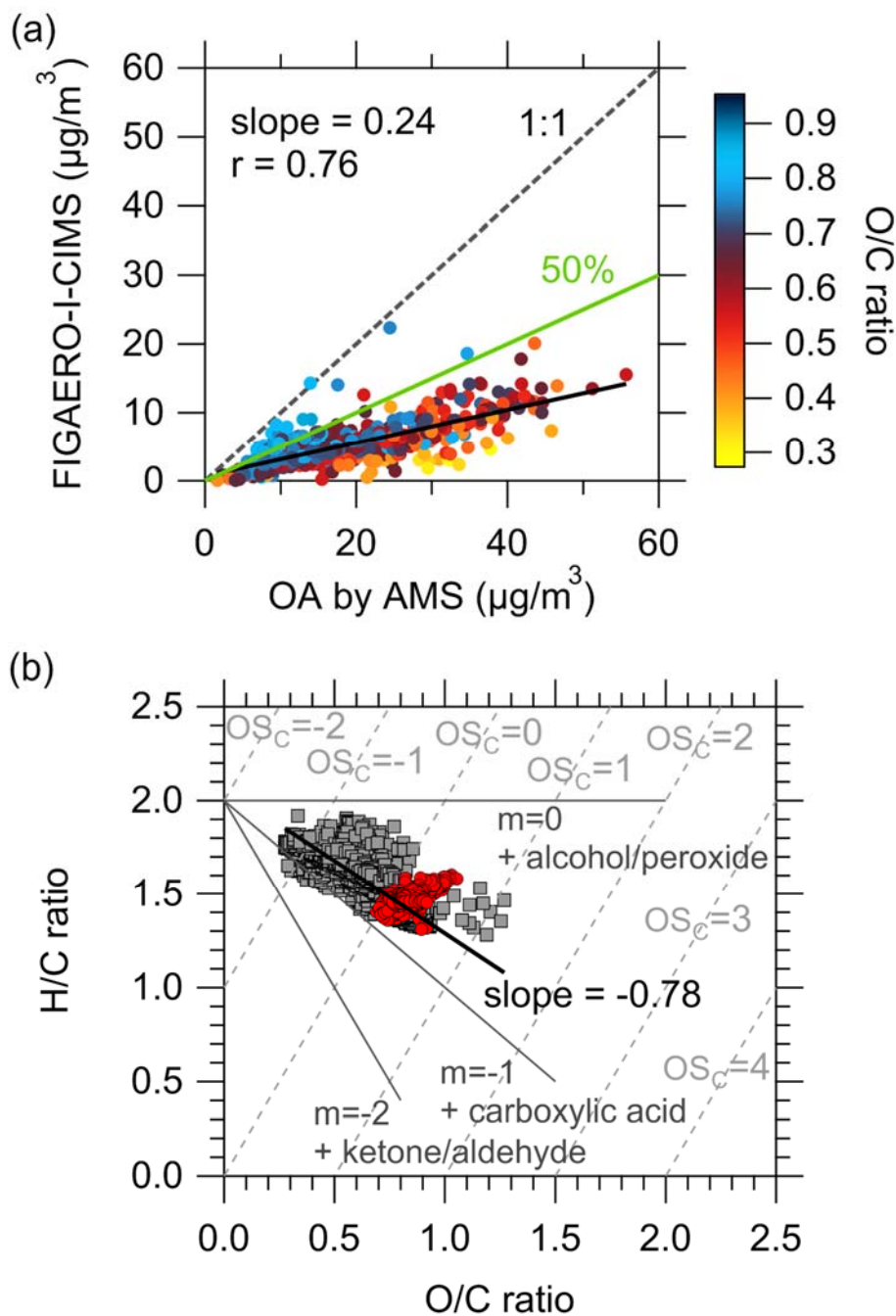
1440



1441

1442 **Figure 15.** (a) Time series of particulate N-containing organics compounds measured
 1443 by FIGAERO-I-CIMS (pON by FIGAERO), particulate ~~inorganic nitrate and~~ organic
 1444 nitrates derived from AMS data (pON by AMS) as well as particulate inorganic nitrate.
 1445 (b) Comparison of pON by FIGAERO~~particulate N-containing organics measured by~~
 1446 FIGAERO-I-CIMS and pON by AMS~~particulate organic nitrates provided by AMS~~,
 1447 color-coded by the concentrations of particulate inorganic nitrate measured by AMS.
 1448 The black line presents the linear fit for nitrate by AMS below $8 \mu\text{g}/\text{m}^3$. (c) The
 1449 determined slopes and correlation coefficients between pON by FIGAERO versus pON
 1450 by AMS by filtering the data below different thresholds of particulate inorganic nitrate
 1451 measured by AMS.





1453

1454 **Figure 16.** (a) Comparison of particulate organic compounds measured by the
 1455 FIGAERO-I-CIMS and AMS, color-coded by O/C ratios measured by AMS. The black
 1456 line is the slope which represents the fraction of OA explained by the measurements of
 1457 FIGAERO-I-CIMS. The green line shows the results from previous work which were
 1458 ~50% (Lopez-Hilfiker et al., 2016; Stark et al., 2017). (b) Van Krevelen diagrams for
 1459 organic aerosol derived from AMS data (gray squares) and FIGAERO-I-CIMS data (red
 1460 circles). Black line is the slope of AMS data. Gray dotted lines are estimated carbon

1461 oxidation state.